Title
H3K36 methylation and the chromodomain protein Eaf3 are required for proper cotranscriptional spliceosome assembly

Author
Leung, Calvin Siu

Publication Date
2019

Peer reviewed|Thesis/dissertation

UNIVERSITY OF CALIFORNIA

Los Angeles

H3K36 methylation and the chromodomain protein Eaf3 are required for proper cotranscriptional spliceosome assembly

A dissertation submitted in partial satisfaction of the requirements for the degree Doctor of Philosophy in Molecular Biology

by

Calvin Siu Leung

2019

ABSTRACT OF THE DISSERTATION

H3K36 methylation and the chromodomain protein Eaf3 are required for proper cotranscriptional spliceosome assembly

by

Calvin Siu Leung

Doctor of Philosophy in Molecular Biology

University of California, Los Angeles, 2019

Professor Tracy L. Johnson, Chair

In the nucleus of the eukaryotic cell, spliceosome assembly and the subsequent catalytic steps of precursor RNA (pre-mRNA) splicing occur cotranscriptionally in the context of a dynamic chromatin environment. A key challenge in the field has been to understand the role that chromatin and, more specifically, histone modification plays in coordinating transcription and splicing. Despite previous work to decipher the coordination between these processes, a mechanistic understanding of the role that chromatin modification plays in spliceosome assembly has remained elusive.

Histone H3K36 trimethylation (H3K36me3) is a highly conserved histone mark found in the body of actively transcribed genes, making it a particularly attractive candidate for having a role in the regulation of pre-mRNA splicing. Although there have been reports that H3K36me3 influences alternative splicing, the underlying mechanisms have remained elusive. Moreover,

despite the prevalence of this mark on actively transcribed genes across eukaryotes, there has not been a mechanistic dissection of its potential role in constitutive splicing. Here we describe how we have addressed these questions and uncovered a core role for H3K36 methylation (H3K36me) in splicing in *Saccharomyces cerevisiae* (*S. cerevisiae*).

RNA-seq analyses of yeast strains deleted of the histone methyltransferase *SET2* or harboring a mutation at the residue lysine 36 revealed widespread and overlapping splicing changes. Through a combination of RNA-seq, ChIP-seq, and biochemical analyses, we determined that the H3K36me effects on splicing are not due defects in transcription, but rather to loss of binding of the chromodomain protein Eaf3. We further show that Eaf3 interacts with the splicing factor Prp45, the human ortholog of SKIP. Consistent with this, Eaf3 is required for the cotranscriptional recruitment of the Prp Nineteen Complex (NTC), which is required for spliceosome activation. Hence, loss of H3K36 methylation has a direct and crucial role in spliceosome assembly. We demonstrate a central role for a highly conserved histone modification in constitutive pre-mRNA splicing. We also show that the reciprocal is true—splicing affects chromatin state.

Although it is established that spliceosome assembly occurs cotranscriptionally, a question that remains is how the activities of the proteins that regulate the dynamic rearrangements of the spliceosome are modulated by transcription and the state of the chromatin. Prp43, an ATPase involved in spliceosome disassembly, has been implicated at numerous steps in the splicing cycle and is therefore an interesting target in the regulation of splicing. Our study aims to determine whether Prp43 plays a role in directing spliceosome rearrangements via chromatin interactions and how interactions between Prp43 and chromatin may affect splicing outcomes. We show that Prp43 associates with chromatin in an RNA-independent manner, but splicing-dependent manner. Furthermore, we observed that Prp43 interacts with H3K36me3, possibly for its role in spliceosome disassembly.

The dissertation of Calvin Siu Leung is approved.

Douglas L. Black

Feng Guo

Alexander Hoffmann

Thomas M. Vondriska

Tracy L. Johnson, Committee Chair

University of California, Los Angeles

2019

This dissertation is dedicated to my parents,

Stanley Kwai Leung and Chinh Ai Phu,

and my brother,

Raymond Siu Leung

TABLE OF CONTENTS

LIST OF FIGURES

Appendix:

LIST OF TABLES

Chapter 2

Chapter 4

LIST OF SUPPLEMENTARY FIGURES

Chapter 2

ACKNOWLEDGEMENTS

I would like to first acknowledge my graduate mentor Dr. Tracy Johnson. I want to thank her for giving me the opportunity to work in her lab. Much of my growth as a scientist is attributed to her. She has always kept me focused and helped guide me whenever I was lost. Her passion for science is contagious and I hope I will be as passionate as her in the future. I have become a better science writer and presenter during my time in the Johnson Lab, which I will forever be grateful for. I would like to thank my committee members Drs. Douglas Black, Feng Guo, Alexander Hoffmann, and Thomas Vondriska for all their feedback and thoughtful guidance during my time as a graduate student. They have constantly advised me on how to proceed with my project, gave critical comments, and always have my best interests at heart. I would like to thank Dr. Matteo Pellegrini, Dr. Marco Morselli, and Matthew Obusan for a productive and fun collaboration that led to a publication in *Cell Reports*. I would also like to thank Dr. Marat Pavlyukov for help with RNA immunoprecipitation and co-immunoprecipitation experiments. I would like to thank the BSCRC HTS facility for their assistance with sequencing the RNA-seq and ChIP-seq libraries.

My research could not have been completed without the assistance and guidance from members of the Johnson Lab. I would like to thank Azad Hossain for his mentoring and words of wisdom throughout my PhD. I would especially like to thank my lab members and good friends Sam Edwards and Denise Ortiz. They made lab fun to come to every day and they are always there when I needed support. We have had many great conversations during “coffee time”, “lunch time”, “snack time”, and “afternoon coffee time”. They are my fitness gurus and are my motivation to go to the gym.

I would also like to thank the members of the Coller Lab, particularly Adriana Corvalan, David Jelinek, and Aaron Ambrus. They have provided me a safe space to hide away from my

research when I needed to. They also motivated me to start running. I would not have run my first marathon without their motivation. I want to express my gratitude to David Jelinek, my “life mentor”. I want to especially thank Adriana for always being there whenever I needed someone to talk to. I have learned so much about tissue culture from her during “TC time”, which I looked forward to everyday.

Lastly, I would like to express my extreme gratitude to my parents Stanley Leung and Chinh Phu and my brother Raymond Leung. My parents have never restricted me in doing anything and have always told me to follow my dreams. They are both immigrants to the United States and have worked hard to allow me to attend college and graduate school. Without their support, I would have not made it into my PhD program. Everything I do is for them and I hope I made them proud.

Reprint of publications

Leung CS, Douglass SM, Morselli M, Obusan MB, Pavlyukov MS, Pellegrini M, and Johnson TL. H3K36 Methylation and the Chromodomain Protein Eaf3 Are Required for Proper Cotranscriptional Spliceosome Assembly. Cell Reports. 2019; 27(13): 3760-3769

As author of an Elsevier journal article, I have permission to include this article in my dissertation (https://www.elsevier.com/about/policies/copyright). This article can be found at https://www.sciencedirect.com/science/article/pii/S2211124719307399?via%3Dihub. I gratefully acknowledge all co-authors for allowing me to include a reprint of this chapter.

VITA

Calvin Leung

Education

BS Biochemistry and Molecular Biology with Highest Honors; GPA: 3.8 2013
University of California, Santa Cruz

Research Experience

Graduate Student Researcher, Tracy L. Johnson Laboratory 2014–Present
UCLA Dept of MCDB

- Used biochemistry, genetic, and high-throughput techniques to investigate interactions between epigenetic marks and the spliceosome
- Identified a novel pathway by which a histone binding protein regulates RNA splicing

Undergraduate Researcher, Harry F. Noller Laboratory 2011–2013
UCSC Dept of MCDB

- Investigated the structure and function of the ribosome and elongation factor G (EF-G)
- Generated and identified lethal mutants of EF-G to better understand the mechanism of translocation during protein synthesis

Awards

- Keystone Symposia Scholarship (Epigenetics and Human Disease) 2019
- UCLA Graduate Division Dissertation Year Fellowship 2018-Present
- RNA Society Meeting Travel Award 2018
- UCLA MBIDP Whitcome Pre-doctoral Fellowship 2017–2018
- UCLA Cellular and Molecular Biology Training Grant 2015–2017
- Certificate of Distinction in Teaching – UCLA Life Sciences Division 2016
- Honorable Mention – NSF Graduate Fellowship Research Program 2015
- UCSC Doug Drexler Chemistry Scholarship 2012

Publications

Leung CS, Douglass SM, Morselli M, Obusan MB, Pavylukov M, Pellegrini M, Johnson TL. (2019) H3K36 methylation and the chromodomain protein Eaf3 are required for proper co-transcriptional spliceosome assembly. *Cell Reports*. (in press).

Douglass SM, **Leung CS**, Johnson TL. (2019) Extensive splicing across the Saccharomyces cerevisiae genome. bioRxiv 515163; doi: https://doi.org/10.1101/515163.

Leung CS, Johnson TL. (2018) The Exon Junction Complex: A Multitasking Guardian of the Transcriptome. *Molecular Cell*. 72(5):799-801.

Sawaya MR, Cascio D, Collazo, M, Bond, C, Cohen, A, DeNicola, A, Eden, K, Jain, K, **Leung, C**, Lubock, N, McCormick, J, Rosinski, J, Spiegelman, L, Athar, Y, Tibrewal, N, Winter, J, Solomon, S.

(2015) Crystal Structure of Proteinase K from Engyodontium album inhibited by METHOXYSUCCINYL-ALA-ALA-PRO-PHE-CHLOROMETHYL KETONE at 1.15 A resolution. RCSB PDB. PDB ID: 4ZAR

Plengpanich W, Young SG, Khovidhunkit W, Bensadoun A, Karnman H, Ploug M, Gardsvoll H, **Leung CS**, Adeyo O, Larsson M, Muanpetch S, Charoen S, Fong LG, Niramitmahapanya S, Beigneux AP. (2014) Multimerization of GPIHBP1 and Familial Chylomicronemia from a Serine-to-Cysteine Substitution in GPIHBP1's Ly6 Domain. *Journal of Biological Chemistry*. 289:19491-19499.

Turlo K, **Leung CS**, Seo JJ, Goulbourne CN, Adeyo O, Gin P, Voss C, Bensadoun A, Fong LG, Young SG,
Beigneux AP. (2014) Equivalent binding of wild-type lipoprotein lipase (LPL) and S447X-LPL to GPIHBP1, the endothelial cell LPL transporter. *Biochimica et Biophysica Acta*. 1841: 963–969.

Bensadoun A, Mottler CD, Pelletier C, Wu D, Seo JJ, **Leung CS**, Adeyo O, Goulbourne CN, Gin P, Fong LG,
Young SG, Beigneux AP. (2014) A new monoclonal antibody, 4-1a, that binds to the amino terminus of human lipoprotein lipase. *Biochimica et Biophysica Acta.* 1841: 970–976.

Schredelseker J, Paz A, López CJ, Altenbach C, **Leung CS**, Drexler MK, Chen JN, Hubbell WL, Abramson J. (2014) High Resolution Structure and Double Electron-Electron Resonance of the Zebrafish Voltage-dependent Anion Channel 2 Reveal an Oligomeric Population. *Journal of Biological Chemistry*. 289: 12566–12577.

Conference Presentations

- Keystone Symposia – Epigenetics and Human Disease 2019 (Poster Presentation) – H3K36 methylation and the chromodomain protein Eaf3 are required for proper co-transcriptional spliceosome assembly.
- RNA Society Meeting 2018 (Poster Presentation) – Dissecting the mechanism of H3K36 methylation in regulating RNA splicing
- ASBMB 2017 (Oral Presentation) – Dissecting the mechanism of H3K36 methylation in regulating pre-mRNA splicing.
- ASBMB 2017 (Poster Presentation) – Dissecting the mechanism of H3K36 methylation in regulating pre-mRNA splicing.

Mentoring

- Kofi Amoah – Bruins-in-Genomics undergraduate student; currently in the UCLA Bioinformatics PhD program
- Anna Marie Rowell – Bruins-in-Genomics undergraduate student; currently in the UW-Madison Cellular & Molecular Pathology PhD program
- Daniel Deny – HHMI EXROP undergraduate student; currently applying for MD/PhD programs

CHAPTER 1:

Background − cotranscriptional pre-mRNA splicing, chromatin, and H3K36 methylation

An introduction to pre-mRNA splicing.

Pre-mRNA splicing is a fundamental process of gene regulation which involves the excision of introns within pre-mRNA and ligation of exons to generate a mature RNA product. This reaction involves two consecutive S_N2-type transesterification reactions and is catalyzed by the spliceosome, a large RNA-protein complex composed of five small nuclear ribonucleoproteins (snRNPs) and many associated protein cofactors (Will and Lührmann, 2011). *In vitro* studies have show that the snRNPs and other splicing factors assemble on the pre-mRNA is an ordered fashion (Bindereif and Green, 1987; Brow, 2002; Pikielny et al., 1986). This assembly is dependent on conserved sequences present within the intron: the 5′ splice site (5′SS), branch site (BS), and 3′ splice site (3′SS) (Frendewey and Keller, 1985; Lamond et al., 1987). The U1 snRNP assembles on the 5′SS and the U2 snRNP subsequently binds to the BS, forming the pre-spliceosome (A complex). The U4/U6.U5 tri-snRNP is then recruited to the A complex to form the pre-catalytic B complex. Following dynamic rearrangements within the B complex, the U1 and U4 snRNPs are destabilized and the activated spliceosome (B^{ACT} complex) is generated. The nineteen complex (NTC) and NTC-associated factors are also recruited with the tri-snRNP and are required for stable association of U5 and U6 with the spliceosome after U1 and U4 disassociation (Chan et al., 2003). The B^{ACT} complex undergoes additional remodeling to generate a catalytically activated spliceosome (B* complex). The B* complex catalyzes the first step of splicing which results in the catalytic step I spliceosome (C complex). The C complex is then remodeled into the catalytic step II spliceosome (C* complex). The C* complex catalyzes the second step and exon ligation occurs, which results in a post-catalytic spliceosome (P complex). The intron lariat spliceosome (ILS complex) is generated following release of the ligated exon from the P complex. The spliceosome is then disassembled and the individual snRNPs and splicing factors are recycled for another round of splicing (Figure 1.1).

Eight highly conserved DExD/H RNA-dependent ATPases are essential to directing the conversion between the various spliceosomal complexes (Cordin and Beggs, 2013). DEAD-box ATPases Sub2 and Prp5 are involved in recognition of the BS during formation of the pre-spliceosome (Libri et al., 2001; Perriman et al., 2003). DEAD-box ATPase Prp28 and DEIH-box ATPase Brr2 facilitate rearrangements during the transitions from the pre-spliceosome to the B^{ACT} complex (Raghunathan and Guthrie, 1998; Staley and Guthrie, 1999). DEAH-box ATPases are important for remodeling the pre-mRNA and spliceosome during the catalytic steps. Prp2 and its co-activator Spp2 are required for spliceosome activation before the first transesterification reaction (Kim and Lin, 1996). Prp16 is required for the second step of splicing (Schwer and Guthrie, 1991). Prp22, the first ATPase involved in spliceosome disassembly, triggers release of spliced mRNA (Company et al., 1991). Prp43 and its co-activators Ntr1 and Ntr2 trigger release of excised intron lariat and disassembly of the ILS complex (Arenas and Abelson, 1997; Tsai et al., 2007).

Aberrant splicing of substrates leads to generation of noncanonical RNA species, which may be detrimental for cellular survival. For example, translation of aberrant RNAs may lead to production of non-functional polypeptides. In addition, RNA mis-splicing has been implicated in human disease (Singh and Cooper, 2012). Therefore, the spliceosome has evolved quality control mechanisms (proofreading) to ensure assembly of complexes on proper substrates and to reject complexes that have assembled on suboptimal substrates. Several studies have linked DExD/H RNA-dependent ATPases in proofreading during pre-mRNA splicing (Cordin and Beggs, 2013; Semlow and Staley, 2012). Prp5 is involved in proofreading the interaction between the U2 snRNP with the BS during pre-spliceosome formation (Liang and Cheng, 2015). Prp28 proofreads the 5′SS:U6 snRNA interaction (Yang et al., 2013). Prp16 rejects substrates prior to 5′SS cleavage when the rate of 5′SS cleavage is slow (Koodathingal et al., 2010). Prp22 enhances fidelity of exon ligation by proofreading the 3′SS and BS (Mayas et al., 2006). Prp43 cooperates with both

Prp16 and Prp22 to discard suboptimal substrates from the spliceosome and disassembles the stalled spliceosome (Semlow and Staley, 2012). Prp43 therefore acts as a general disassembly factor since it is involved in both release of the lariat-intron and discard of suboptimal substrates.

Recently, advances in cryo-EM technology has enabled researchers to elucidate the *Schizosaccharomyces pombe* (*S. pombe*), *S. cerevisiae*, and human structures of the spliceosome at various stages of the splicing cycle at near atomic resolution (Fica and Nagai, 2017; Yan et al., 2019). These cryo-EM snapshots reveal the extensive interplay between the protein components and RNA elements of the spliceosome in its many intermediate stages. The structures not only show the overall architecture of the spliceosome, but also the reveal the organization of the splicing active site, the coordination of the two catalytic metal ions (Hang et al., 2015; Yan et al., 2015), and recognition of intronic and exonic sequences within the pre-mRNA (Fica et al., 2017; Galej et al., 2016; Hang et al., 2015; Wan et al., 2016; Yan et al., 2015; Yan et al., 2016, 2017). The structures also show how the active site of the spliceosome is remodeled following the action of many ATPases involved in the splicing pathway and how Prp8 plays a central role as a structural toggle to promote the catalytic activity of the spliceosome (Fica et al., 2017; Galej et al., 2016; Jia and Sun, 2018). These structures, along with the previous genetic and biochemical work over the past four decades, have enhanced our understanding of the mechanisms of spliceosome assembly and splicing catalysis.

However, a limitation to these structures is that they were imaged as isolated complexes and therefore nuclear interactions between the spliceosome and other nuclear proteins are not shown. This is important because spliceosome assembly and catalysis occur cotranscriptionally, and hence the spliceosome assembles in close proximity to the transcription machinery and the chromatin template. In Chapter 2 we discuss how cotranscriptional association of the splicing factor Prp45 to the splicing machinery is facilitated by the chromodomain protein Eaf3. Prp45 is an intrinsically disordered protein and the recent cryo-EM structures show that Prp45 spans the

entire spliceosome and interacts with several proteins and snRNAs (Wan et al., 2016; Yan et al., 2015; Yan et al., 2016). However, since these structures were elucidated as an isolated complex, Prp45's potential interactions with chromatin and chromatin factors cannot be determined. In addition, given the intrinsically disordered nature of Prp45 (Wan et al., 2016; Yan et al., 2015; Yan et al., 2016), Prp45 may facilitate formation of non-membrane, liquid-phase separated compartments in the nucleus. It is possible that Eaf3 facilitates a high local concentration of Prp45 at sites of transcription such that it is poised to rapidly stabilize the spliceosome during activation. In this model Prp45 and Eaf3 may form phase separated condensates at sites of transcription for spliceosome activation. Because cryo-EM determines structures of isolated biomolecular complexes, potential interactions, such as those in condensates, are not observed.

In the past several years, it has been clear that many splicing factors have additional functions outside of splicing. For example, the human ortholog of Prp45 is SKIP, which has been implicated in both transcription and splicing (Brès et al., 2005; Nagai et al., 2004). Prp19, a core component of the nineteen complex (NTC), has been reported to have roles in splicing, transcription, and other processes in the cell (Chanarat and Sträßer, 2013). While the recent cryo-EM structures have given us insight into the architecture of the spliceosome in great detail, further work needs to be done to characterize interactions between the spliceosome and non-splicing factors and to understand how the multiple functions of particular splicing factors affect their activities in splicing.

Spliceosome assembly and splicing catalysis occurs co-transcriptionally.

In the nucleus, spliceosome assembly and the subsequent catalytic steps of splicing occur co-transcriptionally (Herzel et al., 2017; Merkhofer et al., 2014; Perales and Bentley, 2009; Wallace and Beggs, 2017). ChIP assays have been used to show that U1, U2, and the U4/U6*U5 tri-snRNP and non-snRNP splicing factors are recruited co-transcriptionally to the nascent RNA in a

step-wise manner *in vivo* (Görnemann et al., 2005; Gunderson and Johnson, 2009; Gunderson et al., 2011; Kotovic et al., 2003). In fact, in *S. cerevisiae*, single-molecule sequencing revealed that most intron-containing transcripts are spliced as soon as RNA polymerase II (RNAPII) is 129 nucleotides downstream of the 3′SS (Alpert et al., 2017; Oesterreich et al., 2016). These observations confirm that splicing and transcription rates are closely coordinated.

Models for coupling splicing to transcription.

Here, we discuss two non-mutually exclusive mechanisms to explain coupling of splicing and transcription.

Kinetic model

Because splicing catalysis and transcription are closely coupled, changes in RNAPII elongation may influence nascent RNA processing by affecting splice site identification by the splicing machinery. Insertion of DNA sequences to delay synthesis of a downstream splicing regulatory element in the α-tropomyosin gene results in alternative exon inclusion, suggesting tight temporal coupling between transcription and splicing (Roberts et al., 1998). In a global analysis, inhibition of RNAPII elongation with 5,6-dichloro-1-β-D-ribofuranosyl-benzimidazole (DRB) or camptothecin (CPT) allows more time for the spliceosome to associate with the nascent pre-mRNA and results in increased inclusion of alternative exons, which have weaker strength of splice sites compared to the average strength of splice sites of constitutive exons (Ip et al., 2011). Alternatively, treatment with trichostatin A (TSA) increases chromatin accessibility due to histone hyperacetylation and leads to decreased exon inclusion (Schor et al., 2009). In a more direct approach, use of a slow RNAPII mutant inhibits skipping of a cassette exon in the fibronectin gene (de la Mata et al., 2003). Similarly in yeast, slow RNAPII mutants suppress exon inclusion of the two-intron gene *DYN2* (Howe et al., 2003).

These studies suggest a “window of opportunity” model by which slow RNAPII allows more time for splice site recognition, while fast RNAPII compresses this time. However, this is not always the case. A recent study by the Kaplan group suggested that both slow and fast RNAPII mutants decreased RNAPII occupancy and reduced elongation rate (Malik et al., 2017). RNA-seq analysis of transcripts from both slow and fast RNAPII mutants revealed that there are overlapping effects on inclusion of alternative cassette exons, suggesting that there is an optimal RNAPII elongation rate for pre-mRNA splicing (Fong et al., 2014). The discordance between these studies on the kinetic model of splicing may be because changes in elongation rates may also affect binding of splicing inhibitors and activators, thus affecting exon inclusion or exclusion.

The studies described previously have been examples of experimental manipulations that alter transcription and splicing. In a biological scenario, UV-induced DNA damage reduces RNAPII elongation through CTD hyperphosphorylation and affects cotranscriptional alternative splicing for a subset of genes (Munoz et al., 2009). In another biological scenario, reduction of canonical histones levels leads reduced RNAPII elongation rate, resulting in RNA processing defects (Jimeno-Gonzalez et al., 2015).

Recruitment model via the CTD of RNAPII

In this coupling mechanism, splicing factors physically interact with the transcription machinery to affect co-transcriptional splicing. The C-terminal domain (CTD) is the largest subunit of RNAPII and comprises 26 to 52 tandemly repeated heptapeptides (Phatnani and Greenleaf, 2006). The CTD may also act as a binding scaffold for various nuclear factors and truncation of the CTD leads to defects in transcription, as well as in RNA splicing, 3′ end processing, and transcription termination (McCracken et al., 1997). In mammals, 22 tandem repeats are sufficient for proper transcription, splicing, and 3′ end cleavage of pre-mRNA reporters (Rosonina and Blencowe, 2004). The CTD undergoes extensive posttranslational modification (mainly phosphorylation)

which can affect its many functions (Hsin and Manley, 2012). Generally, the CTD is phosphorylated at the Ser5 (S5P) position at the beginning of genes by kinase Cdk7/Kin28 and is then increasingly phosphorylated at the Ser2 (S2P) position by kinase Cdk9/Bur1 during transcription elongation.

This differential phosphorylation of the CTD also corresponds with association of different mRNA processing factors (Komarnitsky et al., 2000). *In vitro* splicing assays suggest that hyperphosphorylated RNAPII stimulates pre-mRNA splicing by affecting early steps of spliceosome assembly (Hirose et al., 1999). Interestingly, proteomic analysis of purified human RNAPII have revealed that RNAPII associates with serine-arginine (SR) proteins, which are essential splicing factors, and components of the U1 snRNP (Das et al., 2007). A study of the phosphorylated CTD interactome in yeast showed that U1 components physically interact with S5P CTD (Harlen et al., 2016). In a more recent study by the Proudfoot and Carmo-Fonseca groups, it was proposed that S5P CTD (but not S2P) associates with components of active spliceosomes (protein and snRNAs) (Nojima et al., 2018). By performing mass spectrometry immunoprecipitation of RNAPII isoforms following MNase-treatment of chromatin, it was observed the U5 snRNP and most components of the B^{ACT} and C complexes preferentially associate with S5P CTD (Nojima et al., 2018). Together, these studies are consistent with the cotranscriptional formation of splicing intermediates via interaction with the CTD.

Regulation of splicing through chromatin.

Spliceosome assembly and splicing occur co-transcriptionally in the context of a dynamic chromatin environment. The fundamental unit of chromatin is the nucleosome. A nucleosome unit is composed of an octamer of two copies each of core histone proteins: H2A, H2B, H3, and H4 and 147 bp of double-stranded DNA which wraps around the octamer. Nucleosomes not only compact DNA into the nucleus of a eukaryotic cell, but also act as a passive barrier to transcription

factors, RNAPII, and other proteins (Talbert et al., 2019). Nucleosomes must be disassembled or displaced by ATP-dependent remodelers, histone modifications, and histone variants in order for efficient RNAPII elongation (Workman, 2006).

There is a growing body of evidence that has linked chromatin to splicing regulation. The average length of a human internal exon is 145 nt which is close to the amount of DNA that is wrapped around a single nucleosome (Lander et al., 2001). In mammals, nucleosomes are preferentially placed on exons relative to introns (Andersson et al., 2009; Tilgner et al., 2009). Furthermore, nucleosomes occupy constitutively spliced exons more frequently than alternatively spliced exons (Schwartz et al., 2009). Exons flanked with weak splice sites also have more stable nucleosome occupancy compared to exons with strong splice sites (Tilgner et al., 2009). These studies suggest that nucleosomes interfere with RNAPII elongation by acting as “speed bumps” and may be important for exon definition in mammals. The preferential positioning of nucleosomes on exons may direct the splicing machinery to exons and support their splicing by slowing down RNAPII during elongation. Although it has been unclear whether exons are preferentially occupied by nucleosomes in yeast, a recent study from our group shows that the histone variant H2A.Z is positioned near splice sites and the branch site in non-ribosomal ICGs (Neves et al., 2017). A similar pattern of H2A.Z occupancy has been described in fission yeast (Nissen et al., 2017). Loss of H2A.Z leads to defective splicing of suboptimal introns possibly due to altered splicing kinetics; the spliceosome disassembly ATPase Prp43 discards these substrates with stalled spliceosomes (Neves et al., 2017; Nissen et al., 2017).

Regulation of splicing by histone posttranslational modifications and DNA methylation.

There has been an increasing body of evidence implicating histone posttranslational modifications (PTMs) in regulating splicing. N-terminal histone tails that protrude from the nucleosome core can be posttranslationally modified to influence chromatin structure and accessibility. Some PTMs

that have been identified on histones include: acetylation, methylation, phosphorylation, ubiquitylation, sumoylation, and proline isomerization (Kouzarides, 2007). Specific PTMs are enriched in different parts of a gene. For example, H3K4 trimethylation (H3K4me3) is enriched at transcription start sites (TSSs) from yeast to humans and is a predominant feature of active promoters (Karlic et al., 2010; Santos-Rosa et al., 2002). The highly conserved Set1 protein contains a SET histone methyltransferase domain that catalyzes the mono-, di-, and tri-methylation of H3K4 (Shilatifard, 2012). Although H3K4me3 is found predominantly at TSSs, loss of H3K4me3 has little effect on transcription levels (Clouaire et al., 2012). In another study, it was found that H3K4me3 does not influence transcription *in vitro* (Pavri et al., 2006). However, there may be a role for H3K4me3 in regulating pre-mRNA splicing in mammalian cells. H3K4me3 has been proposed to recruit CHD1 to the 5′ end of active genes and depletion of H3K4me3 or CHD1 reduces splicing efficiency due to less stable association of the U2 snRNP with chromatin in human cells (Sims et al., 2007). However, the direct link between CHD1 binding to H3K4me3 and splicing has been unclear in both humans and yeast. Another histone methylation modification that has been implicated in affecting splicing is H3K36 methylation (H3K36me). H3K36 trimethylation (H3K36me3) is globally enriched in exons even after correcting for increased occupancy of nucleosomes in exons (Spies et al., 2009). H3K36me3 is also enriched in the gene body of actively transcribed genes, highlighting its potential role in regulating cotranscriptional splicing (Kolasinska-Zwierz et al., 2009; Weiner et al., 2015). More detail on the role of H3K36me on splicing will be described in subsequent sections.

Other histone modifications besides methylation have also been shown to affect pre-mRNA splicing. In yeast, H2B monoubiquitylation (H2Bub1) is important for efficient recruitment of the U1 and U2 snRNPs onto nascent pre-mRNAs (Hérissant et al., 2014). In human cells, H2Bub1 levels are reduced in exons and correlate with RNAPII pausing at exons, suggesting differential RNAPII kinetics at exons compared to flanking introns (Fuchs et al., 2014). Acetylation

by histone acetyltransferase Gcn5 is also required for proper co-transcriptional recruitment of U2 snRNP in yeast (Gunderson and Johnson, 2009; Gunderson et al., 2011). In mammals, knockdown of Gcn5 leads to changes alternative splicing during ESC reprogramming due Gcn5's role in directly regulating splicing factor gene expression (Hirsch et al., 2015). Histone hyperacetylation by Hu proteins lead to increased RNAPII elongation rate and decreased alternative exon inclusion in the Nf1 gene in neuronal cells (Zhou et al., 2011). Altogether, these studies suggest two non-mutually exclusive models by which histone PTMs can regulate splicing: (1) an adaptor model where PTMs can directly recruit splicing regulators to chromatin and (2) altering RNAPII kinetics.

DNA methylation has also been shown to affect splicing. DNA methylation is an epigenetic mark that is enriched in actively transcribed genes and is critical for regulating gene expression (Zemach et al., 2010). Interestingly, DNA methylation signals are stronger on exons compared to introns and are affected by the GC content of exons and flanking introns (Gelfman et al., 2013). It has also been shown that DNA methylation is enriched at 5′ SSs and depleted at 3′ SSs (Laurent et al., 2010). One potential mechanism by which DNA methylation regulates splicing is by recruiting methyl CpG-binding proteins which then can recruit histone modifying enzymes to affect RNAPII elongation rate. Another non-mutually exclusive model is that DNA methylation directly recruits splicing factors. For example, methyl-CpG-binding protein 2 (MeCP2) directly interacts with the splicing factor Prpf3 and this interaction is important for regulating alternative splicing in mammalian brain (Long et al., 2011).

The role of H3K36 methylation in splicing regulation.

H3K36me is a histone PTM that is conserved from yeast to humans. H3K36me3 is found in the middle to 3′ end of coding genes and its presence is correlated with active transcription (Weiner et al., 2015). In *S. cerevisiae*, the histone methyltransferase Set2 is responsible for the mono-, di-

, and trimethylation of H3K36 (Strahl et al., 2002). In mammals, SETD2 mediates H3K36me3, but not H3K36me1 or H3K36me2 (Edmunds et al., 2008). Unlike in yeast, other histone methyltransferases are present in higher eukaryotes to mediate the mono- and dimethylation of H3K36 (Wagner and Carpenter, 2012). Set2 interacts with RNAPII via its Set2–Rpb1 interacting (SRI) domain, and this interaction is necessary for its cotranscriptional methylation of H3K36 (Kizer et al., 2005). The phosphorylation state of the CTD of RNAPII also plays a role in regulating H3K36me. Partial deletion of the CTD of RNAPII or mutation of Ser2 of the CTD repeats results in reduced Set2 binding to RNAPII and significant reduction of H3K36me (Li et al., 2003).

One of the most well-studied functions for Set2 is to suppress cryptic transcription in yeast. The chromodomain protein Eaf3 in the Rpd3S histone deacetylase complex is recruited to coding regions via interaction with H3K36me (Carrozza et al., 2005; Joshi and Struhl, 2005; Keogh et al., 2005). Recruitment of the Rpd3S complex is necessary for histone deacetylation in transcribed regions following transcription in order to suppress spurious internal transcription from cryptic start sites (Carrozza et al., 2005; Joshi and Struhl, 2005; Keogh et al., 2005; Li et al., 2007). Loss of Set2 also results in genome-wide transcription of antisense RNAs initiated from within coding regions and have been annotated as Set2-repressed antisense transcripts (SRATs) (Venkatesh et al., 2016). Presence of SRATs, however, does not affect abundance of sense transcripts (Venkatesh et al., 2016). In Drosophila, histone replacement revealed that H3K36me does not suppress cryptic transcription, suggesting that H3K36me may not be required for regulating pervasive transcription initiation in metazoans (Meers et al., 2017). Besides its role in preventing cryptic transcription, H3K36me has also been implicated in other functions in the cell including DNA damage response, DNA methylation, mammalian development, and splicing (Dhayalan et al., 2010; Hu et al., 2010; Jha and Strahl, 2014; Luco et al., 2010; Pai et al., 2014).

H3K36me3 was first described to alter alternative splicing of the *FGFR2* gene in fibroblasts via an “adaptor model” through recruitment of the chromodomain-containing protein MRG15 and

polypyrimidine tract-binding protein (PTB) (Luco et al., 2010). Depletion of H3K36me3 by RNAi knockdown of SETD2 resulted in inclusion of PTB-dependent exons in *FGFR2* (Luco et al., 2010). In another study that proposed an adaptor model for H3K36me3, it was suggested that the PWWP domain of Psip1/Ledgf binds to H3K36me3 and recruits splicing factor SRSF1 to regulate alternative splicing (Pradeepa et al., 2012). Genome-wide studies have also identified H3K36me3 to be important for proper splicing (Guo et al., 2014; Simon et al., 2014).

BS69/ZMYND11 was proposed to bind to H3.3K36me3 via its PWWP domain and subsequently recruit U5-snRNP protein EFTUD2 to chromatin to regulate intron retention (IR) in HeLa cells (Guo et al., 2014). Mutation of *SETD2* in human kidney cancer cells led to variation in chromatin accessibility over gene bodies and was associated with widespread RNA processing defects, including aberrant splicing (Simon et al., 2014). Interpretation of the results involving *SETD2* mutation is complicated by the fact that SETD2 also targets the histone variant H3.3 in mammals.

More recently, a study in *S. cerevisiae* proposed that H3K36me is required for proper splicing of a reporter gene and that deletion of *SET2* led to defects in the co-transcriptional recruitment of U2 and U5 snRNP proteins to nascent pre-mRNA (Sorenson et al., 2016). Interestingly, studies by the Bentley and Carmo-Fonseca groups found that inhibition of splicing affects normal distribution of H3K36me3 on coding genes in mammalian cells, suggesting a potential feedback loop between splicing and histone modifications (de Almeida et al., 2011; Kim et al., 2011). However, the potential role of splicing in H3K36me has not been explored.

Although much work has been done correlating H3K36me and changes in splicing, a thorough mechanistic dissection of how this histone modification regulates constitutive splicing (i.e. splicing of most introns in eukaryotes) has been elusive. *SET2* is nonessential in yeast, which makes yeast an attractive model organism for the vigorous study of the effects of H3K36me on

splicing. In Chapter 2, we present a novel mechanism by which H3K36me regulates co-transcriptional splicing in *S. cerevisiae* (Leung et al., 2019). We show that loss of H3K36me leads to widespread accumulation of unspliced pre-mRNA. We suggest an adaptor model where H3K36me recruits the chromodomain protein Eaf3 to intron-containing genes (ICGs). We show that deletion of *EAF3* phenocopies the splicing effects of mutation of H3K36 and that Eaf3 physically interacts with the splicing factor Prp45. We also show that Eaf3 is required for proper co-transcriptional recruitment of Prp45 and the nineteen complex (NTC) to pre-mRNAs. We propose a model by which H3K36me and Eaf3 act between the pre-catalytic B complex and B^{ACT} complex to ensure proper spliceosome assembly and activation (Leung et al., 2019). In Chapter 3, we discuss how splicing may play a role in regulating chromatin state in *S. cerevisiae*. For example. we show that inhibition of splicing using a temperature sensitive Prp45 mutant causes changes in H3K36me3 patterns on an ICG, suggesting a feedback loop between splicing and H3K36me3. Lastly, in Chapter 4, we discuss how H3K36me is involved in recruiting the spliceosome disassembly factor Prp43 to chromatin, further expanding the potential roles H3K36me has on regulating cotranscriptional splicing.

FIGURES

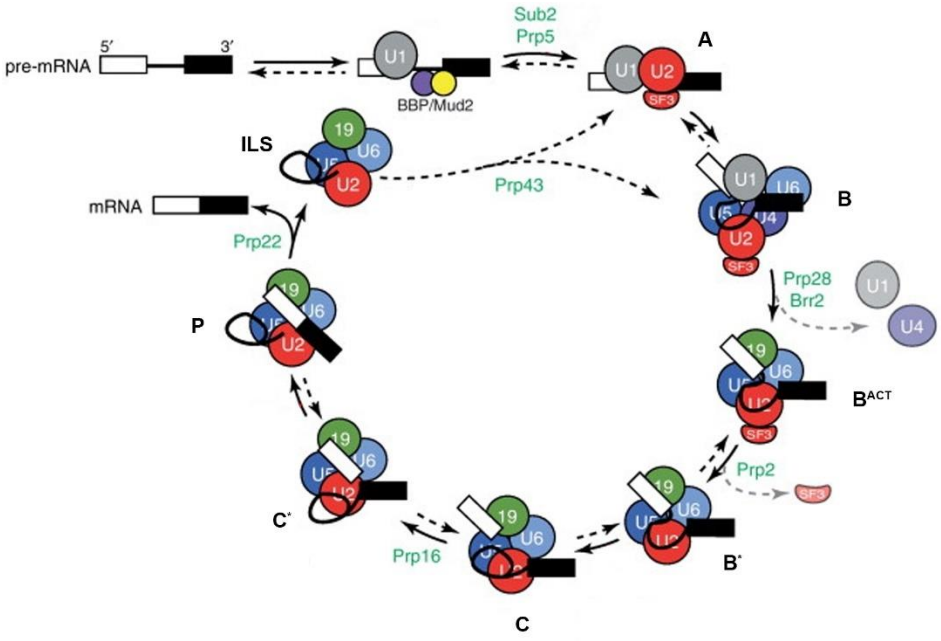

Modified from (Hoskins and Moore, 2012).

Figure 1.1. Assembly and activation of the spliceosome. The A complex (pre-spliceosome) is formed when the U1 snRNP assembles on the 5′SS and the U2 snRNP binds the branch site. The U4/U6.U5 tri-snRNP is then recruited to form the B complex. Following destablization of the U1 and U4 snRNPs by ATPases Prp28 and Brr2, the B^{ACT} complex (activated spliceosome) is generated. The B^{ACT} complex is remodeled by ATPase Prp2, forming the B* complex (catalytically activated spliceosome). Following the first step of splicing, the C complex (catalytic step I spliceosome) is generated. The C complex is further remodeled by the ATPase Prp16 to generate the C* complex (catalytic step II spliceosome). Following exon ligation, the P complex (postcatalytic spliceosome) is generated. The ILS complex (intron lariat spliceosome) is formed following release of the ligated product.

REFERENCES

Alpert, T., Herzel, L., and Neugebauer, K.M. (2017). Perfect timing: splicing and transcription rates in living cells. Wiley Interdiscip Rev RNA *8*.

Andersson, R., Enroth, S., Rada-Iglesias, A., Wadelius, C., and Komorowski, J. (2009). Nucleosomes are well positioned in exons and carry characteristic histone modifications. Genome Res *19*, 1732-1741.

Arenas, J.E., and Abelson, J.N. (1997). Prp43: An RNA helicase-like factor involved in spliceosome disassembly. Proc Natl Acad Sci U S A *94*, 11798-11802.

Bindereif, A., and Green, M.R. (1987). An ordered pathway of snRNP binding during mammalian pre-mRNA splicing complex assembly. EMBO J *6*, 2415-2424.

Brès, V., Gomes, N., Pickle, L., and Jones, K.A. (2005). A human splicing factor, SKIP, associates with P-TEFb and enhances transcription elongation by HIV-1 Tat. Genes Dev *19*, 1211-1226.

Brow, D.A. (2002). Allosteric cascade of spliceosome activation. Annu Rev Genet *36*, 333-360.

Carrozza, M.J., Li, B., Florens, L., Suganuma, T., Swanson, S.K., Lee, K.K., Shia, W.J., Anderson, S., Yates, J., Washburn, M.P.*, et al.* (2005). Histone H3 methylation by Set2 directs deacetylation of coding regions by Rpd3S to suppress spurious intragenic transcription. Cell *123*, 581-592.

Chan, S.P., Kao, D.I., Tsai, W.Y., and Cheng, S.C. (2003). The Prp19p-associated complex in spliceosome activation. Science *302*, 279-282.

Chanarat, S., and Sträßer, K. (2013). Splicing and beyond: the many faces of the Prp19 complex. Biochim Biophys Acta *1833*, 2126-2134.

Clouaire, T., Webb, S., Skene, P., Illingworth, R., Kerr, A., Andrews, R., Lee, J.H., Skalnik, D., and Bird, A. (2012). Cfp1 integrates both CpG content and gene activity for accurate H3K4me3 deposition in embryonic stem cells. Genes Dev *26*, 1714-1728.

Company, M., Arenas, J., and Abelson, J. (1991). Requirement of the RNA helicase-like protein PRP22 for release of messenger RNA from spliceosomes. Nature *349*, 487-493.

Cordin, O., and Beggs, J.D. (2013). RNA helicases in splicing. RNA Biol *10*, 83-95.

Das, R., Yu, J., Zhang, Z., Gygi, M.P., Krainer, A.R., Gygi, S.P., and Reed, R. (2007). SR proteins function in coupling RNAP II transcription to pre-mRNA splicing. Mol Cell *26*, 867-881.

de Almeida, S.F., Grosso, A.R., Koch, F., Fenouil, R., Carvalho, S., Andrade, J., Levezinho, H., Gut, M., Eick, D., Gut, I.*, et al.* (2011). Splicing enhances recruitment of methyltransferase HYPB/Setd2 and methylation of histone H3 Lys36. Nat Struct Mol Biol *18*, 977-983.

de la Mata, M., Alonso, C.R., Kadener, S., Fededa, J.P., Blaustein, M., Pelisch, F., Cramer, P., Bentley, D., and Kornblihtt, A.R. (2003). A slow RNA polymerase II affects alternative splicing in vivo. Mol Cell *12*, 525-532.

Dhayalan, A., Rajavelu, A., Rathert, P., Tamas, R., Jurkowska, R.Z., Ragozin, S., and Jeltsch, A. (2010). The Dnmt3a PWWP domain reads histone 3 lysine 36 trimethylation and guides DNA methylation. J Biol Chem *285*, 26114-26120.

Edmunds, J.W., Mahadevan, L.C., and Clayton, A.L. (2008). Dynamic histone H3 methylation during gene induction: HYPB/Setd2 mediates all H3K36 trimethylation. EMBO J *27*, 406-420.

Fica, S.M., and Nagai, K. (2017). Cryo-electron microscopy snapshots of the spliceosome: structural insights into a dynamic ribonucleoprotein machine. Nat Struct Mol Biol *24*, 791-799.

Fica, S.M., Oubridge, C., Galej, W.P., Wilkinson, M.E., Bai, X.C., Newman, A.J., and Nagai, K. (2017). Structure of a spliceosome remodelled for exon ligation. Nature *542*, 377-380.

Fong, N., Kim, H., Zhou, Y., Ji, X., Qiu, J., Saldi, T., Diener, K., Jones, K., Fu, X.D., and Bentley, D.L. (2014). Pre-mRNA splicing is facilitated by an optimal RNA polymerase II elongation rate. Genes Dev *28*, 2663-2676.

Frendewey, D., and Keller, W. (1985). Stepwise assembly of a pre-mRNA splicing complex requires U-snRNPs and specific intron sequences. Cell *42*, 355-367.

Fuchs, G., Hollander, D., Voichek, Y., Ast, G., and Oren, M. (2014). Cotranscriptional histone H2B monoubiquitylation is tightly coupled with RNA polymerase II elongation rate. Genome Res *24*, 1572-1583.

Galej, W.P., Wilkinson, M.E., Fica, S.M., Oubridge, C., Newman, A.J., and Nagai, K. (2016). Cryo-EM structure of the spliceosome immediately after branching. Nature *537*, 197-201.

Gelfman, S., Cohen, N., Yearim, A., and Ast, G. (2013). DNA-methylation effect on cotranscriptional splicing is dependent on GC architecture of the exon-intron structure. Genome Res *23*, 789-799.

Görnemann, J., Kotovic, K.M., Hujer, K., and Neugebauer, K.M. (2005). Cotranscriptional spliceosome assembly occurs in a stepwise fashion and requires the cap binding complex. Mol Cell *19*, 53-63.

Gunderson, F.Q., and Johnson, T.L. (2009). Acetylation by the transcriptional coactivator Gcn5 plays a novel role in co-transcriptional spliceosome assembly. PLoS Genet *5*, e1000682.

Gunderson, F.Q., Merkhofer, E.C., and Johnson, T.L. (2011). Dynamic histone acetylation is critical for cotranscriptional spliceosome assembly and spliceosomal rearrangements. Proc Natl Acad Sci U S A *108*, 2004-2009.

Guo, R., Zheng, L., Park, J.W., Lv, R., Chen, H., Jiao, F., Xu, W., Mu, S., Wen, H., Qiu, J.*, et al.* (2014). BS69/ZMYND11 reads and connects histone H3.3 lysine 36 trimethylation-decorated chromatin to regulated pre-mRNA processing. Mol Cell *56*, 298-310.

Hang, J., Wan, R., Yan, C., and Shi, Y. (2015). Structural basis of pre-mRNA splicing. Science *349*, 1191-1198.

Harlen, K.M., Trotta, K.L., Smith, E.E., Mosaheb, M.M., Fuchs, S.M., and Churchman, L.S. (2016). Comprehensive RNA Polymerase II Interactomes Reveal Distinct and Varied Roles for Each Phospho-CTD Residue. Cell Rep *15*, 2147-2158.

Hérissant, L., Moehle, E.A., Bertaccini, D., Van Dorsselaer, A., Schaeffer-Reiss, C., Guthrie, C., and Dargemont, C. (2014). H2B ubiquitylation modulates spliceosome assembly and function in budding yeast. Biol Cell *106*, 126-138.

Herzel, L., Ottoz, D.S.M., Alpert, T., and Neugebauer, K.M. (2017). Splicing and transcription touch base: co-transcriptional spliceosome assembly and function. Nat Rev Mol Cell Biol *18*, 637-650.

Hirose, Y., Tacke, R., and Manley, J.L. (1999). Phosphorylated RNA polymerase II stimulates pre-mRNA splicing. Genes Dev *13*, 1234-1239.

Hirsch, C.L., Coban Akdemir, Z., Wang, L., Jayakumaran, G., Trcka, D., Weiss, A., Hernandez, J.J., Pan, Q., Han, H., Xu, X*., et al.* (2015). Myc and SAGA rewire an alternative splicing network during early somatic cell reprogramming. Genes Dev *29*, 803-816.

Hoskins, A.A., and Moore, M.J. (2012). The spliceosome: a flexible, reversible macromolecular machine. Trends Biochem Sci *37*, 179-188.

Howe, K.J., Kane, C.M., and Ares, M., Jr. (2003). Perturbation of transcription elongation influences the fidelity of internal exon inclusion in Saccharomyces cerevisiae. RNA *9*, 993-1006.

Hsin, J.P., and Manley, J.L. (2012). The RNA polymerase II CTD coordinates transcription and RNA processing. Genes Dev *26*, 2119-2137.

Hu, M., Sun, X.J., Zhang, Y.L., Kuang, Y., Hu, C.Q., Wu, W.L., Shen, S.H., Du, T.T., Li, H., He, F*., et al.* (2010). Histone H3 lysine 36 methyltransferase Hypb/Setd2 is required for embryonic vascular remodeling. Proc Natl Acad Sci U S A *107*, 2956-2961.

Ip, J.Y., Schmidt, D., Pan, Q., Ramani, A.K., Fraser, A.G., Odom, D.T., and Blencowe, B.J. (2011). Global impact of RNA polymerase II elongation inhibition on alternative splicing regulation. Genome Res *21*, 390-401.

Jha, D.K., and Strahl, B.D. (2014). An RNA polymerase II-coupled function for histone H3K36 methylation in checkpoint activation and DSB repair. Nat Commun *5*, 3965.

Jia, X., and Sun, C. (2018). Structural dynamics of the N-terminal domain and the Switch loop of Prp8 during spliceosome assembly and activation. Nucleic Acids Res *46*, 3833-3840.

Jimeno-Gonzalez, S., Payan-Bravo, L., Munoz-Cabello, A.M., Guijo, M., Gutierrez, G., Prado, F., and Reyes, J.C. (2015). Defective histone supply causes changes in RNA polymerase II elongation rate and cotranscriptional pre-mRNA splicing. Proc Natl Acad Sci U S A *112*, 14840-14845.

Joshi, A.A., and Struhl, K. (2005). Eaf3 chromodomain interaction with methylated H3-K36 links histone deacetylation to Pol II elongation. Mol Cell *20*, 971-978.

Karlic, R., Chung, H.R., Lasserre, J., Vlahovicek, K., and Vingron, M. (2010). Histone modification levels are predictive for gene expression. Proc Natl Acad Sci U S A *107*, 2926-2931.

Keogh, M.C., Kurdistani, S.K., Morris, S.A., Ahn, S.H., Podolny, V., Collins, S.R., Schuldiner, M., Chin, K., Punna, T., Thompson, N.J*., et al.* (2005). Cotranscriptional set2 methylation of histone H3 lysine 36 recruits a repressive Rpd3 complex. Cell *123*, 593-605.

Kim, S., Kim, H., Fong, N., Erickson, B., and Bentley, D.L. (2011). Pre-mRNA splicing is a determinant of histone H3K36 methylation. Proc Natl Acad Sci U S A *108*, 13564-13569.

Kim, S.H., and Lin, R.J. (1996). Spliceosome activation by PRP2 ATPase prior to the first transesterification reaction of pre-mRNA splicing. Mol Cell Biol *16*, 6810-6819.

Kizer, K.O., Phatnani, H.P., Shibata, Y., Hall, H., Greenleaf, A.L., and Strahl, B.D. (2005). A novel domain in Set2 mediates RNA polymerase II interaction and couples histone H3 K36 methylation with transcript elongation. Mol Cell Biol *25*, 3305-3316.

Kolasinska-Zwierz, P., Down, T., Latorre, I., Liu, T., Liu, X.S., and Ahringer, J. (2009). Differential chromatin marking of introns and expressed exons by H3K36me3. Nat Genet *41*, 376-381.

Komarnitsky, P., Cho, E.J., and Buratowski, S. (2000). Different phosphorylated forms of RNA polymerase II and associated mRNA processing factors during transcription. Genes Dev *14*, 2452-2460.

Koodathingal, P., Novak, T., Piccirilli, J.A., and Staley, J.P. (2010). The DEAH box ATPases Prp16 and Prp43 cooperate to proofread 5' splice site cleavage during pre-mRNA splicing. Mol Cell *39*, 385-395.

Kotovic, K.M., Lockshon, D., Boric, L., and Neugebauer, K.M. (2003). Cotranscriptional recruitment of the U1 snRNP to intron-containing genes in yeast. Mol Cell Biol *23*, 5768-5779.

Kouzarides, T. (2007). Chromatin modifications and their function. Cell *128*, 693-705.

Lamond, A.I., Konarska, M.M., and Sharp, P.A. (1987). A mutational analysis of spliceosome assembly: evidence for splice site collaboration during spliceosome formation. Genes Dev *1*, 532-543.

Lander, E.S., Linton, L.M., Birren, B., Nusbaum, C., Zody, M.C., Baldwin, J., Devon, K., Dewar, K., Doyle, M., FitzHugh, W*., et al.* (2001). Initial sequencing and analysis of the human genome. Nature *409*, 860-921.

Laurent, L., Wong, E., Li, G., Huynh, T., Tsirigos, A., Ong, C.T., Low, H.M., Kin Sung, K.W., Rigoutsos, I., Loring, J*., et al.* (2010). Dynamic changes in the human methylome during differentiation. Genome Res *20*, 320-331.

Leung, C.S., Douglass, S.M., Morselli, M., Obusan, M.B., Pavlyukov, M.S., Pellegrini, M., and Johnson, T.L. (2019). H3K36 Methylation and the Chromodomain Protein Eaf3 Are Required for Proper Cotranscriptional Spliceosome Assembly. Cell Rep *27*, 3760-3769 e3764.

Li, B., Gogol, M., Carey, M., Pattenden, S.G., Seidel, C., and Workman, J.L. (2007). Infrequently transcribed long genes depend on the Set2/Rpd3S pathway for accurate transcription. Genes Dev *21*, 1422-1430.

Li, B., Howe, L., Anderson, S., Yates, J.R., 3rd, and Workman, J.L. (2003). The Set2 histone methyltransferase functions through the phosphorylated carboxyl-terminal domain of RNA polymerase II. J Biol Chem *278*, 8897-8903.

Liang, W.W., and Cheng, S.C. (2015). A novel mechanism for Prp5 function in prespliceosome formation and proofreading the branch site sequence. Genes Dev *29*, 81-93.

Libri, D., Graziani, N., Saguez, C., and Boulay, J. (2001). Multiple roles for the yeast SUB2/yUAP56 gene in splicing. Genes Dev *15*, 36-41.

Long, S.W., Ooi, J.Y., Yau, P.M., and Jones, P.L. (2011). A brain-derived MeCP2 complex supports a role for MeCP2 in RNA processing. Biosci Rep *31*, 333-343.

Luco, R.F., Pan, Q., Tominaga, K., Blencowe, B.J., Pereira-Smith, O.M., and Misteli, T. (2010). Regulation of alternative splicing by histone modifications. Science *327*, 996-1000.

Malik, I., Qiu, C., Snavely, T., and Kaplan, C.D. (2017). Wide-ranging and unexpected consequences of altered Pol II catalytic activity in vivo. Nucleic Acids Res *45*, 4431-4451.

Mayas, R.M., Maita, H., and Staley, J.P. (2006). Exon ligation is proofread by the DExD/H-box ATPase Prp22p. Nat Struct Mol Biol *13*, 482-490.

McCracken, S., Fong, N., Yankulov, K., Ballantyne, S., Pan, G., Greenblatt, J., Patterson, S.D., Wickens, M., and Bentley, D.L. (1997). The C-terminal domain of RNA polymerase II couples mRNA processing to transcription. Nature *385*, 357-361.

Meers, M.P., Henriques, T., Lavender, C.A., McKay, D.J., Strahl, B.D., Duronio, R.J., Adelman, K., and Matera, A.G. (2017). Histone gene replacement reveals a post-transcriptional role for H3K36 in maintaining metazoan transcriptome fidelity. Elife *6*.

Merkhofer, E.C., Hu, P., and Johnson, T.L. (2014). Introduction to cotranscriptional RNA splicing. Methods Mol Biol *1126*, 83-96.

Munoz, M.J., Perez Santangelo, M.S., Paronetto, M.P., de la Mata, M., Pelisch, F., Boireau, S., Glover-Cutter, K., Ben-Dov, C., Blaustein, M., Lozano, J.J.*, et al.* (2009). DNA damage regulates alternative splicing through inhibition of RNA polymerase II elongation. Cell *137*, 708-720.

Nagai, K., Yamaguchi, T., Takami, T., Kawasumi, A., Aizawa, M., Masuda, N., Shimizu, M., Tominaga, S., Ito, T., Tsukamoto, T.*, et al.* (2004). SKIP modifies gene expression by affecting both transcription and splicing. Biochem Biophys Res Commun *316*, 512-517.

Neves, L.T., Douglass, S., Spreafico, R., Venkataramanan, S., Kress, T.L., and Johnson, T.L. (2017). The histone variant H2A.Z promotes efficient cotranscriptional splicing in S. cerevisiae. Genes Dev *31*, 702-717.

Nissen, K.E., Homer, C.M., Ryan, C.J., Shales, M., Krogan, N.J., Patrick, K.L., and Guthrie, C. (2017). The histone variant H2A.Z promotes splicing of weak introns. Genes Dev *31*, 688-701.

Nojima, T., Rebelo, K., Gomes, T., Grosso, A.R., Proudfoot, N.J., and Carmo-Fonseca, M. (2018). RNA Polymerase II Phosphorylated on CTD Serine 5 Interacts with the Spliceosome during Co-transcriptional Splicing. Mol Cell *72*, 369-379 e364.

Oesterreich, F.C., Herzel, L., Straube, K., Hujer, K., Howard, J., and Neugebauer, K.M. (2016). Splicing of Nascent RNA Coincides with Intron Exit from RNA Polymerase II. Cell *165*, 372-381.

Pai, C.C., Deegan, R.S., Subramanian, L., Gal, C., Sarkar, S., Blaikley, E.J., Walker, C., Hulme, L., Bernhard, E., Codlin, S.*, et al.* (2014). A histone H3K36 chromatin switch coordinates DNA double-strand break repair pathway choice. Nat Commun *5*, 4091.

Pavri, R., Zhu, B., Li, G., Trojer, P., Mandal, S., Shilatifard, A., and Reinberg, D. (2006). Histone H2B monoubiquitination functions cooperatively with FACT to regulate elongation by RNA polymerase II. Cell *125*, 703-717.

Perales, R., and Bentley, D. (2009). "Cotranscriptionality": the transcription elongation complex as a nexus for nuclear transactions. Mol Cell *36*, 178-191.

Perriman, R., Barta, I., Voeltz, G.K., Abelson, J., and Ares, M., Jr. (2003). ATP requirement for Prp5p function is determined by Cus2p and the structure of U2 small nuclear RNA. Proc Natl Acad Sci U S A *100*, 13857-13862.

Phatnani, H.P., and Greenleaf, A.L. (2006). Phosphorylation and functions of the RNA polymerase II CTD. Genes Dev *20*, 2922-2936.

Pikielny, C.W., Rymond, B.C., and Rosbash, M. (1986). Electrophoresis of ribonucleoproteins reveals an ordered assembly pathway of yeast splicing complexes. Nature *324*, 341-345.

Pradeepa, M.M., Sutherland, H.G., Ule, J., Grimes, G.R., and Bickmore, W.A. (2012). Psip1/Ledgf p52 binds methylated histone H3K36 and splicing factors and contributes to the regulation of alternative splicing. PLoS Genet *8*, e1002717.

Raghunathan, P.L., and Guthrie, C. (1998). RNA unwinding in U4/U6 snRNPs requires ATP hydrolysis and the DEIH-box splicing factor Brr2. Curr Biol *8*, 847-855.

Roberts, G.C., Gooding, C., Mak, H.Y., Proudfoot, N.J., and Smith, C.W. (1998). Co-transcriptional commitment to alternative splice site selection. Nucleic Acids Res *26*, 5568-5572.

Rosonina, E., and Blencowe, B.J. (2004). Analysis of the requirement for RNA polymerase II CTD heptapeptide repeats in pre-mRNA splicing and 3'-end cleavage. RNA *10*, 581-589.

Santos-Rosa, H., Schneider, R., Bannister, A.J., Sherriff, J., Bernstein, B.E., Emre, N.C., Schreiber, S.L., Mellor, J., and Kouzarides, T. (2002). Active genes are tri-methylated at K4 of histone H3. Nature *419*, 407-411.

Schor, I.E., Rascovan, N., Pelisch, F., Allo, M., and Kornblihtt, A.R. (2009). Neuronal cell depolarization induces intragenic chromatin modifications affecting NCAM alternative splicing. Proc Natl Acad Sci U S A *106*, 4325-4330.

Schwartz, S., Meshorer, E., and Ast, G. (2009). Chromatin organization marks exon-intron structure. Nat Struct Mol Biol *16*, 990-995.

Schwer, B., and Guthrie, C. (1991). PRP16 is an RNA-dependent ATPase that interacts transiently with the spliceosome. Nature *349*, 494-499.

Semlow, D.R., and Staley, J.P. (2012). Staying on message: ensuring fidelity in pre-mRNA splicing. Trends Biochem Sci *37*, 263-273.

Shilatifard, A. (2012). The COMPASS family of histone H3K4 methylases: mechanisms of regulation in development and disease pathogenesis. Annu Rev Biochem *81*, 65-95.

Simon, J.M., Hacker, K.E., Singh, D., Brannon, A.R., Parker, J.S., Weiser, M., Ho, T.H., Kuan, P.F., Jonasch, E., Furey, T.S.*, et al.* (2014). Variation in chromatin accessibility in human kidney cancer links H3K36 methyltransferase loss with widespread RNA processing defects. Genome Res *24*, 241-250.

Sims, R.J., 3rd, Millhouse, S., Chen, C.F., Lewis, B.A., Erdjument-Bromage, H., Tempst, P., Manley, J.L., and Reinberg, D. (2007). Recognition of trimethylated histone H3 lysine 4 facilitates the recruitment of transcription postinitiation factors and pre-mRNA splicing. Mol Cell *28*, 665-676.

Singh, R.K., and Cooper, T.A. (2012). Pre-mRNA splicing in disease and therapeutics. Trends Mol Med *18*, 472-482.

Sorenson, M.R., Jha, D.K., Ucles, S.A., Flood, D.M., Strahl, B.D., Stevens, S.W., and Kress, T.L. (2016). Histone H3K36 methylation regulates pre-mRNA splicing in Saccharomyces cerevisiae. RNA Biol *13*, 412-426.

Spies, N., Nielsen, C.B., Padgett, R.A., and Burge, C.B. (2009). Biased chromatin signatures around polyadenylation sites and exons. Mol Cell *36*, 245-254.

Staley, J.P., and Guthrie, C. (1999). An RNA switch at the 5' splice site requires ATP and the DEAD box protein Prp28p. Mol Cell *3*, 55-64.

Strahl, B.D., Grant, P.A., Briggs, S.D., Sun, Z.W., Bone, J.R., Caldwell, J.A., Mollah, S., Cook, R.G., Shabanowitz, J., Hunt, D.F.*, et al.* (2002). Set2 is a nucleosomal histone H3-selective methyltransferase that mediates transcriptional repression. Mol Cell Biol *22*, 1298-1306.

Talbert, P.B., Meers, M.P., and Henikoff, S. (2019). Old cogs, new tricks: the evolution of gene expression in a chromatin context. Nat Rev Genet *20*, 283-297.

Tilgner, H., Nikolaou, C., Althammer, S., Sammeth, M., Beato, M., Valcárcel, J., and Guigó, R. (2009). Nucleosome positioning as a determinant of exon recognition. Nat Struct Mol Biol *16*, 996-1001.

Tsai, R.T., Tseng, C.K., Lee, P.J., Chen, H.C., Fu, R.H., Chang, K.J., Yeh, F.L., and Cheng, S.C. (2007). Dynamic interactions of Ntr1-Ntr2 with Prp43 and with U5 govern the recruitment of Prp43 to mediate spliceosome disassembly. Mol Cell Biol *27*, 8027-8037.

Venkatesh, S., Li, H., Gogol, M.M., and Workman, J.L. (2016). Selective suppression of antisense transcription by Set2-mediated H3K36 methylation. Nat Commun *7*, 13610.

Wagner, E.J., and Carpenter, P.B. (2012). Understanding the language of Lys36 methylation at histone H3. Nat Rev Mol Cell Biol *13*, 115-126.

Wallace, E.W.J., and Beggs, J.D. (2017). Extremely fast and incredibly close: cotranscriptional splicing in budding yeast. RNA *23*, 601-610.

Wan, R., Yan, C., Bai, R., Huang, G., and Shi, Y. (2016). Structure of a yeast catalytic step I spliceosome at 3.4 A resolution. Science *353*, 895-904.

Weiner, A., Hsieh, T.H., Appleboim, A., Chen, H.V., Rahat, A., Amit, I., Rando, O.J., and Friedman, N. (2015). High-resolution chromatin dynamics during a yeast stress response. Mol Cell *58*, 371-386.

Will, C.L., and Lührmann, R. (2011). Spliceosome structure and function. Cold Spring Harb Perspect Biol *3*.

Workman, J.L. (2006). Nucleosome displacement in transcription. Genes Dev *20*, 2009-2017.

Yan, C., Hang, J., Wan, R., Huang, M., Wong, C.C., and Shi, Y. (2015). Structure of a yeast spliceosome at 3.6-angstrom resolution. Science *349*, 1182-1191.

Yan, C., Wan, R., Bai, R., Huang, G., and Shi, Y. (2016). Structure of a yeast activated spliceosome at 3.5 A resolution. Science *353*, 904-911.

Yan, C., Wan, R., Bai, R., Huang, G., and Shi, Y. (2017). Structure of a yeast step II catalytically activated spliceosome. Science *355*, 149-155.

Yan, C., Wan, R., and Shi, Y. (2019). Molecular Mechanisms of pre-mRNA Splicing through Structural Biology of the Spliceosome. Cold Spring Harb Perspect Biol *11*.

Yang, F., Wang, X.Y., Zhang, Z.M., Pu, J., Fan, Y.J., Zhou, J., Query, C.C., and Xu, Y.Z. (2013). Splicing proofreading at 5' splice sites by ATPase Prp28p. Nucleic Acids Res *41*, 4660-4670.

Zemach, A., McDaniel, I.E., Silva, P., and Zilberman, D. (2010). Genome-wide evolutionary analysis of eukaryotic DNA methylation. Science *328*, 916-919.

Zhou, H.L., Hinman, M.N., Barron, V.A., Geng, C., Zhou, G., Luo, G., Siegel, R.E., and Lou, H. (2011). Hu proteins regulate alternative splicing by inducing localized histone hyperacetylation in an RNA-dependent manner. Proc Natl Acad Sci U S A *108*, E627-635.

CHAPTER 2:

H3K36 methylation and the chromodomain protein Eaf3 are required for proper cotranscriptional spliceosome assembly.

H3K36 Methylation and the Chromodomain Protein Eaf3 Are Required for Proper Cotranscriptional Spliceosome Assembly

Calvin S. Leung,[1] Stephen M. Douglass,[2] Marco Morselli,[2,3,4] Matthew B. Obusan,[2] Marat S. Pavlyukov,[5] Matteo Pellegrini,[1,2,3,4] and Tracy L. Johnson[1,2,6,*]

[1]Molecular Biology Institute, University of California, Los Angeles, Los Angeles, CA 90095, USA
[2]Department of Molecular, Cell, and Developmental Biology, University of California, Los Angeles, Los Angeles, CA 90095, USA
[3]Institute for Genomics and Proteomics, University of California, Los Angeles, Los Angeles, CA 90095, USA
[4]Institute for Quantitative and Computational Biosciences, University of California, Los Angeles, Los Angeles, CA 90095, USA
[5]Shemyakin-Ovchinnikov Institute of Bioorganic Chemistry, Moscow 117997, Russian Federation
[6]Lead Contact
*Correspondence: tljohnson@ucla.edu
https://doi.org/10.1016/j.celrep.2019.05.100

SUMMARY

In the eukaryotic cell, spliceosomes assemble onto pre-mRNA cotranscriptionally. Spliceosome assembly takes place in the context of the chromatin environment, suggesting that the state of the chromatin may affect splicing. The molecular details and mechanisms through which chromatin affects splicing, however, are still unclear. Here, we show a role for the histone methyltransferase Set2 and its histone modification, H3K36 methylation, in pre-mRNA splicing through high-throughput sequencing. Moreover, the effect of H3K36 methylation on pre-mRNA splicing is mediated through the chromodomain protein Eaf3. We find that Eaf3 is recruited to intron-containing genes and that Eaf3 interacts with the splicing factor Prp45. Eaf3 acts with Prp45 and Prp19 after formation of the precatalytic B complex around the time of splicing activation, thus revealing the step in splicing that is regulated by H3K36 methylation. These studies support a model whereby H3K36 facilitates recruitment of an "adapter protein" to support efficient, constitutive splicing.

INTRODUCTION

RNA splicing is a critical and highly regulated process in eukaryotic gene expression. RNA polymerase II (Pol II) catalyzes the synthesis of protein-coding genes to produce unspliced precursor mRNA (pre-mRNA). These genes contain intervening sequences that are removed during pre-mRNA splicing by the spliceosome, a dynamic macromolecular machine composed of five ribonucleoprotein subunits (U1, U2, U4, U5, and U6 small nuclear ribonucleoproteins [snRNPs]) and many associated protein cofactors (Will and Lührmann, 2011). Components of the spliceosome assemble around the splice site consensus sequences located at both ends of the intron. Accurate pre-mRNA splicing by the spliceosome is crucial, and many human diseases are associated with splicing defects or misregulation (Singh and Cooper, 2012).

Alternative splicing allows a single gene to have two or more mature mRNA variants, thus expanding protein diversity in eukaryotes. Alternative splicing occurs in ~95% of human genes, while splicing occurs less frequently in the budding yeast *Saccharomyces cerevisiae*, whose genome has few annotated introns (Ares et al., 1999; Pan et al., 2008). Nonetheless, the spliceosome is highly conserved; over 30% of the messages in yeast are derived from intron-containing genes (ICGs) (Ares et al., 1999), and splicing is regulated in response to changes in environmental conditions (Johnson and Vilardell, 2012), making this biochemically and genetically tractable organism a good model system for studying the basic mechanisms of splicing.

Recent studies have shown that pre-mRNA splicing and transcription are closely linked. Components of the spliceosome have been shown to associate with pre-mRNA as it is being actively transcribed by Pol II, and splicing of many introns is completed before transcription termination (Lacadie et al., 2006; Oesterreich et al., 2016; Pandya-Jones and Black, 2009). A variety of molecular approaches have been used to show that U1, U2, and the U4/U6*U5 tri-snRNP are recruited to the nascent RNA in a stepwise manner (Görnemann et al., 2005; Gunderson and Johnson, 2009; Kotovic et al., 2003). Pol II elongation rates can also affect splicing. Pausing of Pol II at the terminal exon usually promotes splicing, and slowing of the polymerase can allow inclusion of exons that contain weak splice sites by decreasing the synthesis of competing, downstream splice sites (de la Mata et al., 2003; Howe et al., 2003). In some cases, slow elongation rates can also allow for the recruitment of splicing repressors, which leads to exon skipping (Jonkers and Lis, 2015). There is also evidence in yeast and mammals that there may be an optimal elongation rate for splicing of individual introns (Fong et al., 2014; Neves et al., 2017).

Recently, a new layer of complexity has been added to our understanding of cotranscriptional splicing. Specifically, changes in chromatin affect splicing (Hnilicová and Staněk, 2011; Luco and Misteli, 2011). The N-terminal "tails" of histones extend

out from the face of the nucleosome and undergo posttranslational modification. It has been well established that, in mammals, histone modification and positioning of nucleosomes play significant roles in regulating gene activity (Kouzarides, 2007). Nucleosomes are preferentially found on exons, and different sets of histone modifications have been identified at exons and at introns (Andersson et al., 2009; Tilgner et al., 2009). In yeast, deletion of the histone acetyltransferase Gcn5 affects cotranscriptional recruitment of U2 snRNP components (Gunderson and Johnson, 2009; Gunderson et al., 2011); H2B ubiquitylation stimulates recruitment of the early splicing factors (Hérissant et al., 2014); and histone variant H2A.Z is required for efficient splicing (Neves et al., 2017; Nissen et al., 2017).

Studies have previously implicated H3K36 methylation (H3K36me) in regulating alternative pre-mRNA splicing in human cells (Luco et al., 2010; Simon et al., 2014). In yeast and metazoans, H3K36me3 occupies the gene body of actively transcribed genes (Bannister et al., 2005; Krogan et al., 2003). In mammals, worms, and flies, H3K36me3 has been shown to be enriched on exons relative to introns, suggesting a link between this histone modification and alternative splicing (Andersson et al., 2009; Huff et al., 2010; Kolasinska-Zwierz et al., 2009; Schwartz et al., 2009; Spies et al., 2009). It has also been reported that H3K36me is important for proper splicing of a reporter construct in budding yeast (Sorenson et al., 2016). Nonetheless, despite its conservation and likely conserved role in pre-mRNA splicing, the mechanism by which this histone mark regulates pre-mRNA splicing has remained elusive.

Here, we investigate the role of the histone methyltransferase Set2 and its associated chromatin mark, H3K36me, in determining splicing outcomes. Through high-throughput RNA sequencing (RNA-seq), we identify transcripts whose efficient splicing is dependent on the presence of H3K36 methylation. To understand the mechanism by which H3K36me affects splicing, we have analyzed molecular events downstream of H3K36me and have identified the chromodomain-containing protein Eaf3 as a mediator of the interaction between the splicing machinery and H3K36 methylation. Loss of Eaf3 leads to defective splicing of the same genes whose splicing is sensitive to the presence of H3K36me. Moreover, Eaf3 physically interacts with the splicing factor Prp45, the yeast ortholog of human SKIP. Deletion of *EAF3* leads to inefficient recruitment of Prp45 to ICGs, suggesting that Eaf3 is important for cotranscriptional spliceosome assembly. These studies provide a mechanistic basis for a highly conserved histone modification in RNA splicing.

RESULTS

Defective Splicing Is Observed in *set2*Δ and *H3K36A* Mutants

To determine how H3K36me regulates pre-mRNA splicing, we assayed yeast cells in which *SET2*, the gene that encodes the histone methyltransferase for H3K36, is deleted. We also use the histone point mutant strain, *H3K36A*, to verify that the splicing changes we observe are due to loss of histone methylation as opposed to a non-histone target. Western blot analysis confirmed complete loss of H3K36me3 in the *set2*Δ and *H3K36A* mutants (Figure 1A). To observe genome-wide changes in splicing upon loss of H3K36me, total RNA was isolated from wild-type, *set2*Δ, and *H3K36A* cells, and stranded RNA-seq was performed.

We observe a decrease in the splicing efficiency (SE) of a group of ICGs in both the *set2*Δ and *H3K36A* mutants ($p < 0.0001$) compared with wild-type cells (Figure 1B) suggesting that loss of H3K36me leads to decreased SE. Intron accumulation was verified by RT-PCR analysis; representative genes are shown (Figure 1C). To rule out the possibility that the SE changes are due to changes in splicing of *MUD1*, a gene that encodes a splicing factor and shows intron accumulation, protein levels of endogenously HA-tagged Mud1 were examined. Mud1 levels are similar in *set2*Δ compared with wild-type cells (Figure S1A). Furthermore, SEs of all other splicing factor ICGs do not change in either the *set2*Δ or *H3K36A* mutants compared with wild-type cells in our RNA-seq data. RT-PCR analysis of splicing factor encoding ICGs show neither expression nor splicing changes in the *H3K36A* mutant; a representative example is shown in Figure S1B. Because of strict filtering, we knew it was possible that lowly expressed genes that might still display a change in splicing were filtered out. Therefore, we relaxed the read count requirement, and upon reanalysis of the RNA-seq data, we observed a larger set of ICGs that displayed splicing defects in both *set2*Δ and *H3K36A*; a representative RT-PCR analysis is shown (Figure S1C). There is significant overlap of the ICGs that show a decrease in SE in *set2*Δ and *H3K36A* compared with wild-type cells ($p < 0.0001$), indicating that the splicing defects observed are due to loss of H3K36me and not loss of the Set2 protein itself (Figure 1D).

Set2 associates with the phosphorylated carboxyl-terminal domain (CTD) of Pol II via its SRI domain and methylates histones cotranscriptionally (Li et al., 2002; Xiao et al., 2003). To determine whether loss of Set2 binding to the CTD affects splicing, we generated a *set2 SRI*Δ mutant. We confirmed loss of H3K36me3 in the *set2 SRI*Δ mutant (Figure 1E). RT-PCR of the genes *RAD14* and *HPC2* revealed splicing defects similar to those observed in the *set2*Δ mutant (Figure 1F). This further suggests that the splicing defects we observed are not due to non-histone targets of Set2 and that cotranscriptional methylation of H3K36 is important for splicing. It has been previously reported that deletion of the SRI domain of Set2 selectively abolishes H3K36me3 but not H3K36me1 or H3K36me2 (Jha and Strahl, 2014). Therefore, it is likely that the splicing defects we observed in our *set2*Δ and *H3K36A* mutants are due to loss of H3K36me3.

We also analyzed two other H3K36 point mutants, *H3K36R* and *H3K36Q*, and both confer splicing defects consistent with that of *H3K36A* (Figure S1D), further indicating that this residue is important for proper splicing. Moreover, since *H3K36Q* mimics constitutive acetylation, these data suggest that the lack of methylation underlies the splicing defect.

H3K36 Methylation Effects on Splicing Are Unlikely to Be Due to Transcription Defects

Because spliceosome assembly and subsequent splicing catalysis are cotranscriptional, the elongation properties of Pol II can affect splicing (Alexander et al., 2010; de la Mata et al., 2003; Fong et al., 2014). To address whether the observed splicing changes in *set2*Δ and *H3K36A* cells are due to changes in

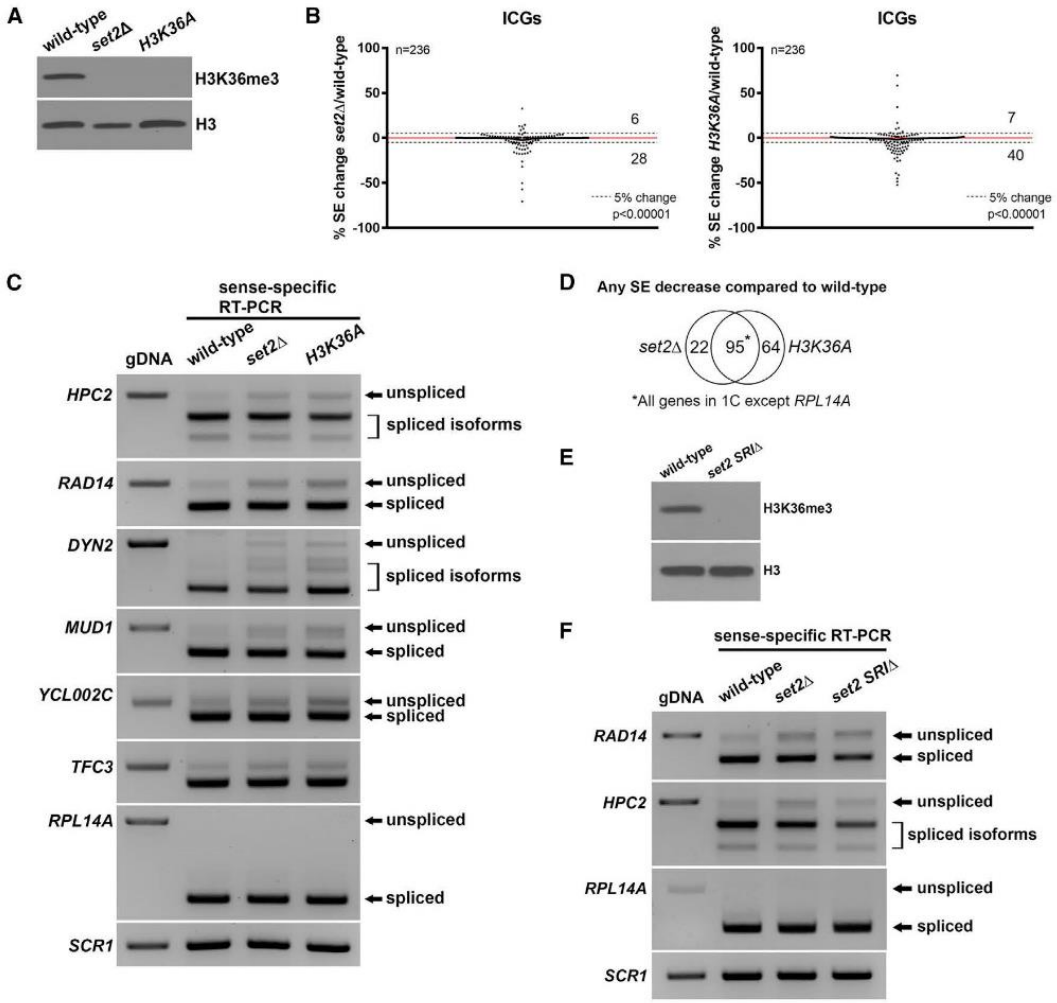

Figure 1. H3K36 Methylation Is Required for Efficient Pre-mRNA Splicing

(A) H3K36me3 is absent in the *set2Δ* and *H3K36A* mutants. Whole cell extracts from wild-type, *set2Δ*, and *H3K36A* cells were subjected to western blotting.

(B) Changes in splicing efficiencies (SEs) of ICGs upon loss of H3K36me represented in a scatterplot. Dashed lines represent a 5% change in SE in the mutant compared to wild-type. Overall splicing decreases in both *set2Δ* and *H3K36A* compared with wild-type (chi-square test, p value indicated). Numbers indicate number of ICGs above and below the dashed lines.

(C) RT-PCR validation of splicing changes observed in RNA-seq analysis. ICGs shown display a $\geq$ 5% decrease in SE in both *set2Δ* and *H3K36A* compared with wild-type. *RPL14A* is a gene that does not show a change in SE. Products were analyzed on a 1.8% agarose gel.

(D) Venn diagram displaying significant overlap of ICGs that display any SE decrease in *set2Δ* and *H3K36A* compared with wild-type cells ($p < 0.0001$, chi-square test).

(E) H3K36me3 is absent in a *set2 SRIΔ* mutant. Whole cell extracts from wild-type and *set2 SRIΔ* were subjected to western blotting.

(F) RT-PCR analysis of splicing changes in *set2 SRIΔ* cells. Products were analyzed on a 1.8% agarose gel. gDNA, genomic DNA. *SCR1* is a loading control.

transcription, we calculated the reads per kilobase of transcript per million mapped reads (RPKM) of all sense transcripts from the stranded RNA-seq data. The RNA abundance of all genes, including splicing factor genes and snRNAs, is strongly correlated between the *set2Δ* and *H3K36A* mutants and wild-type (r_s = 0.9556 and r_s = 0.9051, respectively) (Figure S2A). Expression of ICGs is also strongly correlated between the mutants and wild-type (Figure S2B). In addition, RNA abundance of all genes in *set2Δ* and *H3K36A* cells are also very strongly correlated (r_s = 0.9744), suggesting that the expression profiles of the two mutants are nearly identical (Figure S2C). Recent studies indicate that changes in expression of the highly expressed ribosomal protein intron-containing genes (RP ICGs) leads to changes in splicing because of competition between pre-mRNAs for the spliceosome in yeast (Munding et al., 2013; Awad et al., 2017; Venkataramanan et al., 2017). However, expression of RP ICGs is not significantly altered in the mutants (Figure S2B). When we compare the SE change of ICGs that

show a greater than two-fold decrease in expression to those that show a less than two-fold decrease in expression in the *H3K36A* mutant compared with wild-type, we do not observe a significant difference in SE between the two groups (Figure S2D). Finally, we performed chromatin immunoprecipitation sequencing (ChIP-seq) on the elongating form of Pol II (phospho-S2), in wild-type and *H3K36A* cells. We observed a weak correlation ($r_s = -0.2371$) between SE change and Pol II occupancy change on all ICGs in *H3K36A* compared with wild-type cells, suggesting that the splicing defects observed cannot be easily explained by transcription defects (Figure S2E).

Loss of Chromodomain Protein Eaf3 Leads to Defective Pre-mRNA Splicing

We performed ChIP-seq on H3K36me3 in wild-type cells and observed that H3K36me3 is enriched on ICGs compared with intronless genes (Figure 2A). For example, when we compared the H3K36me3 profile of intron-containing *HPC2* to that of an intronless gene with similar expression and gene length (*PUT4*), we observed more H3K36me3 throughout the *HPC2* gene (Figure 2B). We considered the possibility that a protein binds methyl marks on histones to facilitate recruitment of the splicing machinery. In mammals, MRG15, the yeast homolog of Eaf3, has been suggested to regulate alternative splicing via binding to H3K36me3 (Iwamori et al., 2016; Luco et al., 2010). Eaf3 contains a chromodomain that allows it to bind to methylated H3K36 and is a subunit of the Rpd3S histone deacetylase complex and the NuA4 histone acetyltransferase complex in yeast (Reid et al., 2004). We hypothesized that Eaf3 may recruit the splicing machinery to the chromatin and that the splicing changes in the *set2*Δ and *H3K36A* cells are due to loss of binding of Eaf3 to H3K36. To test this hypothesis, *EAF3* was deleted and stranded RNA-seq was performed to assess splicing. We observe a widespread decrease in SE ($p = 0.0077$) (Figure 2C). RT-PCR confirmed the splicing changes observed from the RNA-seq analysis for the same subset of genes (Figure 2D). There is a significant ($p < 0.0001$) overlap between ICGs that show any decrease in SE in *eaf3*Δ and *H3K36A* compared with wild-type (Figure 2E). ChIP analysis of endogenously HA-tagged Eaf3 (Eaf3-HA) reveals significant decrease in Eaf3 occupancy on ICGs in the *set2*Δ mutant; *HPC2* and *RAD14* are shown here (Figure 2F). Levels of Eaf3-HA protein are identical between wild-type and *set2*Δ cells (Figure 2G). When we performed ChIP of Eaf3-HA on *ECM33*, a gene that does not show a splicing defect in the absence of H3K36me, we did not observe a significant decrease in Eaf3-HA occupancy, suggesting that loss of Eaf3 on an ICG may be correlated with a decrease in splicing of that ICG (Figure 2H, left). We also analyzed Eaf3-HA occupancy ± *SET2* on an intronless gene, *ADH1*, and observe only a modest and not significant decrease of Eaf3 on the gene (Figure 2H, right). These results suggest that Eaf3 requires other proteins in addition to H3K36me to stabilize its interaction with chromatin, but that its loss, nonetheless, has a deleterious effect on splicing.

To determine whether Eaf3 interacts with the spliceosome, we performed RNA immunoprecipitation (RIP) without crosslinking on HA-tagged Eaf3. Eaf3-HA was immunoprecipitated and qPCR was performed to determine whether any of the spliceosomal snRNAs co-precipitate. Interestingly, we observed enrichment of the snRNAs relative to other small RNA controls (Figure 2I). Loss of Set2 results in decreased binding between Eaf3-HA and the five snRNAs, indicating that this interaction is mediated through interaction between Eaf3 and chromatin, perhaps before release of U1 snRNA before spliceosome activation (Figure 2I). To determine whether the binding of snRNAs to Eaf3 was specific, we also performed RIP with HA-tagged Chd1, another yeast chromodomain protein. In contrast to Eaf3, we did not observe a strong interaction between Chd1-HA and snRNAs (Figure S3A).

Previous studies have implicated Eaf3 in recruitment of the Rpd3S complex, which includes Rpd3, to deacetylate the histone H3 tail (Keogh et al., 2005). Moreover, Eaf3 also recruits the NuA4 histone acetyltransferase, which acetylates the four conserved lysines on the histone H4 tail, to chromatin (Sathianathan et al., 2016). We considered the possibility that the inability to acetylate the histone H4 tail or deacetylate the histone H3 tail might underlie the splicing defect observed in the *eaf3*Δ mutant. To test this, we performed RT-PCR to analyze splicing of selected ICGs in *eaf3*Δ, *rpd3*Δ, and *H4K5,8,12,16R* cells. Neither deletion of *RPD3* nor mutation of H4 phenocopy the splicing defects observed in the *eaf3*Δ mutant (data not shown).

RNA abundance in the *eaf3*Δ mutant is strongly correlated with RNA abundance in the *H3K36A* mutant, which suggests that their overall expression profiles are nearly identical ($r_s = 0.9754$) (Figure S3B). Lastly, we performed ChIP-seq on Pol II (phospho-S2) and, similar to the *H3K36A* mutant, we did not observe a correlation ($r_s = -0.09173$) between change in SE and change in the occupancy of the elongating Pol II on ICGs in the *eaf3*Δ mutant (Figure S3C).

Eaf3 Is Required for the Efficient Cotranscriptional Recruitment of Splicing Factor Prp45

Eaf3 has been previously reported to physically interact with the splicing factor Prp45 using a high-throughput yeast two-hybrid screen (Albers et al., 2003). We confirmed this physical interaction by performing a co-immunoprecipitation (coIP) between Eaf3-HA and endogenously Myc-tagged Prp45 (Prp45-Myc) (Figure 3A). This result is consistent with physical interaction between the two proteins, although we suspected that the interaction was weak and/or transient. To address this and confirm that the interaction occurred *in vivo*, we performed crosslinking of whole cells followed by coIP (Figure 3B). We next analyzed the cotranscriptional recruitment of Prp45 in the absence of Eaf3. Spliceosome assembly has been shown to occur in a stepwise manner cotranscriptionally by ChIP-qPCR, and ChIP signals are routinely used as a proxy for the timing of association of splicing factors with the pre-mRNA (Kotovic et al., 2003; Görnemann et al., 2005; Gunderson and Johnson, 2009; Gunderson et al., 2011). The recruitment profile of Prp45 has recently been reported using this approach (Hálová et al., 2017). We performed ChIP on endogenously tagged Prp45 (Prp45-HA) in wild-type, *set2*Δ, and *eaf3*Δ cells on *HPC2* and *RAD14*, two genes that displayed strong splicing defects in the mutants. In wild-type cells, we observed a Prp45 ChIP pattern similar to what has been previously described (Figure 3C). Deletion of Eaf3 leads to decreased Prp45-HA occupancy compared to wild-type, indicating less stable association of Prp45-HA on both *HPC2* and

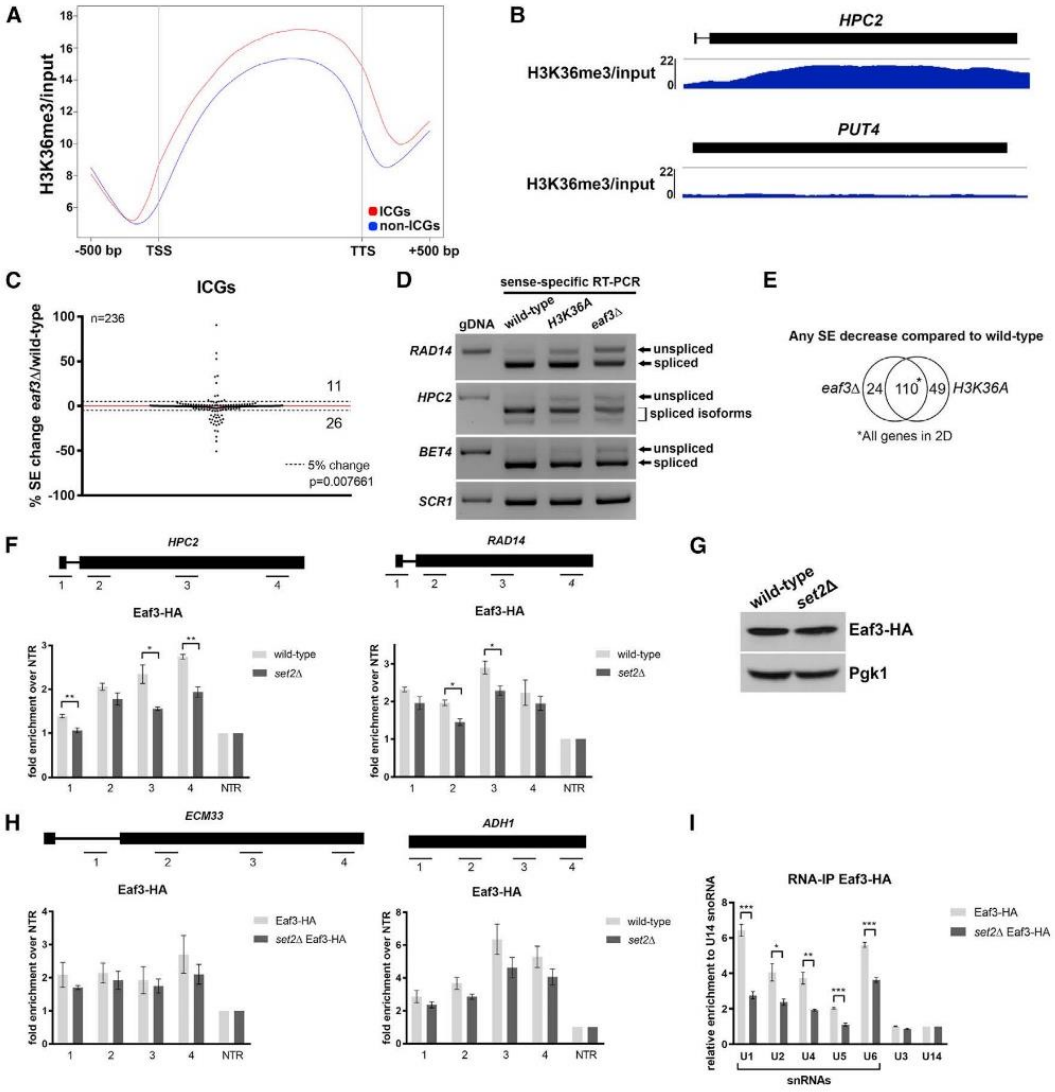

Figure 2. Eaf3 Is Required for Efficient Pre-mRNA Splicing

(A) Metagene plot of H3K36me3 ChIP-seq enrichment across the transcribed region and 500 nucleotides (nt) upstream of the transcription start site (TSS) and 500 nt downstream of the transcription termination site (TTS) of ICGs and non-ICGs.

(B) Genome-browser tracks of H3K36me3 ChIP-seq enrichment on ICG *HPC2* (RPKM: 7.355; length: 1962 bp) and intronless gene *PUT4* (RPKM: 7.658; length: 1884 bp).

(C) Scatterplot of percentage change in splicing efficiency (SE) of all ICGs in *eaf3*Δ over wild-type. Dashed lines represent a 5% change in SE. Numbers indicate number of ICGs above and below the dashed lines.

(D) RT-PCR validation of splicing changes observed in the *eaf3*Δ mutant. Products were run on a 1.8% agarose gel. *SCR1* is a loading control.

(E) Venn diagram displaying significant overlap of ICGs that display any SE decrease in *eaf3*Δ and *H3K36A* compared to wild-type cells ($p < 0.0001$, chi-square test).

(F) Occupancy of Eaf3-HA on ICGs *HPC2* (left) and *RAD14* (right) relative to a non-transcribed region (NTR) on chromosome V (Chr. V) in wild-type (light gray bars) and *set2*Δ cells (dark gray bars).

(G) Western blot analysis of Eaf3-HA protein levels in wild-type and *set2*Δ cells. Pgk1 is a loading control.

(H) Occupancy of Eaf3-HA on ICG *ECM33* relative to a NTR on Chr. V in wild-type and *set2*Δ cells (left). Occupancy of Eaf3-HA on intronless gene *ADH1* relative to a NTR on Chr. V in wild-type and *set2*Δ cells (right).

(I) Spliceosomal snRNAs co-immunoprecipitated with Eaf3. Bar graph depicting the five spliceosomal snRNAs that are immunoprecipitated with Eaf3 in wild-type and *set2*Δ cells under non-crosslinking conditions. U3 and U14 are snoRNAs. Bars represent the average of 3 biological replicates. Error bars represent the SEM. p values were determined by 2-tailed unpaired t test. *$p \leq 0.05$; **$p \leq 0.01$; ***$p \leq 0.001$.

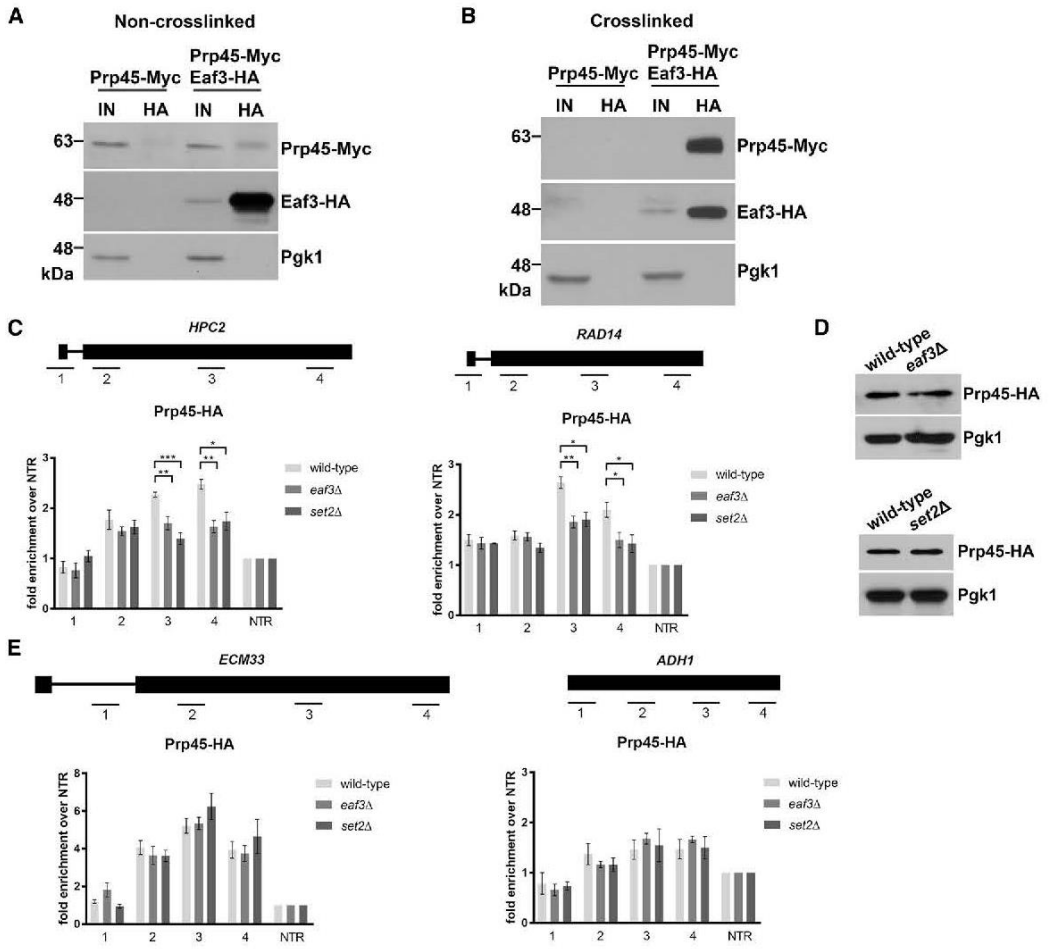

Figure 3. Eaf3 Is Required for the Proper Cotranscriptional Recruitment of Prp45

(A) Non-crosslinked co-immunoprecipitation (coIP) of Eaf3-HA and Prp45-Myc. Eaf3-HA was immunoprecipitated with an anti-HA antibody. Input is 2% of total lysate used for pull-down. Products were analyzed by western blotting with an anti-HA antibody and anti-Myc antibody.

(B) Crosslinked coIP of Eaf3-HA and Prp45-Myc. Whole cell extracts were crosslinked with 1% formaldehyde. Eaf3-HA was immunoprecipitated with an anti-HA antibody. Input is 2% of total lysate used for pull-down. Products were analyzed by western blotting with an anti-HA antibody and anti-Myc antibody.

(C) Occupancy of Prp45-HA on ICGs *HPC2* (left) and *RAD14* (right) relative to a non-transcribed region (NTR) on Chr. V in wild-type (light gray bars), *eaf3*Δ (medium gray bars), and *set2*Δ (dark gray bars).

(D) Western blot analysis of Prp45-HA protein levels in wild-type and *eaf3*Δ (top), and *set2*Δ (bottom) cells. Pgk1 is a loading control.

(E) Occupancy of Prp45-HA on ICG *ECM33* and intronless gene *ADH1* relative to a NTR on Chr. V. in wild-type, *eaf3*Δ, and *set2*Δ. Bars represent the average of at least 3 biological replicates. Error bars represent the SEM. p values were determined by 2-tailed unpaired t test. *, $p \leq 0.05$; **$p \leq 0.01$; ***$p \leq 0.001$.

RAD14 (Figure 3C). In the *set2*Δ mutant, we observed an almost identical reduction in Prp45-HA binding to the *eaf3*Δ mutant (Figure 3C); Prp45-HA protein levels are identical in wild-type and the two mutants (Figure 3D). This suggests that the inefficient recruitment of Prp45 to *HPC2* and *RAD14* in *set2*Δ is due to loss of Eaf3 binding to chromatin. ChIP of Prp45 on a gene that does not show a splicing defect in the absence of *eaf3*Δ or *set2*Δ, shows no change in Prp45 occupancy (Figure 3E, left), indicating that, for this gene, Prp45 occupancy is not sensitive to Set2 or Eaf3. The intronless gene *ADH1* shows negligible Prp45 occupancy which does not appear to be affected by Set2 or Eaf3 (Figure 3E, right).

Efficient Cotranscriptional Recruitment of Prp19 Depends on the Presence of Eaf3

Prp45 has been shown to interact with components of the nineteen complex (NTC) (Fabrizio et al., 2009), a complex important for spliceosome activation. Moreover, Prp45 has been shown to be necessary for NTC recruitment early in cotranscriptional spliceosome assembly (Hálová et al., 2017). Because efficient recruitment of Prp45 depends on Eaf3, we hypothesized that recruitment of the NTC would also be negatively affected by the absence of Eaf3. We endogenously HA-tagged Prp19 and determined that protein levels of Prp19 do not change in an *eaf3*Δ mutant (Figure 4A). We then performed ChIP of

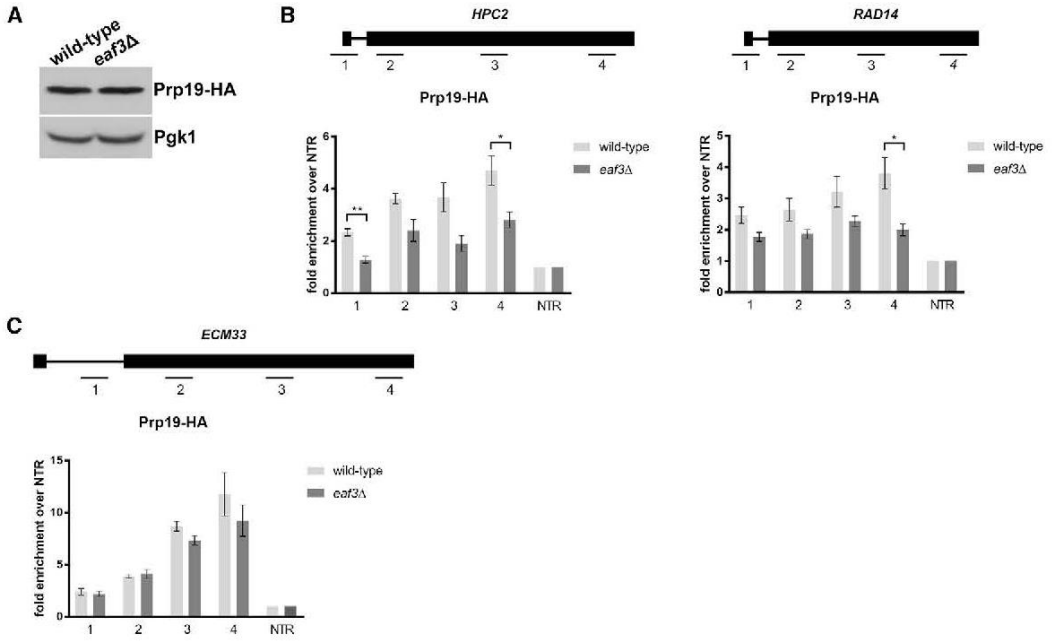

Figure 4. Prp19 Is Inefficiently Recruited to ICGs in the Absence of Eaf3

(A) Western blot analysis of Prp19-HA protein levels in wild-type and *eaf3*Δ cells. Pgk1 is a loading control.

(B) Occupancy of Prp19-HA on ICGs *HPC2* (left) and *RAD14* (right) relative to a non-transcribed region (NTR) on Chr. V in wild-type (light gray bars) and *eaf3*Δ (medium gray bars).

(C) Occupancy of Prp19-HA on ICG *ECM33* relative to a NTR on Chr. V. in wild-type and *eaf3*Δ cells. Bars represent the average of at least 3 biological replicates. Error bars represent the SEM. p values were determined by 2-tailed unpaired t test. *$p \leq 0.05$; **$p \leq 0.01$; ***$p \leq 0.001$.

Prp19-HA in wild-type and *eaf3*Δ cells and observed a significant decrease in recruitment of Prp19-HA to ICGs *HPC2* and *RAD14* (Figure 4B) in the absence of Eaf3. Similar to what was observed when we ChIP Prp45 (Figure 3E), there was no change of occupancy of Prp19-HA on *ECM33* (Figure 4C).

The NTC plays a critical role in catalytic activation of the spliceosome and associates with the spliceosome along with the U4/U6*U5 tri-snRNP around the time of U4/U6 unwinding and concomitant release of U1 and U4 (Fabrizio et al., 2009). Prp45 physically interacts with the NTC and co-purifies with the precatalytic complex B (Albers et al., 2003; Fabrizio et al., 2009), suggesting that the NTC, as well as NTC-associated protein Prp45, facilitates the transition from the precatalytic complex B to the activated complex B^{ACT}. Eaf3 also appears to play an important role in these steps (Figure 5).

DISCUSSION

Posttranslational modifications on histones have been implicated in the regulation of RNA splicing (Andersson et al., 2009; Hérissant et al., 2014; Hnilicová and Staněk, 2011). H3K36me3 was first reported to regulate exon selection in the *FGFR2* gene in human cells via recruitment of chromatin-associated protein MRG15 and polypyrimidine tract-binding protein (PTB) (Luco et al., 2010). Nonetheless, the sometimes subtle, gene-specific splicing effects and incomplete overlap between MRG15- and PTB-splicing dependent events left open the possibility that there were other effects of H3K36me3 on splicing that remained to be elucidated. Another report suggested that PWWP domain-containing protein Psip1/p52 binds to H3K36me3 and recruits SR-containing proteins and splicing factors to regulate alternative splicing of a specific set of genes (Pradeepa et al., 2012). Studies have also linked H3K36 methylation to genome-wide splicing effects, although the underlying mechanisms have been less clear (Guo et al., 2014; Simon et al., 2014). H3K36me has also been implicated in regulating splicing in yeast via a gene expression reporter (Sorenson et al., 2016). This reporter screen made use of the intron in *RPL28*, an efficiently spliced ICG (Sorenson and Stevens, 2014), which does not uncover the effects of H3K36me loss on splicing genome-wide or its role in expression of genes that are less efficiently spliced.

H3K36 Methylation Is Required for Constitutive Splicing in Yeast

Here we show that H3K36me3 is required for efficient constitutive pre-mRNA splicing genome-wide (Figure 1B). We observed that H3K36 methylation is central to core splicing events and not exclusively to exon inclusion events. Our data are consistent with a recruitment model by which H3K36me recruits the chromodomain protein Eaf3 to mediate the interaction between chromatin and the spliceosome. Indeed, deletion of *EAF3* phenocopies the splicing of the same genes that are sensitive to loss of H3K36me (Figure 2E).

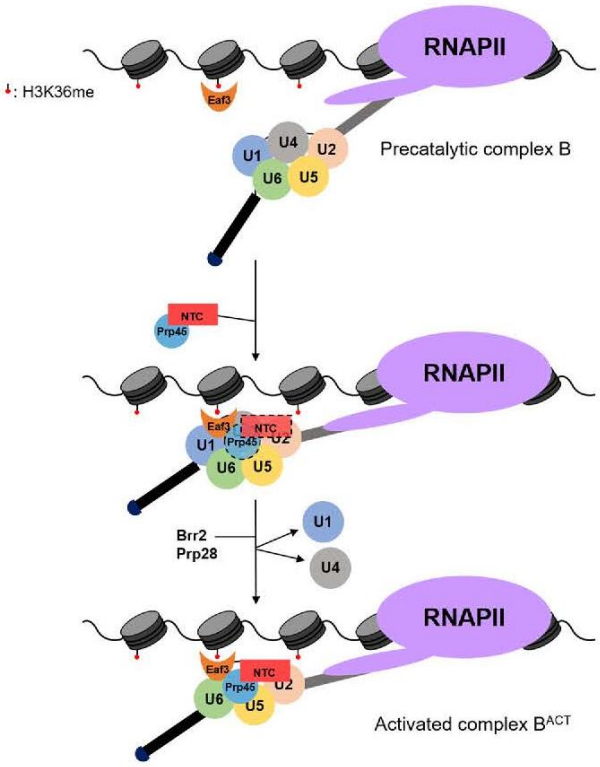

Figure 5. Eaf3 Recognizes H3K36 Methylation to Regulate Pre-mRNA Splicing

Eaf3 recruits Prp45 and the nineteen complex (NTC) to the precatalytic complex B to promote spliceosome activation. The putative NTC and Prp45 interaction with the spliceosome prior to U1 and U4 snRNP release may be transient (indicated by dashed lines).

One of the additional reported functions of H3K36 methylation is to suppress cryptic and antisense transcription within gene bodies through recruitment of the Rpd3S complex (Keogh et al., 2005). Since Eaf3 is also a component of the Rpd3S complex, it is tempting to speculate that antisense transcription might affect splicing of the sense transcript. However, from our stranded RNA-seq analysis, we did not observe a significant correlation between antisense transcription and changes in SE (data not shown). Although antisense transcription does not seem to affect RNA splicing, we observe several antisense transcripts that are spliced, albeit rather inefficiently (Douglass et al., 2019).

Eaf3 Interaction with Prp45 Affects Its Role in Splicing

We reveal a mechanism by which the chromodomain-containing protein Eaf3 binds methylated H3K36 and interacts physically with Prp45 (Figures 3A and 3B) to facilitate stable Prp45 association during cotranscriptional spliceosome assembly (Figure 3C). Recent cryo-EM structures of *S. cerevisiae* and *S. pombe* spliceosomes have revealed that Prp45 is an intrinsically disordered protein that spans over 150 Å and stabilizes the catalytic center through extensive contacts with several proteins and snRNAs (Wan et al., 2016; Yan et al., 2015; Yan et al., 2016). We propose that because Prp45 is found throughout the splicing process and after spliceosome assembly (Albers et al., 2003), Eaf3 is well positioned to link the spliceosome to chromatin until the splicing reaction is completed (Figure 5).

Interestingly, the human ortholog of Prp45 is SKIP, a protein involved in both transcription and splicing (Brès et al., 2005; Makarov et al., 2002; Nagai et al., 2004; Neubauer et al., 1998). In yeast, Prp45 fused with a DNA-binding domain has been shown to activate transcription of a reporter gene (Martínková et al., 2002). Like SKIP, it is possible that Prp45 bridges transcription initiation and pre-mRNA processing but may depend on Eaf3 or other factors for its binding to chromatin since Prp45 lacks many of the binding motifs found in SKIP.

Eaf3 Is Required for the Proper Cotranscriptional Recruitment of Prp19

All five spliceosomal snRNAs immunoprecipitate with Eaf3, suggesting that, perhaps, its role in splicing occurs when all five snRNPs are present. Since we show Eaf3 interacts with Prp45, which is associated with the NTC, we hypothesize that Eaf3 acts between the precatalytic complex B and the activated complex B^{ACT}. Indeed, in the absence of Eaf3, cotranscriptional recruitment of Prp19 to ICGs *HPC2* and *RAD14* is diminished (Figure 4B). We propose a model whereby Eaf3 stabilizes Prp45 and NTC interactions with the precatalytic complex B spliceosome to facilitate major structural rearrangements within the spliceosome, including the irreversible loss of U4 that occurs immediately after NTC association (Hoskins et al., 2016).

Prp19 has been implicated in a variety of processes, in addition to splicing, in both yeast and higher eukaryotes. These include genome maintenance, recruitment of ubiquitylated proteins to the proteasome, liquid droplet formation, and importantly, transcription elongation (Chanarat and Sträßer, 2013). This raises the possibility that Eaf3's role in directing NTC activity may extend beyond effects on splicing, a question we are currently addressing.

STAR★METHODS

Detailed methods are provided in the online version of this paper and include the following:

- KEY RESOURCES TABLE
- LEAD CONTACT AND MATERIALS AVAILABILITY
- EXPERIMENTAL MODEL AND SUBJECT DETAILS
- METHOD DETAILS
  - RNA Isolation
  - RNA-seq Library Preparation and Analysis
  - RT-PCR Analysis
  - Western Blot Analysis
  - ChIP-seq Library Preparation and ChIP-seq Analysis
  - ChIP-qPCR Analysis
  - RNA Immunoprecipitation
  - Co-immunoprecipitation and crosslinked co-immunoprecipitation
- QUANTIFICATION AND STATISTICAL ANALYSIS
- DATA AND CODE AVAILABILITY

SUPPLEMENTAL INFORMATION

Supplemental Information can be found online at https://doi.org/10.1016/j.celrep.2019.05.100.

ACKNOWLEDGMENTS

This work was supported by the National Institute of General Medical Sciences (GM-085474 to T.L.J.), as well as the Cellular and Molecular Biology Training Program Ruth L. Kirschstein National Research Service Award (GM007185 to C.S.L.), the Whitcome Predoctoral Fellowship (to C.S.L.), and the UCLA Dissertation Year Fellowship (to C.S.L.). M.S.P. was supported by the Russian Foundation for Basic Research grants 17-29-06056 and 18-29-01027 and Russian Science Foundation grant 19-44-02027.

AUTHOR CONTRIBUTIONS

C.S.L. and T.L.J. conceived the study and designed the experiments. C.S.L., S.M.D., M.M., M.B.O., and M.S.P. performed the experiments and data analyses. C.S.L. performed the stranded RNA-seq. C.S.L. and S.M.D. performed the RNA-seq analysis. M.M. and M.B.O. performed the ChIP-seq. M.M., M.B.O., and M.P. contributed to the ChIP-seq analysis. M.S.P. performed the RIP experiments. C.S.L. and T.L.J. wrote the manuscript.

DECLARATION OF INTERESTS

The authors declare no competing interest.

Received: November 5, 2018
Revised: March 8, 2019
Accepted: May 27, 2019
Published: June 25, 2019

REFERENCES

Albers, M., Diment, A., Muraru, M., Russell, C.S., and Beggs, J.D. (2003). Identification and characterization of Prp45p and Prp46p, essential pre-mRNA splicing factors. RNA *9*, 138–150.

Alexander, R.D., Innocente, S.A., Barrass, J.D., and Beggs, J.D. (2010). Splicing-dependent RNA polymerase pausing in yeast. Mol. Cell *40*, 582–593.

Andersson, R., Enroth, S., Rada-Iglesias, A., Wadelius, C., and Komorowski, J. (2009). Nucleosomes are well positioned in exons and carry characteristic histone modifications. Genome Res. *19*, 1732–1741.

Ares, M. (2012). Isolation of total RNA from yeast cell cultures. Cold Spring Harb. Protoc. *2012*, 1082–1086.

Ares, M., Jr., Grate, L., and Pauling, M.H. (1999). A handful of intron-containing genes produces the lion's share of yeast mRNA. RNA *5*, 1138–1139.

Awad, A.M., Venkataramanan, S., Nag, A., Galivanche, A.R., Bradley, M.C., Neves, L.T., Douglass, S., Clarke, C.F., and Johnson, T.L. (2017). Chromatin-remodeling SWI/SNF complex regulates coenzyme Q_6 synthesis and a metabolic shift to respiration in yeast. J. Biol. Chem. *292*, 14851–14866.

Bannister, A.J., Schneider, R., Myers, F.A., Thorne, A.W., Crane-Robinson, C., and Kouzarides, T. (2005). Spatial distribution of di- and tri-methyl lysine 36 of histone H3 at active genes. J. Biol. Chem. *280*, 17732–17736.

Brès, V., Gomes, N., Pickle, L., and Jones, K.A. (2005). A human splicing factor, SKIP, associates with P-TEFb and enhances transcription elongation by HIV-1 Tat. Genes Dev. *19*, 1211–1226.

Chanarat, S., and Sträßer, K. (2013). Splicing and beyond: the many faces of the Prp19 complex. Biochim. Biophys. Acta *1833*, 2126–2134.

de la Mata, M., Alonso, C.R., Kadener, S., Fededa, J.P., Blaustein, M., Pelisch, F., Cramer, P., Bentley, D., and Kornblihtt, A.R. (2003). A slow RNA polymerase II affects alternative splicing in vivo. Mol. Cell *12*, 525–532.

Douglass, S., Leung, C.S., and Johnson, T.L. (2019). Extensive splicing across the Saccharomyces cerevisiae genome. bioRxiv. https://doi.org/10.1101/515163.

Fabrizio, P., Dannenberg, J., Dube, P., Kastner, B., Stark, H., Urlaub, H., and Lührmann, R. (2009). The evolutionarily conserved core design of the catalytic activation step of the yeast spliceosome. Mol. Cell *36*, 593–608.

Fong, N., Kim, H., Zhou, Y., Ji, X., Qiu, J., Saldi, T., Diener, K., Jones, K., Fu, X.D., and Bentley, D.L. (2014). Pre-mRNA splicing is facilitated by an optimal RNA polymerase II elongation rate. Genes Dev. *28*, 2663–2676.

Görnemann, J., Kotovic, K.M., Hujer, K., and Neugebauer, K.M. (2005). Cotranscriptional spliceosome assembly occurs in a stepwise fashion and requires the cap binding complex. Mol. Cell *19*, 53–63.

Gunderson, F.Q., and Johnson, T.L. (2009). Acetylation by the transcriptional coactivator Gcn5 plays a novel role in co-transcriptional spliceosome assembly. PLoS Genet. *5*, e1000682.

Gunderson, F.Q., Merkhofer, E.C., and Johnson, T.L. (2011). Dynamic histone acetylation is critical for cotranscriptional spliceosome assembly and spliceosomal rearrangements. Proc. Natl. Acad. Sci. USA *108*, 2004–2009.

Guo, R., Zheng, L., Park, J.W., Lv, R., Chen, H., Jiao, F., Xu, W., Mu, S., Wen, H., Qiu, J., et al. (2014). BS69/ZMYND11 reads and connects histone H3.3 lysine 36 trimethylation-decorated chromatin to regulated pre-mRNA processing. Mol. Cell *56*, 298–310.

Hálová, M., Gahura, O., Převorovský, M., Cit, Z., Novotný, M., Valentová, A., Abrhámová, K., Půta, F., and Folk, P. (2017). Nineteen complex-related factor Prp45 is required for the early stages of cotranscriptional spliceosome assembly. RNA *23*, 1512–1524.

Hérissant, L., Moehle, E.A., Bertaccini, D., Van Dorsselaer, A., Schaeffer-Reiss, C., Guthrie, C., and Dargemont, C. (2014). H2B ubiquitylation modulates spliceosome assembly and function in budding yeast. Biol. Cell *106*, 126–138.

Hnilicová, J., and Staněk, D. (2011). Where splicing joins chromatin. Nucleus *2*, 182–188.

Hoskins, A.A., Rodgers, M.L., Friedman, L.J., Gelles, J., and Moore, M.J. (2016). Single molecule analysis reveals reversible and irreversible steps during spliceosome activation. eLife *5*, e14166.

Howe, K.J., Kane, C.M., and Ares, M., Jr. (2003). Perturbation of transcription elongation influences the fidelity of internal exon inclusion in Saccharomyces cerevisiae. RNA *9*, 993–1006.

Huff, J.T., Plocik, A.M., Guthrie, C., and Yamamoto, K.R. (2010). Reciprocal intronic and exonic histone modification regions in humans. Nat. Struct. Mol. Biol. *17*, 1495–1499.

Iwamori, N., Tominaga, K., Sato, T., Riehle, K., Iwamori, T., Ohkawa, Y., Coarfa, C., Ono, E., and Matzuk, M.M. (2016). MRG15 is required for pre-mRNA splicing and spermatogenesis. Proc. Natl. Acad. Sci. USA *113*, E5408–E5415.

Jha, D.K., and Strahl, B.D. (2014). An RNA polymerase II-coupled function for histone H3K36 methylation in checkpoint activation and DSB repair. Nat. Commun. *5*, 3965.

Johnson, T.L., and Vilardell, J. (2012). Regulated pre-mRNA splicing: the ghostwriter of the eukaryotic genome. Biochim. Biophys. Acta *1819*, 538–545.

Jonkers, I., and Lis, J.T. (2015). Getting up to speed with transcription elongation by RNA polymerase II. Nat. Rev. Mol. Cell Biol. *16*, 167–177.

Keogh, M.C., Kurdistani, S.K., Morris, S.A., Ahn, S.H., Podolny, V., Collins, S.R., Schuldiner, M., Chin, K., Punna, T., Thompson, N.J., et al. (2005). Cotranscriptional set2 methylation of histone H3 lysine 36 recruits a repressive Rpd3 complex. Cell *123*, 593–605.

Kolasinska-Zwierz, P., Down, T., Latorre, I., Liu, T., Liu, X.S., and Ahringer, J. (2009). Differential chromatin marking of introns and expressed exons by H3K36me3. Nat. Genet. *41*, 376–381.

Kotovic, K.M., Lockshon, D., Boric, L., and Neugebauer, K.M. (2003). Cotranscriptional recruitment of the U1 snRNP to intron-containing genes in yeast. Mol. Cell. Biol. *23*, 5768–5779.

Kouzarides, T. (2007). Chromatin modifications and their function. Cell *128*, 693–705.

Krogan, N.J., Kim, M., Tong, A., Golshani, A., Cagney, G., Canadien, V., Richards, D.P., Beattie, B.K., Emili, A., Boone, C., et al. (2003). Methylation of

histone H3 by Set2 in Saccharomyces cerevisiae is linked to transcriptional elongation by RNA polymerase II. Mol. Cell. Biol. *23*, 4207–4218.

Lacadie, S.A., Tardiff, D.F., Kadener, S., and Rosbash, M. (2006). In vivo commitment to yeast cotranscriptional splicing is sensitive to transcription elongation mutants. Genes Dev. *20*, 2055–2066.

Langmead, B., Trapnell, C., Pop, M., and Salzberg, S.L. (2009). Ultrafast and memory-efficient alignment of short DNA sequences to the human genome. Genome Biol. *10*, R25.

Li, J., Moazed, D., and Gygi, S.P. (2002). Association of the histone methyltransferase Set2 with RNA polymerase II plays a role in transcription elongation. J. Biol. Chem. *277*, 49383–49388.

Longtine, M.S., McKenzie, A., 3rd, Demarini, D.J., Shah, N.G., Wach, A., Brachat, A., Philippsen, P., and Pringle, J.R. (1998). Additional modules for versatile and economical PCR-based gene deletion and modification in Saccharomyces cerevisiae. Yeast *14*, 953–961.

Luco, R.F., and Misteli, T. (2011). More than a splicing code: integrating the role of RNA, chromatin and non-coding RNA in alternative splicing regulation. Curr. Opin. Genet. Dev. *21*, 366–372.

Luco, R.F., Pan, Q., Tominaga, K., Blencowe, B.J., Pereira-Smith, O.M., and Misteli, T. (2010). Regulation of alternative splicing by histone modifications. Science *327*, 996–1000.

Makarov, E.M., Makarova, O.V., Urlaub, H., Gentzel, M., Will, C.L., Wilm, M., and Lührmann, R. (2002). Small nuclear ribonucleoprotein remodeling during catalytic activation of the spliceosome. Science *298*, 2205–2208.

Martínková, K., Lebduska, P., Skružný, M., Folk, P., and Půta, F. (2002). Functional mapping of Saccharomyces cerevisiae Prp45 identifies the SNW domain as essential for viability. J. Biochem. *132*, 557–563.

Morselli, M., Pastor, W.A., Montanini, B., Nee, K., Ferrari, R., Fu, K., Bonora, G., Rubbi, L., Clark, A.T., Ottonello, S., et al. (2015). In vivo targeting of de novo DNA methylation by histone modifications in yeast and mouse. eLife *4*, e06205.

Munding, E.M., Shiue, L., Katzman, S., Donohue, J.P., and Ares, M., Jr. (2013). Competition between pre-mRNAs for the splicing machinery drives global regulation of splicing. Mol. Cell *51*, 338–348.

Nagai, K., Yamaguchi, T., Takami, T., Kawasumi, A., Aizawa, M., Masuda, N., Shimizu, M., Tominaga, S., Ito, T., Tsukamoto, T., and Osumi, T. (2004). SKIP modifies gene expression by affecting both transcription and splicing. Biochem. Biophys. Res. Commun. *316*, 512–517.

Neubauer, G., King, A., Rappsilber, J., Calvio, C., Watson, M., Ajuh, P., Sleeman, J., Lamond, A., and Mann, M. (1998). Mass spectrometry and EST-database searching allows characterization of the multi-protein spliceosome complex. Nat. Genet. *20*, 46–50.

Neves, L.T., Douglass, S., Spreafico, R., Venkataramanan, S., Kress, T.L., and Johnson, T.L. (2017). The histone variant H2A.Z promotes efficient cotranscriptional splicing in *S. cerevisiae*. Genes Dev. *31*, 702–717.

Nissen, K.E., Homer, C.M., Ryan, C.J., Shales, M., Krogan, N.J., Patrick, K.L., and Guthrie, C. (2017). The histone variant H2A.Z promotes splicing of weak introns. Genes Dev. *31*, 688–701.

Oesterreich, F.C., Herzel, L., Straube, K., Hujer, K., Howard, J., and Neugebauer, K.M. (2016). Splicing of Nascent RNA Coincides with Intron Exit from RNA Polymerase II. Cell *165*, 372–381.

Pan, Q., Shai, O., Lee, L.J., Frey, B.J., and Blencowe, B.J. (2008). Deep surveying of alternative splicing complexity in the human transcriptome by high-throughput sequencing. Nat. Genet. *40*, 1413–1415.

Pandya-Jones, A., and Black, D.L. (2009). Co-transcriptional splicing of constitutive and alternative exons. RNA *15*, 1896–1908.

Pradeepa, M.M., Sutherland, H.G., Ule, J., Grimes, G.R., and Bickmore, W.A. (2012). Psip1/Ledgf p52 binds methylated histone H3K36 and splicing factors and contributes to the regulation of alternative splicing. PLoS Genet. *8*, e1002717.

Reid, J.L., Moqtaderi, Z., and Struhl, K. (2004). Eaf3 regulates the global pattern of histone acetylation in Saccharomyces cerevisiae. Mol. Cell. Biol. *24*, 757–764.

Sathianathan, A., Ravichandran, P., Lippi, J.M., Cohen, L., Messina, A., Shaju, S., Swede, M.J., and Ginsburg, D.S. (2016). The Eaf3/5/7 Subcomplex Stimulates NuA4 Interaction with Methylated Histone H3 Lys-36 and RNA Polymerase II. J. Biol. Chem. *291*, 21195–21207.

Schwartz, S., Meshorer, E., and Ast, G. (2009). Chromatin organization marks exon-intron structure. Nat. Struct. Mol. Biol. *16*, 990–995.

Simon, J.M., Hacker, K.E., Singh, D., Brannon, A.R., Parker, J.S., Weiser, M., Ho, T.H., Kuan, P.F., Jonasch, E., Furey, T.S., et al. (2014). Variation in chromatin accessibility in human kidney cancer links H3K36 methyltransferase loss with widespread RNA processing defects. Genome Res. *24*, 241–250.

Singh, R.K., and Cooper, T.A. (2012). Pre-mRNA splicing in disease and therapeutics. Trends Mol. Med. *18*, 472–482.

Sorenson, M.R., and Stevens, S.W. (2014). Rapid identification of mRNA processing defects with a novel single-cell yeast reporter. RNA *20*, 732–745.

Sorenson, M.R., Jha, D.K., Ucles, S.A., Flood, D.M., Strahl, B.D., Stevens, S.W., and Kress, T.L. (2016). Histone H3K36 methylation regulates pre-mRNA splicing in Saccharomyces cerevisiae. RNA Biol. *13*, 412–426.

Spies, N., Nielsen, C.B., Padgett, R.A., and Burge, C.B. (2009). Biased chromatin signatures around polyadenylation sites and exons. Mol. Cell *36*, 245–254.

Stempor, P., and Ahringer, J. (2016). SeqPlots - Interactive software for exploratory data analyses, pattern discovery and visualization in genomics. Wellcome Open Res. *1*, 14.

Tilgner, H., Nikolaou, C., Althammer, S., Sammeth, M., Beato, M., Valcárcel, J., and Guigó, R. (2009). Nucleosome positioning as a determinant of exon recognition. Nat. Struct. Mol. Biol. *16*, 996–1001.

Trapnell, C., Pachter, L., and Salzberg, S.L. (2009). TopHat: discovering splice junctions with RNA-Seq. Bioinformatics *25*, 1105–1111.

Venkataramanan, S., Douglass, S., Galivanche, A.R., and Johnson, T.L. (2017). The chromatin remodeling complex Swi/Snf regulates splicing of meiotic transcripts in Saccharomyces cerevisiae. Nucleic Acids Res. *45*, 7708–7721.

Wan, R., Yan, C., Bai, R., Huang, G., and Shi, Y. (2016). Structure of a yeast catalytic step I spliceosome at 3.4 Å resolution. Science *353*, 895–904.

Will, C.L., and Lührmann, R. (2011). Spliceosome structure and function. Cold Spring Harb. Perspect. Biol. *3*, a003707.

Xiao, T., Hall, H., Kizer, K.O., Shibata, Y., Hall, M.C., Borchers, C.H., and Strahl, B.D. (2003). Phosphorylation of RNA polymerase II CTD regulates H3 methylation in yeast. Genes Dev. *17*, 654–663.

Yan, C., Hang, J., Wan, R., Huang, M., Wong, C.C., and Shi, Y. (2015). Structure of a yeast spliceosome at 3.6-angstrom resolution. Science *349*, 1182–1191.

Yan, C., Wan, R., Bai, R., Huang, G., and Shi, Y. (2016). Structure of a yeast activated spliceosome at 3.5 Å resolution. Science *353*, 904–911.

Zhang, Y., Liu, T., Meyer, C.A., Eeckhoute, J., Johnson, D.S., Bernstein, B.E., Nusbaum, C., Myers, R.M., Brown, M., Li, W., and Liu, X.S. (2008). Model-based analysis of ChIP-Seq (MACS). Genome Biol. *9*, R137.

STAR★METHODS

KEY RESOURCES TABLE

REAGENT or RESOURCE	SOURCE	IDENTIFIER
Antibodies		
Anti-H3K36me3	Abcam	Cat# ab9050; RRID:AB_306966
Anti-Histone H3	Abcam	Cat# ab1791; RRID:AB_302613
Anti-HA (12CA5)	Roche	Cat# 11583816001; RRID:AB_514505
Anti-Myc (9E10)	Roche	Cat# 11667149001; RRID:AB_390912
Anti-RNAPII S2P	Abcam	Cat# ab5095; RRID:AB_304749
Chemicals, Peptides, and Recombinant Proteins		
Bovine Serum Albumin	Rockland	Cat# BSA-50
Non-fat Dry Milk	Genesee Scientific	Cat# 20-241
Agencourt AMPure XP	Beckman Coulter	Cat# A63880
cOmplete, Mini, EDTA-free Protease Inhibitor Cocktail	Roche	Cat# 4693159001
Formaldehyde	Fisher Scientific	Cat# BP531-500
iTaq Universal SYBR® Green Supermix	Bio-Rad	Cat# 172-5121
GammaBind G Sepharose	GE Healthcare	Cat# 17-0885-01
Pierce Anti-HA Magnetic Beads	ThermoFisher Scientific	Cat# 88836
Maxima Reverse Transcriptase	ThermoFisher Scientific	Cat# EP0742
RiboLock RNase Inhibitor	ThermoFisher Scientific	Cat# EO0382
RNase A	ThermoFisher Scientific	Cat# AM2270
Proteinase K	Roche	Cat# 03115828001
DNase I recombinant	Roche	Cat# 4716728001
Glass Beads	BioSpec	Cat# 11079105
Protein A Dynabeads	ThermoFisher Scientific	Cat# 10001D
HiBind DNA columns	VWR	Cat# 95043-212
UltraPure Ethidium Bromide	ThermoFisher Scientific	Cat# 15585011
Critical Commercial Assays		
TruSeq Stranded mRNA Library Preparation Kit	Illumina	Cat# RS-122-2101
Ribo-Zero Gold rRNA Removal Kit (Yeast)	Illumina	Cat# MRZY1324
Ovation Ultralow DR Kit	NuGEN	Cat# 0344
Deposited Data		
RNA-seq and ChiP-seq data	This study	GEO: GSE120051
Experimental Models: Organisms/Strains		
Yeast strains, see Table S1	This study	N/A
Oligonucleotides		
Primers for PCR, RT-PCR, and qPCR, see Table S3	This study	N/A
Recombinant DNA		
pFA6a-3HA-kanMX6	Longtine et al., 1998	N/A
pFA6a-3HA-HIS3MX6	Longtine et al., 1998	N/A
pFA6A-13Myc-kanMX6	Longtine et al., 1998	N/A
Software and Algorithms		
Prism 7	GraphPad	N/A
TopHat 2.0.14	Trapnell et al., 2009	https://ccb.jhu.edu/software/tophat/index.shtml
MACS2	Zhang et al., 2008	https://github.com/taoliu/MACS
SeqPlots 3.7	Stempor and Ahringer, 2016	https://bioconductor.org/packages/release/bioc/html/seqplots.html

(*Continued on next page*)

Continued		
REAGENT or RESOURCE	SOURCE	IDENTIFIER
Bowtie 0.12.8	Langmead et al., 2009	http://bowtie-bio.sourceforge.net/index.shtml
Microsoft Excel (Version 1812)	Microsoft	N/A
ImageJ	NIH	https://imagej.nih.gov/ij/

LEAD CONTACT AND MATERIALS AVAILABILITY

Further information and requests for resources and reagents should be directed to and will be fulfilled by the Lead Contact, Tracy L. Johnson (tljohnson@ucla.edu).

EXPERIMENTAL MODEL AND SUBJECT DETAILS

The *S. cerevisiae* strains used in this study are listed in Table S1. All strains were grown in YPD (1% yeast extract, 2% peptone, and 2% dextrose) at 30°C. All strains are derived from BY4741. Individual deletion strains were obtained from GE Dharmacon. 3HA- and 13Myc- endogenous C-terminal tagged strains were generated by homologous recombination following PCR amplification from the pFA6a-3HA-kanMX6, pFA6a-3HA-His3MX6, and pFA6A-13Myc-kanMX6 plasmids as described previously (Longtine et al., 1998).

METHOD DETAILS

RNA Isolation

RNA was isolated from yeast during log-phase (OD_{600} = 0.5–0.6) by hot phenol:chloroform:isoamyl alcohol (PCA) extraction with SDS as described previously (Ares, 2012). Ethanol precipitation was performed to concentrate the RNA.

RNA-seq Library Preparation and Analysis

Stranded RNA-seq libraries were prepared using the TruSeq Stranded Total RNA Kit (Illumina). Prior to library preparation, isolated total RNA from 2 biological replicates was treated with DNase I (Roche) and was subsequently depleted of ribosomal RNA using the Ribo-Zero Gold rRNA Removal Kit (Illumina). 100 bp single-end reads (Illumina HiSeq 4000) were aligned to the sacCer3 assembly (UCSC 2011) using TopHat 2.0.14 (Trapnell et al., 2009) with a maximum of 2 read mismatches, 0 splice mismatches, and a minimum anchor of 8 nucleotides. An average of 38,326,464 reads were obtained per sample, of which an average of 32,533,221 reads were mapped (84.9% of input). RPKMs were calculated by dividing read counts that aligned within a gene by the length of the gene in kilobases per million mapped reads. For intron-containing genes, exonic reads were quantitated by aligned reads that mapped entirely in an exon as defined by the Ares Lab Yeast Intron Database. Unspliced reads were defined as reads mapped within an annotated intron and reads mapped partially in an intron. Spliced reads were defined as splice junction reads. Introns that contained annotated snoRNAs were omitted from the splicing analysis. Spliced and unspliced read counts were normalized by the total number of unique alignments that can contribute to its count value. For spliced reads, this is simply read length minus one (99). For unspliced reads, we normalized by dividing by the intron length plus the read length minus one. Splicing efficiency (SE) was calculated using the formula: $SE = \frac{\text{normalized spliced reads}}{\text{normalized spliced reads} + \text{normalized unspliced reads}} \times 100\%$. SEs for all ICGs are listed in Table S2. For splicing analysis, ICGs with less than 3 total spliced reads between biological replicates were filtered out. For the relaxed read count splicing reanalysis, we eliminated the requirement for 3 total spliced reads and added a 0.01 normalized spliced pseudocount for ICGs that had a 0 spliced read count. Genes with an RPKM of less than 1 were filtered out prior to all data analysis.

RT-PCR Analysis

Following total RNA isolation, 20 µg of RNA was treated with DNase I (Roche). 500 ng–1 µg of DNase-treated RNA was used for cDNA synthesis. Sense-specific cDNA was generated using Maxima Reverse Transcriptase (ThermoFisher Scientific) and gene-specific primers. Gene-specific primers and RT primers are listed in Table S3. 1–2 µL of cDNA was used as the template in a 50 µL PCR reaction. Primers that flank the intron were used to observe splicing changes. The PCR products were run on a 1.8% agarose gel. Agarose gels were stained with ethidium bromide (ThermoFisher Scientific). Gels were then imaged on Image Lab (Bio-Rad).

Western Blot Analysis

50 mL of log-phase yeast were pelleted and resuspended in 500 µL of lysis buffer (50 mM HEPES pH 7.5, 150 mM NaCl, 1 mM EDTA, 1% Triton X-100, 0.1% sodium deoxycholate) with protease inhibitors. An equal volume of 0.5 mm acid-washed glass beads (BioSpec) was added to the cell resuspension and the samples were lysed in a cell disruptor for 5 minutes at 4°C. Proteins were separated in a 10% SDS-PAGE gel for Eaf3-HA, Prp45-HA, and Prp45-Myc and a 15% SDS-PAGE gel for histone H3 and histone H3K36me3. HA blots were probed with anti-HA antibody (clone 12CA5, Roche), Myc blots were probed with anti-Myc antibody

(clone 9E10, Roche), histone H3 blots were probed with anti-histone H3 (clone ab1791, Abcam), and histone H3K36me3 blots were probed with anti-histone H3K36me3 (clone ab9050, Abcam).

ChIP-seq Library Preparation and ChIP-seq Analysis

ChIP-seq has been described previously (Morselli et al., 2015) with the following modifications. 1% formaldehyde was added to 50 OD of yeast cells and gently rotated for 15 minutes at room temperature. 125mM glycine was then added to the cells and rotated for 5 minutes at room temperature to quench the crosslinking reaction. Cells were pelleted at 4°C at 4000 rpm and washed twice with 25 mL of ice-cold PBS. The pellet was resuspended in 400 μL of ice cold lysis buffer (50 mM HEPES pH 7.5, 140 mM NaCl, 1 mM EDTA, 1% Triton X-100, 0.1% sodium deoxycholate). An equal volume of 0.5 mm acid-washed glass beads was added, and the resuspension was placed in a cell disruptor at 4°C for 5 minutes. The lysates were then sonicated using a Covaris S2 programmed to run 16 cycles (total sonication time: 8 minutes, duty cycle: 5%, intensity: 5%). DNA was sonicated to an average size of 300 bp. Following sonication, the samples were centrifuged for 10 minutes at 4°C. The supernatant was collected, and 10 μL from each sample of the was collected for input and stored at −20°C. 50 μL of each sample was incubated overnight at 4°C with 4 μg of anti-H3K36me3 (clone ab9050, Abcam) or anti-RNAPII S2P (clone ab5095, Abcam). The samples were incubated for 2 hours at 4°C with Protein A Dynabeads (ThermoFisher Scientific). The beads were washed with low salt buffer (140 mM NaCl), high salt buffer (500 mM NaCl), LiCl buffer, and TE (10 mM Tris-HCl, pH 8.0, 1 mM EDTA) buffer. Beads were resuspended with elution buffer and incubated for 10 min at 65°C. Following elution, all tubes were incubated at 65°C overnight to reverse crosslinks. An RNase cocktail mix was added to all samples and incubated for 1 hour at 37°C. Proteinase K was added and the samples were incubated for 1 hour at 60°C. Sample were purified using 1.8 volumes of AMPure XP beads (Beckman Coulter). The real-time reaction was performed using iTaq Universal SYBR (Bio-Rad) on a CFX96 Real-Time PCR system (Bio-Rad). For ChIP-seq analysis, an Ovation Ultralow DR kit (NuGEN) was used to prepare the libraries using 1 ng of purified DNA. An Illumina HiSeq 4000 system was used for sequencing using 50 bp single-end reads. Reads were aligned to the sacCer3 (UCSC 2011) reference genome using Bowtie 0.12.8 (Langmead et al., 2009) with up to 2 mismatches. Peak calling was performed using Model-Based Analysis of ChIP-Seq (MACS2) (Zhang et al., 2008). A q-value cutoff of 0.05 was used when identifying significantly enriched regions of the genome using MACS2. Metagene profiles and heatmaps were generated using SeqPlots 3.7 (Stempor and Ahringer, 2016).

ChIP-qPCR Analysis

50 mL of log-phase yeast cells were crosslinked with 1% formaldehyde for 15 minutes at room temperature. The reaction was then quenched with 125mM glycine for 5 minutes at room temperature. Cells were pelleted and washed twice with 25 mL of ice-cold PBS and resuspended in 400 μL of lysis buffer (50 mM HEPES pH 7.5, 140 mM NaCl, 1 mM EDTA, 1% Triton X-100, 0.1% sodium deoxycholate). The cells were then lysed by bead beating at 4°C for 5 minutes. The lysates were then sonicated using a Branson Digital Sonifier to run 15 cycles (total sonication time: 7.5 minutes, amplification: 15%) to an average size of 300 bp. The samples were then clarified for 10 minutes at 4°C. 10 μL from each sample of the was collected for input and 700 μL was incubated overnight at 4°C with 4 μg of anti-HA (clone 12CA5, Roche). 50 μL of GammaBind G Sepharose beads (GE Healthcare) were added to each sample and incubated for 2 hours at 4°C. The beads were washed four times in lysis buffer and twice in TE. The washed beads were then resuspended with elution buffer and incubated for 10 min at 65°C. All samples were incubated at 65°C overnight to reverse crosslinks. RNase A (ThermoFisher Scientific) was added to all samples and incubated for 1 hour at 37°C. Proteinase K (Roche) was added and the samples were incubated for 1 hour at 60°C. Following proteinase K treatment, DNA was extracted by column purification. Purified DNA was used for qPCR analysis using gene-specific primers (Table S3). The real-time reaction was performed using iTaq Universal SYBR (Bio-Rad) on a CFX96 Real-Time PCR system (Bio-Rad).

RNA Immunoprecipitation

150 mL of log-phase yeast were pelleted and resuspended in 1 mL of lysis buffer with RiboLock RNase inhibitor (ThermoFisher Scientific) and protease inhibitors. An equal volume of acid-washed beads was added to the resuspension. The cells were then lysed in a cell disruptor for 5 minutes at 4°C. The lysate was then centrifugated at 13,000 rpm at 4°C for 20 minutes. 10 μL of clarified lysate was removed as input. 40 μL of Pierce anti-HA magnetic beads (ThermoFisher Scientific) was added to the 1 mL of clarified lysate and rotated at 4°C overnight. Beads were washed once with lysis buffer and three times with TBS 0.05% tween. Acidic elution was performed, and samples were neutralized with Tris-HCl pH 8.5. The samples were treated with DNase I (Roche) and acid phenol: chloroform extraction was performed to isolate immunoprecipitated RNA. cDNA was synthesized from the extracted RNA using the Maxima First Strand cDNA Synthesis Kit (ThermoFisher Scientific). qPCR analysis for pull-down of snRNAs and control RNAs was performed using iTaq Universal SYBR (Bio-Rad) on a CFX96 Real-Time PCR system (Bio-Rad). Primers for qPCR analysis are listed in Table S3.

Co-immunoprecipitation and crosslinked co-immunoprecipitation

150 mL of log-phase yeast were crosslinked in 1% formaldehyde for 15 minutes at room temperature and quenched in 125 mM glycine for 5 minutes at room temperature for the crosslinked co-immunoprecipitation. Non-crosslinked and crosslinked cultures were then pelleted and resuspended in 1 mL of lysis buffer with protease inhibitors. Acid-washed beads were added to the resuspension and samples were lysed in a cell disruptor for 5 minutes at 4°C. The lysates were centrifuged at 13,000 rpm at 4°C

for 20 minutes to remove the insoluble material. 1 mL of lysate was precleared with 50 μL of GammaBind G Sepharose beads (GE Healthcare). 10 μL of precleared lysate was removed as input. 4 μg of anti-HA antibody (clone: 12CA5, Roche) was added to the 700 μL of clarified lysate and rotated at 4°C overnight. Samples were incubated with 25 μL of GammaBind G Sepharose beads (GE Healthcare) for two hours at 4°C. Beads were then washed five times with lysis buffer and eluted by boiling with 2X SDS-PAGE loading buffer. Crosslinked samples were incubated at 95°C for 30 minutes to reverse crosslinks.

QUANTIFICATION AND STATISTICAL ANALYSIS

Data in bar graphs represent the average of at least 3 biological replicates. Error bars represent the standard error of the mean (SEM). P values were determined by 2-tailed unpaired Student's t test. *, $p \leq 0.05$; **, $p \leq 0.01$; ***, $p \leq 0.001$. Chi-square test was used in RNA-seq splicing analysis to determine the statistical significance of changes in SE in the mutants compared to wild-type. Spearman's rank correlation was used to measure the association of gene expression between wild-type and mutants. Statistical analyses were performed in Microsoft Excel (Version 1812) or Prism 7 (GraphPad).

DATA AND CODE AVAILABILITY

The accession number for the RNA-seq and ChIP-seq data reported in this paper is GEO: GSE120051.

Cell Reports, Volume *27*

Supplemental Information

H3K36 Methylation and the Chromodomain Protein Eaf3 Are Required for Proper Cotranscriptional Spliceosome Assembly

Calvin S. Leung, Stephen M. Douglass, Marco Morselli, Matthew B. Obusan, Marat S. Pavlyukov, Matteo Pellegrini, and Tracy L. Johnson

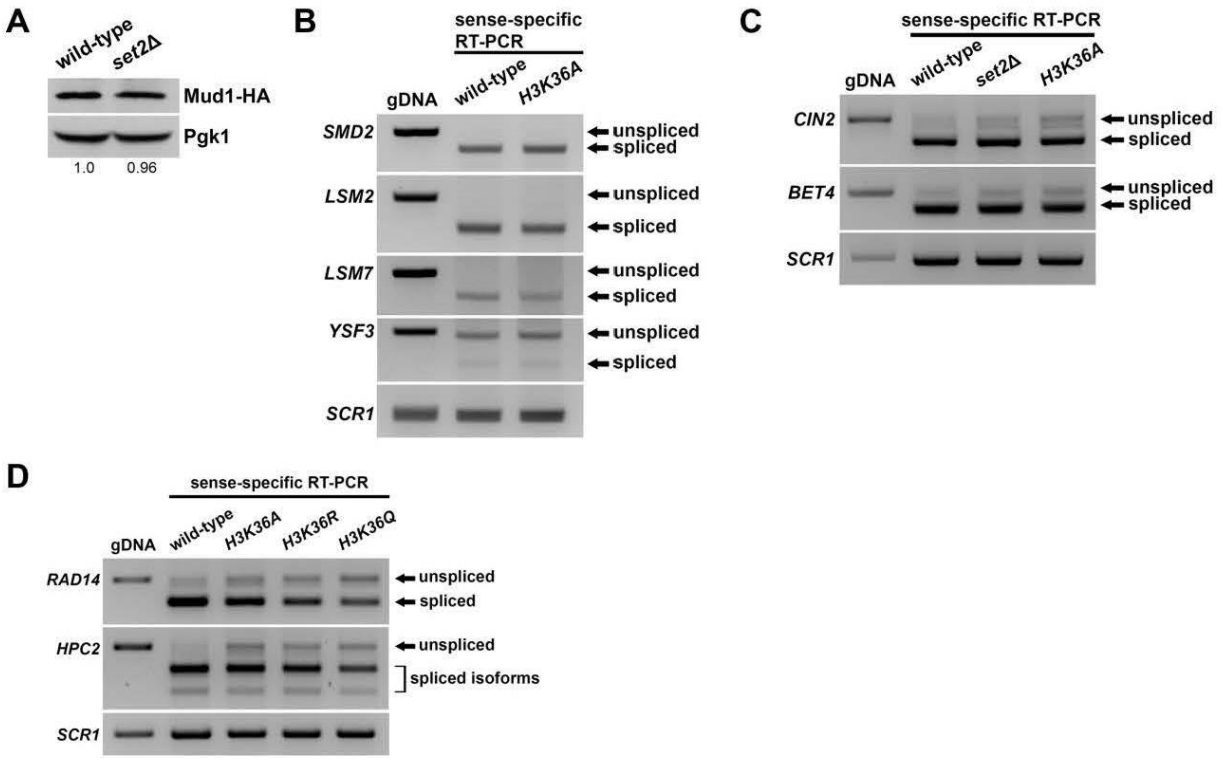

Figure S1. Splicing defects are observed in the absence of H3K36 methylation. Related to Figure 1. A. Western blot analysis of Mud1-HA protein levels in wild-type and *set2*Δ cells. Pgk1 is a loading control. Band intensities were quantified using ImageJ. The intensity of Mud1-HA normalized to Pgk1 in *set2*Δ was compared to the intensity of Mud1-HA normalized to Pgk1 in wild-type (defined as 1.0). **B.** RT-PCR of splicing factor ICGs. Products were analyzed on a 1.8% agarose gel. **C.** RT-PCR of ICGs that are lowly expressed and display a splicing defect in both *set2*Δ and *H3K36A* compared to wild-type. Products were analyzed on a 1.8% agarose gel. **D.** Splicing defects are observed in *H3K36R* and *H3K36Q* mutants. Products were analyzed on a 1.8% agarose gel. gDNA: genomic DNA. *SCR1* is a loading control.

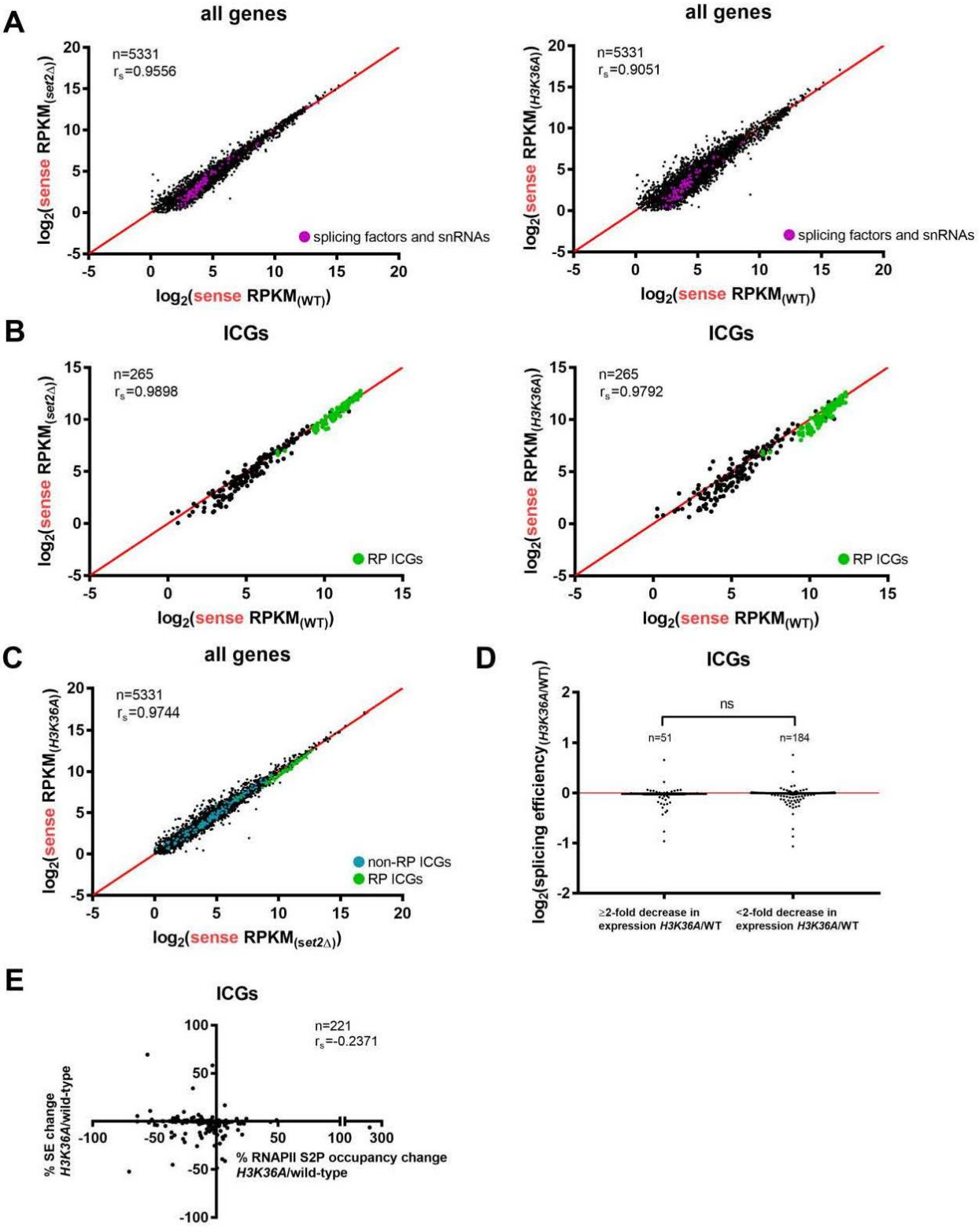
A
all genes
n=5331
r_s=0.9556
splicing factors and snRNAs
$\log_2$(sense RPKM$_{(set2\Delta)}$)
$\log_2$(sense RPKM$_{(WT)}$)
all genes
n=5331
r_s=0.9051
splicing factors and snRNAs
$\log_2$(sense RPKM$_{(H3K36A)}$)
$\log_2$(sense RPKM$_{(WT)}$)
B
ICGs
n=265
r_s=0.9898
RP ICGs
$\log_2$(sense RPKM$_{(set2\Delta)}$)
$\log_2$(sense RPKM$_{(WT)}$)
ICGs
n=265
r_s=0.9792
RP ICGs
$\log_2$(sense RPKM$_{(H3K36A)}$)
$\log_2$(sense RPKM$_{(WT)}$)
C
all genes
n=5331
r_s=0.9744
non-RP ICGs
RP ICGs
$\log_2$(sense RPKM$_{(H3K36A)}$)
$\log_2$(sense RPKM$_{(set2\Delta)}$)
D
ICGs
ns
n=51
n=184
$\log_2$(splicing efficiency$_{(H3K36A/WT)}$)
≥2-fold decrease in expression *H3K36A*/WT
<2-fold decrease in expression *H3K36A*/WT
E
ICGs
n=221
r_s=-0.2371
% SE change *H3K36A*/wild-type
% RNAPII S2P occupancy change *H3K36A*/wild-type

Figure S2. RNA expression profiles in *set2*Δ and *H3K36A* cells. Related to Figure 1. **A.** XY-scatter plot of wild-type sense RPKM, *set2*Δ sense RPKM (left), and *H3K36A* sense RPKM (right) of all genes. All splicing factors and spliceosomal snRNAs are labeled in purple. Spearman's correlation coefficient indicated. Red line represents the x=y line. **B.** XY-scatter plot of wild-type sense RPKM, *set2*Δ sense RPKM (left), and *H3K36A* sense RPKM (right) of all ICGs. Ribosomal protein intron-containing genes (RP ICGs) are labeled in green. Spearman's correlation coefficient indicated. **C.** XY-scatter plot of *set2*Δ sense RPKM and *H3K36A* sense RPKM of all ICGs. Non-ribosomal protein intron-containing genes (non-RP ICGs) are labeled in blue and ribosomal protein intron-containing genes (RP ICGs) are labeled in green. Spearman's correlation coefficient indicated. **D.** Scatter plot representing change in splicing efficiency (SE) of ICGs that show a ≥2-fold decrease in expression in *H3K36A* compared to wild-type and ICGs that show a <2-fold decrease in expression in *H3K36A* compared to wild-type. Solid black line represents the median. Red line represents the y=0 line. Unpaired t test was used to test significance. **E.** XY-scatter plot of % RNAPII S2P ChIP-seq occupancy change and % SE change of all ICGs in *H3K36A*/wild-type cells.

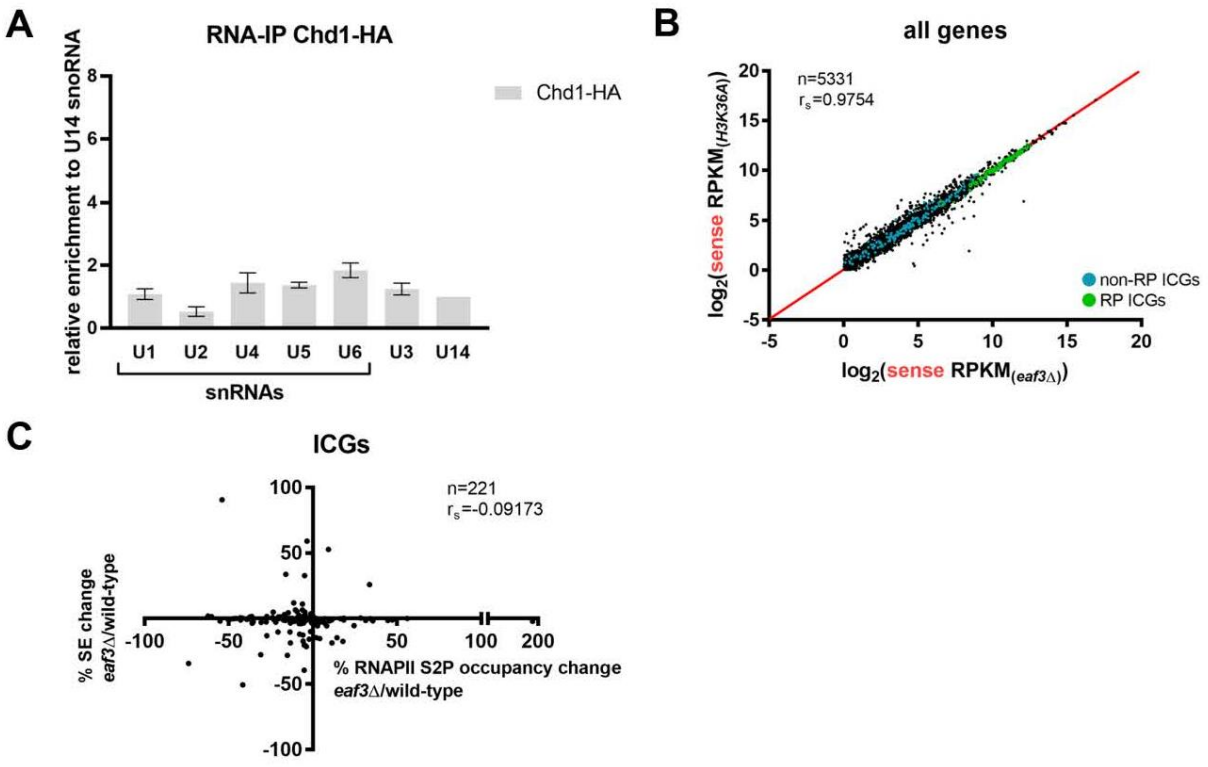

Figure S3. ***eaf3*Δ and *H3K36A* cells have similar RNA expression profiles. Related to Figure 2. A.** Spliceosomal snRNAs co-immunoprecipitated with Chd1-HA. Bar graph depicting the five spliceosomal snRNAs that are pulled-down with Chd1-HA in wild-type cells under non-crosslinking conditions. U3 and U14 are snoRNAs. Bars represent the average of 3 biological replicates. Error bars represent the standard error of the mean (SEM). **B.** XY-scatter plot of *eaf3*Δ sense RPKM and *H3K36A* sense RPKM of all genes. Non-ribosomal protein intron-containing genes (non-RP ICGs) are labeled in blue and ribosomal protein intron-containing genes (RP ICGs) are labeled in green. Spearman's correlation coefficient indicated. Red line represents the x=y line. **C.** XY-scatter plot of % RNAPII S2P ChIP-seq occupancy change and % SE change of all ICGs in *eaf3*Δ/wild-type cells.

Table S1. Strains used in this study. Related to STAR Methods.

Name	Genotype	Reference
BY4741	MATa his3Δ1 leu2Δ0 met15Δ0 ura3Δ0	Open Biosystems
TJY7170	MATa *set2*Δ::KANMX4 his3Δ1 leu2Δ0 met15Δ0 ura3Δ0	GE Dharmacon
TJY7152	MATa his3Δ200 leu2Δ0 lys2Δ0 trp1Δ63 ura3Δ0 met15Δ0 can1::MFA1pr-HIS3 hht1-hhf1::NatMX4 hht2-hhf2::[*H3K36A*-HHFS]*-URA3	GE Dharmacon
TJY7171	MATa *set2 SRI*Δ::HIS3 his3Δ1 leu2Δ0 met15Δ0 ura3Δ0	This study
TJY7153	MATa *eaf3*Δ::KANMX4 his3Δ1 leu2Δ0 met15Δ0 ura3Δ0	GE Dharmacon
TJY7158	MATa EAF3-HA::HIS3MX6 his3Δ1 leu2Δ0 met15Δ0 ura3Δ0	This study
TJY7159	MATa *set2*Δ::KANMX4 EAF3-HA:HIS3 his3Δ1 leu2Δ0 met15Δ0 ura3Δ0	This study
TJY7214	MATa PRP45-HA::KANMX6 his3Δ1 leu2Δ0 met15Δ0 ura3Δ0	This study
TJY7209	MATa PRP45-Myc::HIS3MX6 his3Δ1 leu2Δ0 met15Δ0 ura3Δ0	This study
TJY7216	MATa EAF3-HA::HIS3MX6 PRP45-Myc::HIS3MX6 his3Δ1 leu2Δ0 met15Δ0 ura3Δ0	This study
TJY7215	MATa *eaf3*Δ::KANMX4 PRP45-HA::HIS3MX6 his3Δ1 leu2Δ0 met15Δ0 ura3Δ0	This study
TJY7238	MATa *set2*Δ::KANMX4 PRP45-HA::HIS3MX6 his3Δ1 leu2Δ0 met15Δ0 ura3Δ0	This study
TJY7240	MATa PRP19-HA::HIS3MX6 his3Δ1 leu2Δ0 met15Δ0 ura3Δ0	This study
TJY7241	MATa *eaf3*Δ::KANMX4 PRP19-HA:HIS3 his3Δ1 leu2Δ0 met15Δ0 ura3Δ0	This study
TJY7242	MATa his3Δ200 leu2Δ0 lys2Δ0 trp1Δ63 ura3Δ0 met15Δ0 can1::MFA1pr-HIS3 hht1-hhf1::NatMX4 hht2-hhf2::[*H3K36R*-HHFS]*-URA3	GE Dharmacon
TJY7243	MATa his3Δ200 leu2Δ0 lys2Δ0 trp1Δ63 ura3Δ0 met15Δ0 can1::MFA1pr-HIS3 hht1-hhf1::NatMX4 hht2-hhf2::[*H3K36Q*-HHFS]*-URA3	GE Dharmacon
TJY7244	MATa MUD1-HA::KANMX4 his3Δ1 leu2Δ0 met15Δ0 ura3Δ0	This study
TJY7245	MATa *set2*Δ::KANMX4 MUD1-HA::HIS3MX6 his3Δ1 leu2Δ0 met15Δ0 ura3Δ0	This study
TJY7246	MATa CHD1-HA::KANMX4 his3Δ1 leu2Δ0 met15Δ0 ura3Δ0	This study

Table S3. Primer sequences used for RT-PCR, RT-qPCR, and ChIP-qPCR. Related to STAR Methods.

Name	Sequence (5′ to 3′)	Purpose
HPC2 sense	AACACCACCTCTTTTCATGGTACCA	RT-PCR
HPC2 F	CCTCCACGA CCATATTCAA ACGATTGG	RT-PCR
HPC2 R	GGAACCAGAAATTATAATGGGAGACGG	RT-PCR
RAD14 sense	TGTCAATTTCTTCAGTTTCTAGCCC	RT-PCR
RAD14 F	CGTAGTGAAGGTATCGAACGTAACGC	RT-PCR
RAD14 R	GTGTTAGTGTTAGCAAGCGCAGACG	RT-PCR
DYN2 sense	CGCCAGTGGACCGATATAGAAATAA	RT-PCR
DYN2 F	GGAAAGCCTCCAAAACTACTGCCAG	RT-PCR
DYN2 R	GAAAACTAAAAACGCCAGTGGACCG	RT-PCR
MUD1 sense	GGTAACGTCATTGTTTTGTAGCTTGT	RT-PCR
MUD1 F	CGGCCTCATCAAACCTAAAGAAACC	RT-PCR
MUD1 R	GAAACCGGTCTGCTTCTTCTTGAG	RT-PCR
YCL002C sense	TTATAGTTTTCCTTTTGGCAACCGTG	RT-PCR
YCL002C F	ATGCTTGTTA TTGTTCTGCAGGGC	RT-PCR
YCL002C R	AACTGCCTTAAAACCATCATGCAGC	RT-PCR
TFC3 sense	ACCAATTATGATTGACCCAATAGCC	RT-PCR
TFC3 F	GACGATTTATCCTGACGAACTCGTAC	RT-PCR
TFC3 R	CCTGATTTGGCAACTTCGAGAAGTA	RT-PCR
RPL14A sense	TTAAGCCTTAGCCAAAGCCTTCTTG	RT-PCR
RPL14A F	CAAGGCTTCTAACTGGAGATTAGTCG	RT-PCR
RPL14A R	CAATCTTCTTAGCCCAAGATGAAGC	RT-PCR
SCR1 sense/R	CACAATGTGCGAGTAAATCCTGATG	RT-PCR
SCR1 F	AAGGGATAGTTCTCTATTCCGCACC	RT-PCR
CIN2 sense	CTATAAGTAAGCGCGAAACAACTGC	RT-PCR
CIN2 F	GCTTAAGCATAAATGGACTTTACTGCG	RT-PCR
CIN2 R	GCTGAATCACCCTTCTCCAAGAC	RT-PCR
BET4 sense	CACTTATGCTGCTCCAGGAGATG	RT-PCR
BET4 F	ACTATAAAGCAGTAGGTCAGCAATG	RT-PCR
BET4 R	TCCAATAGACTTTGGGGTAATCCTTC	RT-PCR
YSF3 sense/R	CTACCTCTCTTCTCGTAAGTAGGCTT	RT-PCR
YSF3 F	GGTTATATTACACAATTCGAAACAGTGAAA	RT-PCR
LSM2 sense/R	TCTTTCAGTCATTACCTCCCTTCTGG	RT-PCR
LSM2 F	CAAGACTTTA GTTGACCAAG AAGTGGT	RT-PCR
SMD2 sense/R	ACTCAACAGGGGTTTTTAACACAACG	RT-PCR
SMD2 F	CGCCTTTGACAGTTGATTAGAGGAGT	RT-PCR
LSM7 sense/R	TATAGTACATCAGAACCTTCGGCGG	RT-PCR
LSM7 F	CAAAAAAACATGCATCAGCAACACTCC	RT-PCR
U1 F	ATTGAAGTCATTGATGCAAACTCCT	qPCR
U1 R	GGTGTCAAACTTCTCCAGGCAG	qPCR

U2 F	TATCGATGGGAAGAAATGGTGC	qPCR
U2 R	CTCTTGCAGCGCCACCAG	qPCR
U4 F	CGCATATCAGTGAGGATTCGTC	qPCR
U4 R	CCAAAAATTCCCTACATAGTCTTGAAGTA	qPCR
U5 F	TACAGATCAATGGCGGAGGG	qPCR
U5 R	AAATATGGCAAGCCCACAGTAAC	qPCR
U6 F	AAGTAACCCTTCGTGGACATTTG	qPCR
U6 R	TCTCTTTGTAAAACGGTTCATCCTTAT	qPCR
U3 F	CAAAAGAGCCACTGAATCCAACT	qPCR
U3 R	TAGATGGCCGAACCGCTAAG	qPCR
U14 F	GGTGATGAAAGACTGGTTCCTTA	qPCR
U14 R	AAGGTCTCTAAAGAAGAGCGGTC	qPCR
HPC2 1 F	ACCTCCACGACCATATTCAAACG	ChIP-qPCR
HPC2 1 R	CCCTAACGAAGGGCGGATAATTG	ChIP-qPCR
HPC2 2 F	TTCCTCCAGTACAAACCCGATGG	ChIP-qPCR
HPC2 2 R	ATCACGGGGGATGGTGAATG	ChIP-qPCR
HPC2 3 F	CTCCAGCAAAAAGCCTACGTCTG	ChIP-qPCR
HPC2 3 R	TCTTGGTCGTTGTTGGCTTTGG	ChIP-qPCR
HPC2 4 F	TCTCCGAAGAAGAAGTCGCATCC	ChIP-qPCR
HPC2 4 R	CCGAATCATCAATGAACGGATCTTC	ChIP-qPCR
RAD14 1 F	GTATCGAACGTAACGCTATGACTCC	ChIP-qPCR
RAD14 1 R	ACCCACGGTTAAAATACAAACACAG	ChIP-qPCR
RAD14 2 F	GGCAGCAATCGGGATGATAATG	ChIP-qPCR
RAD14 2 R	TGTTAGTGTTAGCAAGCGCAGACG	ChIP-qPCR
RAD14 3 F	TGCACCTCCTCCAGAGCATATTTC	ChIP-qPCR
RAD14 3 R	CATCATGTAGCACAGGATCCATCTC	ChIP-qPCR
RAD14 4 F	AATGGCAACGTCGTGAAGAAGG	ChIP-qPCR
RAD14 4 R	GCTCTTGTTTTCAGTCGCATTTCC	ChIP-qPCR
ECM33 1 F	AAGAGGAAACGGGTTTCGAG	ChIP-qPCR
ECM33 1 R	ACTCGCCCTAATCCTATGACAG	ChIP-qPCR
ECM33 2 F	ACCAGTGCTTCTTTCGGTTC	ChIP-qPCR
ECM33 2 R	GGTAGAAATGGCAGGCAAAG	ChIP-qPCR
ECM33 3 F	AGGCCGCTTTCAGTAACTTG	ChIP-qPCR
ECM33 3 R	ACTTCAATGGCACCACCAAC	ChIP-qPCR
ECM33 4 F	TAGTGGTGATGCCTCCAATG	ChIP-qPCR
ECM33 4 R	TGGAACAAGTTCTGGAGCAG	ChIP-qPCR
ADH1 1 F	TGGTGTCTGTCACACTGACTTG	ChIP-qPCR
ADH1 1 R	TTCGTGACCACCGACTAATG	ChIP-qPCR
ADH1 2 F	TCACGCTGACTTGTCTGGTTAC	ChIP-qPCR
ADH1 2 R	AATGTGAGCGGCTTGAACAG	ChIP-qPCR
ADH1 3 F	TTGACGGTGGTGAAGGTAAG	ChIP-qPCR
ADH1 3 R	CACCGACAATGTCCTTTTCC	ChIP-qPCR
ADH1 4 F	TCAACCAAGTCGTCAAGTCC	ChIP-qPCR
ADH1 4 R	TCTGGCGAAGAAGTCCAAAG	ChIP-qPCR

CHAPTER 3:

The role of splicing on H3K36me3 in *S. cerevisiae*.

INTRODUCTION

Spliceosome assembly occurs co-transcriptionally while the pre-mRNA is still tethered to the chromatin template by RNAPII. The basic repeat unit of chromatin is the nucleosome which is composed of DNA wrapped around an octamer of the core histones H2A, H2B, H3, and H4. Histones can be posttranslationally modified at their N-terminal ends and these modifications can regulate chromatin compaction and gene transcription (Kouzarides, 2007). Several studies have revealed that there is a link between nucleosome positioning and exon-intron structure, where nucleosome occupancy is higher on exons than in introns (Andersson et al., 2009; Schwartz et al., 2009; Spies et al., 2009; Tilgner et al., 2009). Additionally, certain histone modifications are preferentially found on exons. For example, in human, mouse, and worms, internal exons are enriched for H3K36 trimethylation (H3K36me3), suggesting that this histone modification marks exons at the chromatin level (Andersson et al., 2009; Kolasinska-Zwierz et al., 2009; Spies et al., 2009). Interestingly, H3K36me3 is enriched on constitutive exons compared to alternative exons (Kolasinska-Zwierz et al., 2009).

H3K36 co-transcriptionally methylated by the histone methyltransferase Set2/Setd2 (Krogan et al., 2003; Li et al., 2002; Strahl et al., 2002; Wagner and Carpenter, 2012). H3K36me3 is enriched in the mid- to 3′ coding region of genes and is a highly-conserved transcription-correlated histone mark (Barski et al., 2007; Weiner et al., 2015). Set2 interacts the C-terminal domain (CTD) of RNA polymerase II (RNAPII) via its Set2 Rpb1 interacting domain (SRI) when Ser2 of the CTD is phosphorylated and this interaction is necessary for the methylation of H3K36 (Kizer et al., 2005; Li et al., 2003; Xiao et al., 2003). Set2 and its associated chromatin mark, H3K36 methylation (H3K36me), has been implicated in affecting many functions in the nucleus including transcription, DNA damage repair, and RNA splicing (McDaniel and Strahl, 2017).

Studies in mammals have revealed that loss of H3K36me modulates alternative splicing (Guo et al., 2014; Luco et al., 2010; Simon et al., 2014). More recently, H3K36me was found to affect constitutive splicing genome-wide in *S. cerevisiae* via recruitment of the chromodomain protein Eaf3 and the splicing factor Prp45 (Leung et al., 2019). These past studies have focused on a "how chromatin affects splicing" model whereby the chromatin state regulates splicing locally. However, because splicing and transcription are tightly coordinated, a key question is how splicing affects the state of the chromatin. Specifically, because histone-modifying proteins have no DNA sequence specificity, what targets these modifiers to specific sites in different contexts? A non-mutually exclusive model is that co-transcriptional spliceosome assembly and splicing can affect chromatin via recruitment of chromatin modifiers. Interestingly, a study by the Bentley group suggested that globally inhibiting splicing with spliceostatin A (SSA) affects proper establishment and maintenance of H3K36me3 levels in mammals (Kim et al., 2011). Addition of SSA to cells redistributes H3K36me3 from the 5′ to 3′ end of genes (Kim et al., 2011). Another report shows that splicing inhibition by addition of meayamycin or knockdown of splicing factor SAP130 reduces H3K36me3 and Setd2 recruitment to intron-containing genes (ICGs) (de Almeida et al., 2011). These two studies suggest that there may be a splicing and histone modification feedback loop that reinforces efficient splicing.

Here, we show that in *S. cerevisiae*, ICGs are enriched for H3K36me3 compared to intronless genes. Furthermore, we show that upon splicing inhibition using a temperature sensitive *PRP45* mutant (*prp45*(1-169)), there is a shift in H3K36me3 to the 3′ end of an ICG. This chapter will explore the functional implications of these observations in splicing and highlight future experiments that will further elucidate how splicing affects the state of chromatin.

RESULTS AND DISCUSSION

We first investigated whether ICGs were enriched in the histone modification H3K36me3. We performed ChIP-seq on H3K36me3 and performed metagene analysis of H3K36me3 to compare occupancy in ICGs and intronless genes genome-wide (Figure 3.1). Genes were aligned from their annotated transcription start site (TSS) to their transcription termination site (TTS). The metagene plots also included 500 nucleotides (nt) upstream and downstream of their TSS and TTS, respectively. We observe that levels of H3K36me3 are low at the TSS and peak toward the 3′ end of ICGs and intronless genes (Figure 3.1). Interestingly, levels of H3K36me3 are higher in ICGs compared to intronless genes, especially towards the 3′ end (Figure 3.1). This result suggests that placement of H3K36me3 on chromatin not only depends on transcription, but also by splicing. Although ICGs are enriched for H3K36me3, our previous results discussed in Chapter 2 showed that only a subset of ICGs depend on Set2 and H3K36me for splicing. This may be because these ICGs tend to be lowly expressed and therefore need more “support” for efficient splicing, while highly expressed ICGs have strong local concentrations of the spliceosome at their loci and may not depend on H3K36me for its efficient splicing.

It was observed that when splicing is inhibited with the splicing inhibitor SSA in mammalian cells, there is a global redistribution of H3K36me3 away from the 5′ end of ICGs toward the 3′ end, although the purpose of this repositioning has been unclear (Kim et al., 2011). We hypothesized that a similar redistribution of H3K36me3 may occur in budding yeast as well when splicing in inhibited. To begin to address this, we generated the temperature-sensitive mutant *prp45*(1-169) as previously described and characterized (Gahura et al., 2009) and confirmed that this mutant has a severe splicing defect at 37°C by performing RT-PCR on ICGs; an example is shown in Figure 3.2A. We then performed ChIP-qPCR of H3K36me3 on the gene *ECM33* before and after shifting the strain to its non-permissive temperature of 37°C. *ECM33* was chosen because its long second exon allows resolution of changes in the 3′ end of the gene. In wild-type cells at 37°C, H3K36me3 is low at the 5′ end of the ICG *ECM33* but increases towards the 3′ end

(Figure 3.2B). Interestingly, we observe a shift in H3K36me3 from the 5′ to 3′ end of *ECM33* in the *prp45*(1-169) at 37°C (Figure 3.2B). This result suggests that when splicing is inhibited using the temperature-sensitive mutant, normal levels and positioning of H3K36me3 is changed.

Together, these results suggest that there may be a role for splicing in the establishment of normal levels and location of H3K36me3 on ICGs. We demonstrate that ICGs are enriched for H3K36me3, raising the possibility that the splicing machinery may recruit Set2 to these genes (Figure 3.1). Our previous study revealed that H3K36me recruits the splicing machinery to the chromatin (Leung et al., 2019). This leads to a model where Set2 is recruited to ICGs by Ser2-P RNAPII, where it can then co-transcriptionally deposit its H3K36me3 mark. Likely through a network of protein-protein interactions, spliceosome recruitment then enhances H3K36me3 at ICGs. Intriguingly, we also observe a shift in H3K36me3 toward the 3′ end of an actively transcribed gene when splicing is inhibited (Figure 3.2B). This redistribution of H3K36me3 could be correlated with quality control of splicing. For example, shifts in H3K36me3 may be a signal for disassembly factors to release stalled spliceosomes and discard the unspliced RNA. This possibility will be explored in more detail in Chapter 4.

Future studies are needed to further characterize the molecular details of the interaction between the splicing machinery and H3K36me3. We plan to perform a genome-wide survey of H3K36me3 upon splicing inhibition by ChIP-seq. To efficiently inhibit splicing, we will employ an auxin-inducible degron (AID) system to specifically and rapidly degrade Prp45 to inhibit splicing. The AID system is a powerful tool for altering protein levels rapidly, and has been used previously to deplete splicing factors (Maudlin and Beggs, 2019; Mendoza-Ochoa et al., 2019). As another approach to inhibit splicing, we will also use pladienolide B to block splicing by inhibiting SF3B1. Pladienolide B has been used previously to inhibit splicing in yeast (Hansen et al., 2019). These experiments will allow us to assay how H3K36me3 positioning changes globally on ICGs and

intronless genes. In addition, we can perform ChIP-seq on late splicing factors to determine whether there are defects in release of these factors.

MATERIALS AND METHODS

H3K36me3 metagene analysis

H3K36me3 ChIP-seq was performed as previously described (Leung et al., 2019). H3K36me3 metagene profiles were generated using SeqPlots 3.7 (Stempor and Ahringer, 2016). The accession number for the H3K36me3 data is GEO: GSE120051. Genes used in this analysis are all intron-containing genes in *S. cerevisiae*.

RNA isolation and RT-PCR

RNA isolation was performed as previously described (Ares, 2012). Briefly, wild-type and *prp45*(1-169) cells were grown at 30°C to an OD_{600} of 0.6. The cultures were then temperature shifted from 30°C to 37°C for 2 hours. Cells were pelleted and RNA was isolated by hot phenol:chloroform extraction followed by ethanol precipitation. Isolated RNA was treated with DNase (Roche) and cDNA was generated using the Maxima First Strand cDNA Synthesis Kit (ThermoFisher Scientific). Splicing analysis was performed using gene-specific primers as previously described (Leung et al., 2019).

ChIP-qPCR

ChIP-qPCR was performed as previously reported (Leung et al., 2019). Briefly, wild-type and *prp45*(1-169) cells were grown at 30°C to an OD_{600} of 0.6. The cultures were then temperature shifted to 37°C for 2 hours. Following the temperature shift, the cells were then crosslinked with 1% formaldehyde for 15 minutes and quenched with 125 mM glycine for 5 minutes. Cells were pelleted and washed with 1X PBS. Cells were lysed and DNA was sonicated to an average length of 300 nt. Sonicated lysates were incubated with anti-H3K36me3 antibody (Abcam) overnight at

4°C. GammaBind G Beads (GE Healthcare) were added to the samples for 2 hours at 4°C. Beads were washed four times in lysis buffer and twice in TE. Beads were then resuspended in elution buffer and eluted sample was incubated overnight at 65°C to reverse crosslinks. Following incubation with with RNase A (ThermoFisher) and Proteinase K (Roche), DNA was eluted by column purification. qPCR with gene-specific primers was performed using iTaq Universal SYBR (Bio-Rad). Gene-specific primers for *ECM33* and the non-transcribed region have been described previously (Leung et al., 2019).

FIGURES

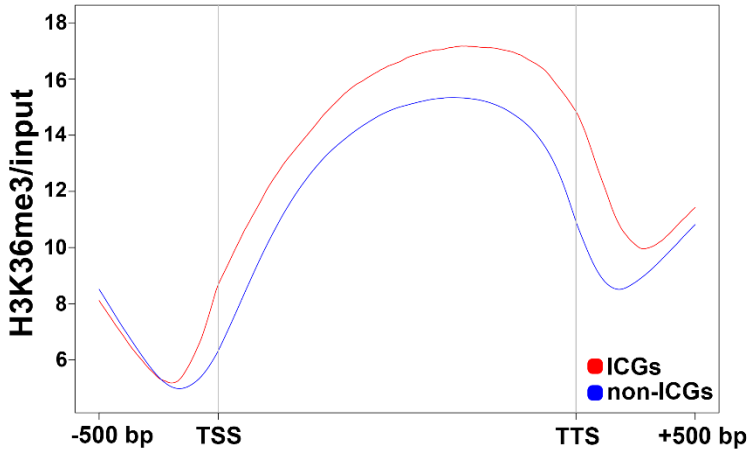

Figure 3.1. H3K36me3 is enriched in ICGs. Metagene plot of H3K36me3 on all ICGs and non-ICGs from 500 bp upstream of the transcription start site (TSS) to 300 bp downstream of the transcription termination site (TTS).

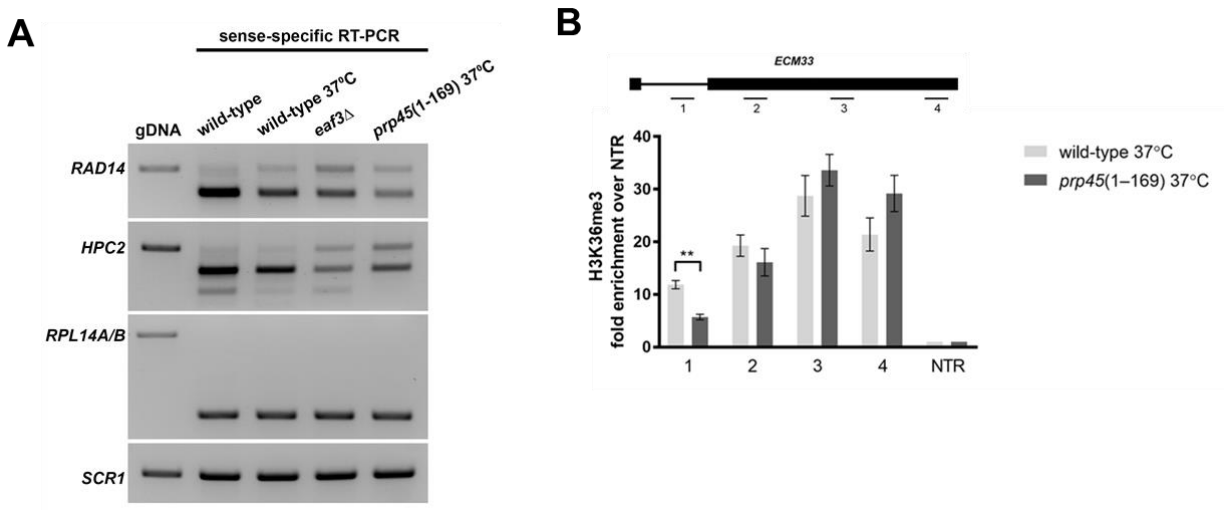

Figure 3.2. Splicing inhibition affects H3K36me3 levels. A. RT-PCR analysis of wild-type 30°C, wild-type 37°C, *eaf3*Δ 30°C and *prp45*(1-169) 37°C. Products were run on a 1.8% gel. **B.** Occupancy of H3K36me3 on *ECM33* relative to a non-transcribed region (NTR) on Chr. V in wild-type (light grey bars) and *prp45*(1-169) (dark grey bars). Bars represent an average of three biological replicates. Error bars represent the standard error of the mean (SEM). Student's t test was used to test for significance.

REFERENCES

Andersson, R., Enroth, S., Rada-Iglesias, A., Wadelius, C., and Komorowski, J. (2009). Nucleosomes are well positioned in exons and carry characteristic histone modifications. Genome Res *19*, 1732-1741.

Ares, M. (2012). Isolation of total RNA from yeast cell cultures. Cold Spring Harb Protoc *2012*, 1082-1086.

Barski, A., Cuddapah, S., Cui, K., Roh, T.Y., Schones, D.E., Wang, Z., Wei, G., Chepelev, I., and Zhao, K. (2007). High-resolution profiling of histone methylations in the human genome. Cell *129*, 823-837.

de Almeida, S.F., Grosso, A.R., Koch, F., Fenouil, R., Carvalho, S., Andrade, J., Levezinho, H., Gut, M., Eick, D., Gut, I.*, et al.* (2011). Splicing enhances recruitment of methyltransferase HYPB/Setd2 and methylation of histone H3 Lys36. Nat Struct Mol Biol *18*, 977-983.

Gahura, O., Abrhámová, K., Skruzný, M., Valentová, A., Munzarová, V., Folk, P., and Půta, F. (2009). Prp45 affects Prp22 partition in spliceosomal complexes and splicing efficiency of non-consensus substrates. J Cell Biochem *106*, 139-151.

Guo, R., Zheng, L., Park, J.W., Lv, R., Chen, H., Jiao, F., Xu, W., Mu, S., Wen, H., Qiu, J.*, et al.* (2014). BS69/ZMYND11 reads and connects histone H3.3 lysine 36 trimethylation-decorated chromatin to regulated pre-mRNA processing. Mol Cell *56*, 298-310.

Hansen, S.R., Nikolai, B.J., Spreacker, P.J., Carrocci, T.J., and Hoskins, A.A. (2019). Chemical Inhibition of Pre-mRNA Splicing in Living Saccharomyces cerevisiae. Cell Chem Biol *26*, 443-448 e443.

Kim, S., Kim, H., Fong, N., Erickson, B., and Bentley, D.L. (2011). Pre-mRNA splicing is a determinant of histone H3K36 methylation. Proc Natl Acad Sci U S A *108*, 13564-13569.

Kizer, K.O., Phatnani, H.P., Shibata, Y., Hall, H., Greenleaf, A.L., and Strahl, B.D. (2005). A novel domain in Set2 mediates RNA polymerase II interaction and couples histone H3 K36 methylation with transcript elongation. Mol Cell Biol *25*, 3305-3316.

Kolasinska-Zwierz, P., Down, T., Latorre, I., Liu, T., Liu, X.S., and Ahringer, J. (2009). Differential chromatin marking of introns and expressed exons by H3K36me3. Nat Genet *41*, 376-381.

Kouzarides, T. (2007). Chromatin modifications and their function. Cell *128*, 693-705.

Krogan, N.J., Kim, M., Tong, A., Golshani, A., Cagney, G., Canadien, V., Richards, D.P., Beattie, B.K., Emili, A., Boone, C.*, et al.* (2003). Methylation of histone H3 by Set2 in Saccharomyces cerevisiae is linked to transcriptional elongation by RNA polymerase II. Mol Cell Biol *23*, 4207-4218.

Leung, C.S., Douglass, S.M., Morselli, M., Obusan, M.B., Pavlyukov, M.S., Pellegrini, M., and Johnson, T.L. (2019). H3K36 Methylation and the Chromodomain Protein Eaf3 Are Required for Proper Cotranscriptional Spliceosome Assembly. Cell Rep *27*, 3760-3769 e3764.

Li, B., Howe, L., Anderson, S., Yates, J.R., 3rd, and Workman, J.L. (2003). The Set2 histone methyltransferase functions through the phosphorylated carboxyl-terminal domain of RNA polymerase II. J Biol Chem *278*, 8897-8903.

Li, J., Moazed, D., and Gygi, S.P. (2002). Association of the histone methyltransferase Set2 with RNA polymerase II plays a role in transcription elongation. J Biol Chem *277*, 49383-49388.

Luco, R.F., Pan, Q., Tominaga, K., Blencowe, B.J., Pereira-Smith, O.M., and Misteli, T. (2010). Regulation of alternative splicing by histone modifications. Science *327*, 996-1000.

Maudlin, I.E., and Beggs, J.D. (2019). Spt5 modulates co-transcriptional spliceosome assembly in Saccharomyces cerevisiae. RNA.

McDaniel, S.L., and Strahl, B.D. (2017). Shaping the cellular landscape with Set2/SETD2 methylation. Cell Mol Life Sci *74*, 3317-3334.

Mendoza-Ochoa, G.I., Barrass, J.D., Terlouw, B.R., Maudlin, I.E., de Lucas, S., Sani, E., Aslanzadeh, V., Reid, J.A.E., and Beggs, J.D. (2019). A fast and tuneable auxin-inducible degron for depletion of target proteins in budding yeast. Yeast *36*, 75-81.

Schwartz, S., Meshorer, E., and Ast, G. (2009). Chromatin organization marks exon-intron structure. Nat Struct Mol Biol *16*, 990-995.

Simon, J.M., Hacker, K.E., Singh, D., Brannon, A.R., Parker, J.S., Weiser, M., Ho, T.H., Kuan, P.F., Jonasch, E., Furey, T.S.*, et al.* (2014). Variation in chromatin accessibility in human kidney cancer links H3K36 methyltransferase loss with widespread RNA processing defects. Genome Res *24*, 241-250.

Spies, N., Nielsen, C.B., Padgett, R.A., and Burge, C.B. (2009). Biased chromatin signatures around polyadenylation sites and exons. Mol Cell *36*, 245-254.

Stempor, P., and Ahringer, J. (2016). SeqPlots - Interactive software for exploratory data analyses, pattern discovery and visualization in genomics. Wellcome Open Res *1*, 14.

Strahl, B.D., Grant, P.A., Briggs, S.D., Sun, Z.W., Bone, J.R., Caldwell, J.A., Mollah, S., Cook, R.G., Shabanowitz, J., Hunt, D.F.*, et al.* (2002). Set2 is a nucleosomal histone H3-selective methyltransferase that mediates transcriptional repression. Mol Cell Biol *22*, 1298-1306.

Tilgner, H., Nikolaou, C., Althammer, S., Sammeth, M., Beato, M., Valcárcel, J., and Guigó, R. (2009). Nucleosome positioning as a determinant of exon recognition. Nat Struct Mol Biol *16*, 996-1001.

Wagner, E.J., and Carpenter, P.B. (2012). Understanding the language of Lys36 methylation at histone H3. Nat Rev Mol Cell Biol *13*, 115-126.

Weiner, A., Hsieh, T.H., Appleboim, A., Chen, H.V., Rahat, A., Amit, I., Rando, O.J., and Friedman, N. (2015). High-resolution chromatin dynamics during a yeast stress response. Mol Cell *58*, 371-386.

Xiao, T., Hall, H., Kizer, K.O., Shibata, Y., Hall, M.C., Borchers, C.H., and Strahl, B.D. (2003). Phosphorylation of RNA polymerase II CTD regulates H3 methylation in yeast. Genes Dev *17*, 654-663.

CHAPTER 4:

Characterizing the role of DEAH-box ATPase Prp43 in determining splicing outcomes.

INTRODUCTION

Pre-mRNA splicing and transcription both take place in close proximity to chromatin structure and are closely linked (Alpert et al., 2017; Merkhofer et al., 2014). snRNP and non-snRNP proteins have been shown to be recruited to pre-mRNA as it is being actively transcribed by RNAPII in both yeast and mammalian cells and splicing catalysis occurs before transcription termination (Alpert et al., 2017; Oesterreich et al., 2016). Because splicing and transcription are tightly coupled, perturbation of RNA polymerase II (RNAPII) elongation rates can affect constitutive and alternative splicing (de la Mata et al., 2003; Howe et al., 2003; Lacadie et al., 2006). Additionally, the carboxy terminal domain (CTD) of RNAPII has been suggested to recruit splicing factors to sites of transcription (Misteli and Spector, 1999; Nojima et al., 2018).

There is also strong evidence that changes to chromatin affect splicing (Hnilicová and Staněk, 2011). In eukaryotic cell nuclei, histones compact and structure DNA into nucleosomes, and the histone tails are posttranslationally modified to affect chromatin structure and function (Kouzarides, 2007). In mammals, nucleosomes are preferentially positioned over internal exons independent of transcription level and certain histone modifications are more prevalent on exons compared to introns (Andersson et al., 2009). Recent studies have also revealed that histone modifications are involved in recruiting the splicing machinery to chromatin (Leung et al., 2019; Luco et al., 2010; Sims et al., 2007).

Remarkably, purification of chromatin-associated RNA fractions from cells has allowed for the genome-wide study of chromatin-associated transcripts. In a recent study, high-throughput sequencing of chromatin-associated RNA revealed accumulation of fully transcribed and partially unspliced transcripts still bound to chromatin, suggesting that the transcripts are bound to the chromatin until they are fully spliced (Bhatt et al., 2012). However, it is not clear how the spliceosome remains associated with the chromatin until splicing is completed.

Prp43: a DEAH-box spliceosomal disassembly factor.

Prp43 is an essential DEAH-box RNA ATPase that is involved the late stages of splicing in *S. cerevisiae*. Prp43 is required for the ATP-dependent release of the lariat-intron and the disassembly of the post-splicing complex (Arenas and Abelson, 1997). The G-patch protein Ntr1/Spp382 is required for activation of the ATPase activity of Prp43. Ntr1/Spp382 binds to Prp43 *in vivo* and stimulates its RNA unwinding activity *in vitro*, although the actual substrate(s) for the Prp43-driven unwinding activity are not known (Tsai et al., 2007).

Intriguingly, Prp43 not only promotes spliceosome disassembly after optimal pre-mRNA splicing, but also participates in the dissociation of spliceosomes stalled with suboptimal substrates at both the first and second catalytic steps of splicing, indicating that Prp43 plays an important role in proofreading and fidelity in splicing (Koodathingal et al., 2010; Mayas et al., 2010). Prp43 is required for the release of pre-mRNA rejected by Prp16 and splicing intermediates prior to 5′ splice cleavage (Koodathingal et al., 2010). Prp43 also discards suboptimal intermediates that have been stalled in the DEAH-box Prp22-mediated rejection pathway (Mayas et al., 2010). Hence, Prp43 is responsible for entry into the non-reversible discard pathway and couples discard to rejection (Figure 4.1). However, the role of Prp43 in this discard pathway in the context of co-transcriptional splicing is not known.

Because of its role in spliceosome disassembly and in the non-reversible RNA discard pathway, Prp43 is an interesting target in the regulation of splicing. Recent studies show that the second step of pre-mRNA splicing is highly regulated. For example, in fission yeast Prp43 has been shown to be not only involved in the discard of suboptimal or defective substrates, but also in the release of the functional telomerase RNA product, generated from release of RNA before the second catalytic step (Chen et al., 2014). Moreover, in mammals it is known that almost all pre-mRNA splicing occurs while the transcript is still attached to the chromatin, so the timing of

the release of the product is critical (Bhatt et al., 2012). Interestingly, there is a recent report that splicing factors that drive energy-dependent spliceosome rearrangements (such as EFTUD2) during splicing are bound directly to chromatin (Guo et al., 2014). In *S. cerevisiae*, high-throughput studies hint at potential physical interactions between Prp43 and chromatin and chromatin-associated proteins, such as the core histones, H2A.Z, and components of the SWI/SNF complex (Lebaron et al., 2005). Furthermore, a recent report from our lab showed that in the absence of the histone variant H2A.Z in *S. cerevisiae*, transcription elongation and spliceosome kinetics are disrupted creating an environment whereby Prp43 can disassemble stalled spliceosomes (Neves et al., 2017). These observations lead to a model whereby Prp43 interacts either directly or indirectly with chromatin to disassemble spliceosomes following optimal or defective splicing and that splicing fidelity is compromised when Prp43 is not associated with nucleosomes.

Here, we show Prp43 physically interacts with chromatin and that this interaction is not dependent on the presence of RNA. We also show that Set2 and its associated chromatin mark, H3K36me3, are important for Prp43's interaction with chromatin. Additionally, decreased expression of intron-containing genes (ICGs) abrogates the interaction between Prp43 and chromatin. The interaction between Prp43 and its splicing cofactor Ntr1/Spp382 decreases as well, suggesting that Prp43's splicing function is important for its interaction with chromatin and vice versa. Further studies will be done to elucidate the role of chromatin in regulating Prp43's function in the discard pathway when splicing is slow or inhibited.

RESULTS

Prp43 shows RNA-independent interaction with Histone H3.

If Prp43 facilitates disassembly of spliceosomes co-transcriptionally, we predicated that Prp43 may associate with chromatin. We first endogenously HA-tagged Prp43 in a haploid yeast strain (Prp43-3HA). Exponentially growing cells from the Prp43-3HA strain were lysed and the soluble

proteins were separated from the chromatin-enriched insoluble pellet by centrifugation at 15,000 x g. Previous studies showed that, because of their high molecular weight, the chromatin fibers migrate with the pellet (Kai et al., 2001; Li and Stern, 2005). Western blot analysis of the fractions with an anti-Histone H3 antibody confirmed that the insoluble pellet was chromatin-enriched compared to the supernatant (Figure 4.2A). Western blotting of the fractions with an anti-HA antibody showed that Prp43 is present in both the soluble and insoluble fractions (Figure 4.2A). Due to its role in the final maturation steps of rRNA in the cytoplasm, it was not surprising to detect Prp43 in the soluble fraction (Pertschy et al., 2009). Pgk1, a highly soluble protein that localizes to the cytoplasm, was immunoblotted to confirm proper separation of soluble and insoluble proteins (Figure 4.2A). These data suggest that Prp43 is associated with the insoluble chromatin pellet.

Due to the co-transcriptional nature of splicing, however, it is possible that Prp43 is present in the chromatin-enriched fraction because it interacts either directly or indirectly with the elongating pre-mRNA undergoing splicing on the chromatin. To address this, we performed a co-immunoprecipitation (co-IP) experiment between Histone H3 and Prp43. Exponentially growing cells from the Prp43-3HA strain were lysed and the whole cell extract (WCE) was subjected to micrococcal nuclease (MNase) digestion to release soluble chromatin. WCEs were then treated with RNase A and RNase T1 for 30 minutes at 37°C to degrade RNA present in the extracts. An anti-Histone H3 antibody was used to immunoprecipitate bulk chromatin from the cell lysates and co-precipitating proteins were then detected by Western blotting. Prp43-3HA was observed to co-precipitate with Histone H3, and that this interaction persists under RNase conditions, suggesting that this interaction occurs even in the absence of RNA (Figure 4.2B)

Prp43's interaction with chromatin is stimulated by Set2 and its chromatin mark H3K36me3.

Histone marks have been shown to affect splicing and mediate interactions between splicing factors and histones (Hnilicová and Staněk, 2011). Although less than 5% of all genes in *S. cerevisiae* contain an intron, ICGs account for almost one-third of total cellular transcription (Ares et al., 1999). We hypothesized that chromatin marks associated with active transcription (i.e. H3K36me3) may direct recruitment of Prp43 to actively transcribed ICGs, which are enriched for H3K36me3 (Leung et al., 2019). We prepared WCEs from wild-type and *set2*Δ cells and separated the soluble from the chromatin-enriched insoluble fraction by high-speed centrifugation as described above. We then probed for Prp43-3HA in each fraction by Western blotting (Figure 4.3A). Prp43-3HA is de-enriched in the insoluble pellet in *set2*Δ cells decreases compared to wild-type cells (Figure 4.3A). To complement this analysis, we immunoprecipitated H3K36me3, the chromatin mark associated with Set2, in wild-type cells and observe that Prp43-3HA coimmunoprecipitates with H3K36me3 marked chromatin (Figure 4.3B). In addition, when we repeat the Histone H3–Prp43-3HA co-IP experiment in *set2*Δ cells, we observe that interaction between Histone H3 and Prp43-3HA decreases compared to wild-type (Figure 4.3C). This decrease in interaction between Prp43 and Histone H3 may be due a decrease in ICG expression in *set2*Δ cells. However, we have previously shown that expression of ICGs do not change significantly in *set2*Δ compared to wild-type cells (Leung et al., 2019).

To test whether there is a functional interaction between Prp43 and Set2, we generated a temperature-sensitive (ts) mutant of Prp43—*prp43-1*. At its permissive temperature of 25°C, *prp43-1* grows similarly to wild-type cells, but when it is grown at 37°C, there is a severe growth defect (Figure 4.3D). When the *prp43-1* ts mutation is combined with a *SET2* knockout, we observe an even more drastic growth defect (Figure 4.3D). These results suggest that Prp43 and Set2 play supporting roles in a common process.

Proteins that bind to methylated histone lysines often contain a domain such as a chromodomain, PHD finger, PWWP, or WD40 repeats (Wilkinson and Gozani, 2014). Because

Prp43 lacks a domain that is known to bind methylated histone lysines, it is possible that Prp43's interaction with chromatin is indirect, suggesting that another protein may be mediating the interaction between Prp43 and methylated histones. A potential interacting protein may be Eaf3, which has been implicated in mediating interaction between Prp45 and chromatin in *S. cerevisiae* (Leung et al., 2019). Experiments to address this possibility are in progress.

Additionally, we are addressing the possibility that Prp43 interacts directly with histones by using a histone peptide array with histone tail peptides containing a range of posttranslational modifications. These experiments require purified Prp43 protein. To purify recombinant Prp43, we transformed the plasmid pET16-PRP43, which expresses an N-terminal 6His-tagged wild-type Prp43 under the control of a T7 promoter, into the *E. coli* strain BL21-Codon Plus(DE3)RIL. 1 mg of recombinant 6His-tagged Prp43 was purified by affinity chromatography from a 50 mL culture of *E. coli*. The elution profile was gauged by SDS-PAGE (Figure 4.3E). Following purification, we used an ATPase assay and have confirmed that the purified protein has ATPase activity (data not shown). With active, purified recombinant Prp43, we plan on applying it to the histone peptide array to determine which, if any, modified peptides Prp43 may directly interact with.

Prp43's interaction with chromatin decreases when ICGs are downregulated.

One interesting feature of Prp43 is that its nuclear versus cytoplasmic activities are regulated by interacting proteins that act in different compartments (Robert-Paganin et al., 2015). These proteins contain a glycine-rich patch (G-patch) that facilitates Prp43 interaction. One model that this suggests is that Prp43 is recruited to the sites at which it acts through its G-patch interacting co-factors. In fact, it was shown that overexpression of certain G-patch proteins leads to redistribution of Prp43 within the cell (Heininger et al., 2016).

Rapamycin is a chemical that inhibits the TOR kinases that regulate cell proliferation and mRNA translation in yeast (Thomas and Hall, 1997). Additionally, rapamycin globally represses

expression of the highly expressed ribosomal protein genes (Cardenas et al., 1999; Venkataramanan et al., 2017). In *S. cerevisiae*, nearly one-third of all ICGs are ribosomal protein genes (RPGs) and ribosomal protein mRNAs account for nearly 90% of all mRNA transcripts from intron-containing genes (Ares et al., 1999). To determine whether Prp43 indeed interacts with chromatin only when ICGs are transcribed (i.e. when Prp43 is performing is splicing function) we treated actively growing cells with rapamycin and performed a co-IP experiment between Prp43-3HA and Histone H3. Addition of rapamycin to cells resulted in a significant reduction in the interaction between Prp43 and Histone H3 (Figure 4.4A). This result suggests that when ICGs are not actively transcribed, Prp43 is not enriched on chromatin since there is less need to disassemble spliceosomes.

We also considered the possibility that the addition of rapamycin leads to Prp43 re-distribution in the cell. We analyzed Prp43 interaction with G-patch proteins in the presence of rapamycin and observed that Prp43's interaction with Spp382/Ntr1, the G-patch protein involved in activating Prp43 for spliceosome disassembly, was disrupted. However, Prp43's interaction with Sqs1, the G-patch protein involved in activating Prp43 for ribosomal biogenesis, did not change (Figure 4.4B). So while expression of intron-containing RNAs helps direct Prp43 interaction with chromatin and splicing factors, the cytoplasmic interactions are not affected. This result also suggests a potential model where Spp382/Ntr1 binds to Prp43 and then directs Prp43 to the chromatin for cotranscriptional spliceosome disassembly. When ICGs are downregulated upon addition of rapamycin, interaction between Prp43 and Spp382/Ntr1 decreases because there is less need for spliceosome disassembly.

Co-transcriptional recruitment of Prp43 to ICGs can be assayed by ChIP.

One of the long outstanding questions has been when and where DExH/D family proteins associate with their substrates co-transcriptionally. Due to their weak and transient interactions

with the spliceosome it has not been clear how readily the cotranscriptional association could be detected by standard methods. To address this, we performed chromatin immunoprecipitation (ChIP)-qPCR to investigate occupancy of Prp43 along the ICG *ECM33*. Satisfingly, we were able to capture Prp43 on this particular ICG; Figure 4.5 shows the fold accumulation of Prp43-3HA on *ECM33* relative to the non-transcribed region (NTR) in a wild-type strain. Prp43 is most enriched toward the end of the gene, which correlates well with the fact that H3K36me3 is more enriched toward the 3′ end of genes as well as the fact that Prp43 primarily acts at the end of splicing.

DISCUSSION AND FUTURE DIRECTIONS

Splicing is tightly coordinated with gene transcription and studies have shown that splicing and transcription are not only coupled in time, but also functionally (Alpert et al., 2017; Merkhofer et al., 2014). A model for the kinetic coupling of splicing and transcription suggests that there is an optimal elongation rate for proper RNA splicing and processing (Fong et al., 2014; Neves et al., 2017). This model suggests that spliceosome disassembly and release may be affected when this kinetic coupling is perturbed (due to a change in the chromatin environment or other factors), leading to release of the spliceosome on the chromatin. Because Prp43 is involved in disassembling the spliceosome following optimal and defective splicing, we considered the possibility that Prp43 interacts with chromatin to affect spliceosome release.

Prp43 physically interacts with chromatin.

We demonstrate that the ATPase Prp43 physically interacts with Histone H3, a core histone protein, by co-IP (Figure 4.2B). We also show that this interaction persists in the presence of RNase, suggesting that Prp43's interaction with chromatin is not through chromatin and instead may be interacting directly or indirectly with chromatin (Figure 4.2B).

H3K36 methylation is one of the most well-studied histone modifications in the regulation of co-transcriptional splicing (Andersson et al., 2009; Guo et al., 2014; Kim et al., 2011;

Kolasinska-Zwierz et al., 2009; Leung et al., 2019; Luco et al., 2010; Simon et al., 2014; Sorenson et al., 2016). We previously demonstrated that H3K36me recruits the splicing machinery to chromatin via the chromodomain protein Eaf3 (Leung et al., 2019). Here, we show that Prp43 interacts with H3K36me3 and that Set2 has a role in mediating the interaction between Prp43 and chromatin (Figure 4.3B,C). These results suggest that H3K36me may not only be recruiting early splicing factors for efficient co-transcriptional spliceosome assembly, but also factors that are involved in the disassembly of the spliceosome. To further explore the Prp43–H3K36me3 interaction, we plan to assay whether this interaction is direct via histone peptide array and identify domains in Prp43 that are important for this interaction.

A possible role for H3K36me3 in the spliceosome discard pathway.

In mammals, H3K36me3 shifts from the 5′ end of genes to the 3′ end when splicing is inhibited using the splicing inhibitor spliceostatin A (Kim et al., 2011). We also show that a similar shift in H3K36me3 positioning occurs in yeast when splicing is inhibited using a ts *prp45* mutant (Figure 3.2B). We propose that H3K36me3 may be a signal to recruit proofreading factors such as Prp43 to disassemble stalled spliceosomes on the nascent pre-mRNA. To uncover the mechanism by which Prp43 directs release of co-transcriptionally spliced RNA and/or RNAs to be discarded, we performed Prp43 ChIP-qPCR in wild-type and were able to detect Prp43 recruitment to the ICG *ECM33* (Figure 4.5). We next plan to perform Prp43 ChIP-seq to observe distribution of Prp43 occupancy genome-wide under wild-type and *prp45* ts conditions. In addition to using the ts *prp45* mutant, we will also look at Prp43 occupancy in Prp2, 16, and 22 mutants, all of which trigger Prp43 disassembly. We plan to either use ts mutants of these ATPases or rapidly degrade these proteins using a degron system. In addition, we will look at how H3K36me3 changes in these mutants and Prp43 occupancy will be compared to H3K36me3 in wild-type cells and in the Prp mutant backgrounds.

While it is understood that splicing and transcription are coupled, the ramifications of splicing occurring on chromatin has been unclear. Here, we propose that Prp43 interacts with chromatin and regulates the time the pre-mRNA remains chromatin-associated. We propose that Prp43 physically interacts with the chromatin to disassemble wild-type spliceosomes and also stalled spliceosomes, releasing the RNA to the nucleoplasm for export or degradation.

MATERIALS AND METHODS

Yeast strains, media, and growth

The yeast strains used in this study are listed in Table 4.1. Strains were grown in YPD (1% yeast extract, 2% peptone, and 2% dextrose) at 30°C under constant shaking to an OD_{600} of 0.6–0.8. The *set2*Δ mutant was obtained from GE Dharmacon. Tagged strains were generated as previously described (Longtine et al., 1998). For rapamycin treatment, cultures were grown to an OD_{600} of 0.5 and then incubated with 200 ng/µL rapamycin for 30 minutes.

Generating whole cell extracts

Cell pellets were resuspended in 400–700 µL FA lysis buffer (50 mM HEPES pH 7.5, 150 mM NaCl, 1 mM EDTA, 1% Triton X-100, 0.1% sodium deoxycholate, 1 mM PMSF) with protease inhibitors. 500 µm diameter acid-washed beads (Biospec) were added to the resuspension and subsequently continuously vortexed for 5 minutes at 4°C. Beads and cell debris were removed by centrifugation at 13,000 rpm at 4°C.

Separating soluble and insoluble fractions

50 mL yeast cultures were grown to an OD_{600} of 0.8 and pelleted. WCE were generated and subjected to centrifugation at 13,000 rpm for 30 min at 4°C. The supernatant was removed and labeled as the soluble fraction. 2X SDS-PAGE loading buffer was added to the supernatant and the sample was boiled for 5 minutes at 95°C. The insoluble pellet was resuspended in 1X SDS-

PAGE loading buffer and subsequently boiled for 10 minutes at 95°C. The supernatant and pellet fractions were run on a 10–15% SDS-PAGE gel and subjected to Western blotting with anti-HA (Roche, 12CA5), anti-H3 (Abcam, 1791), and anti-Pgk1 (ThermoFisher, 22C5D8) antibodies.

Co-immunoprecipitation

150 mL yeast cultures were grown to an OD_{600} of 0.8 and pelleted. Pellets were then lysed in FA lysis buffer with protease inhibitors by bead beating and cleared by high speed centrifugation. 700 µL of lysate was removed for the immunoprecipitation (IP) fraction. 10 µL was removed for the input (IN) fraction. 4 µg of anti-H3 or anti-Myc (Roche, 9E10) antibody was added to the IP fraction and the sample was placed on a nutator at 4°C overnight. 25 µL of GammaBind G beads (GE Healthcare) was then added to the IP sample and incubated for 2 hours at 4°C. Beads were washed four times with FA lysis buffer and the bound proteins were eluted with 2X SDS-PAGE loading buffer by boiling at 95°C for 5 minutes. IN and IP samples were then subjected to SDS-PAGE followed by Western blot analysis.

Chromatin immunoprecipitation

50 mL yeast cultures were grown to an OD_{600} of 0.8 and crosslinked with 1% formaldehyde for 15 minutes at room temperature. Crosslinking was then quenched after adding 125 mM glycine for 5 minutes. Cells were then pelleted and flash frozen in liquid N_2. WCEs were generated and subjected to sonication for a total sonication time of 7.5 minutes at 15% amplitude (300 bp average sonicated DNA size). Sonicated lysates were cleared by high speed centrifugation. 500 µL of supernatant was removed for ChIP and 10 µL was saved as the input fraction. 4 µg of anti-HA antibody was added to the supernatant and the sample was incubated at 4°C overnight on a nutator. 25 µL of GammaBind G beads were added to the samples for 2 hours at 4°C. Beads were washed four times in FA lysis buffer and two times in TE (10 mM Tris pH 8, 1 mM EDTA). Beads were then incubated with elution buffer (50 mM Tris pH 8, 5 mM EDTA, 1% SDS) for 10

minutes at 65°C. The eluted samples were then incubated at 65°C overnight to reverse crosslinks. The following day, the decrosslinked samples were subjected to RNase and Proteinase K treatment. DNA was then isolated by column purification and qPCR analysis was then performed using gene-specific primers.

FIGURES

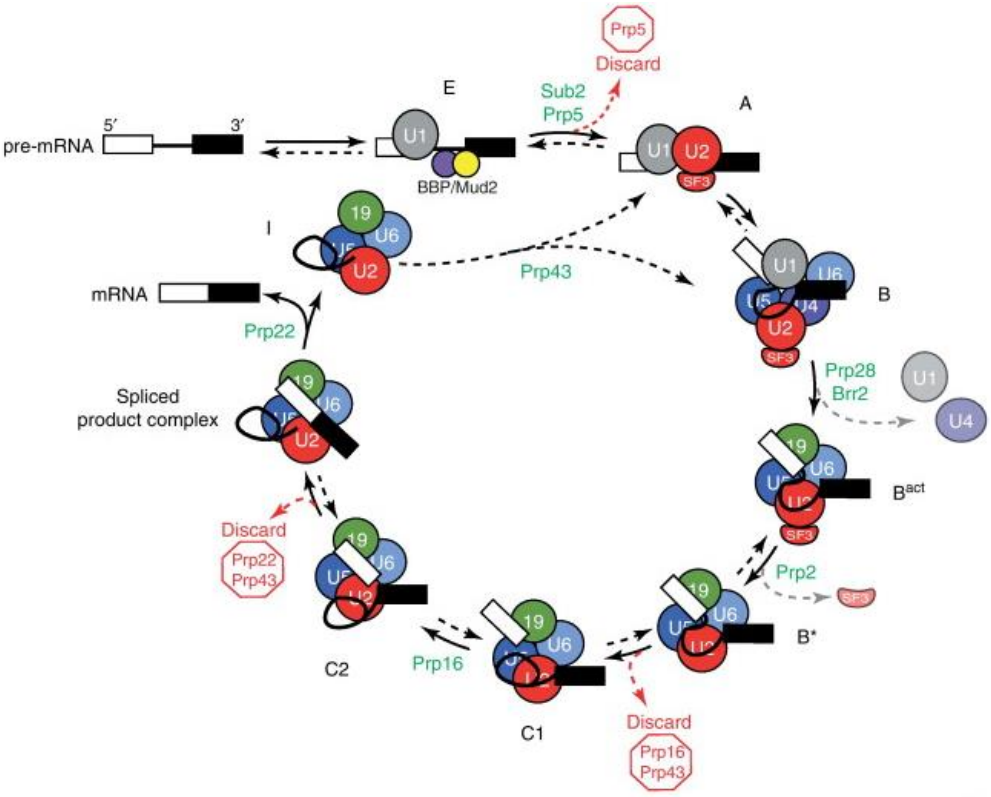

Figure 4.1. Adapted from (Hoskins and Moore, 2012). Prp43 is involved in the spliceosome discard pathway.

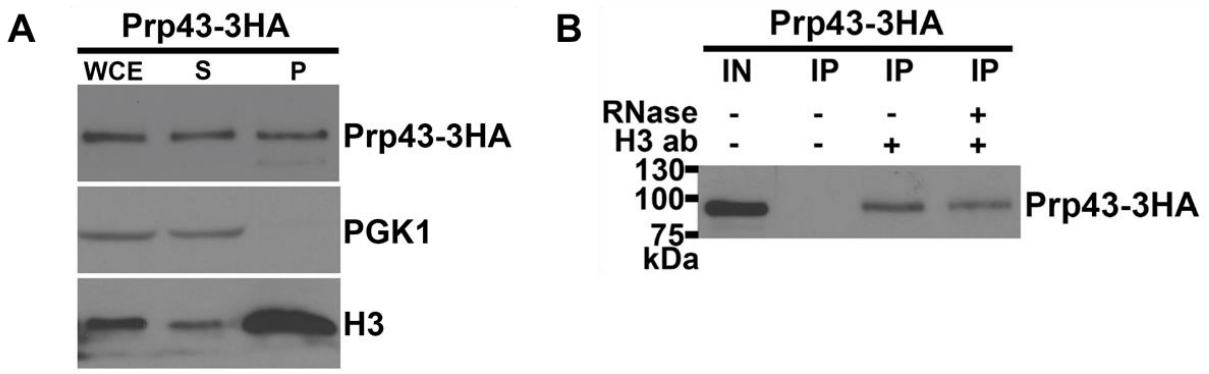

Figure 4.2. Prp43 is associated with chromatin. A. Western blot analysis of whole cell extracts (WCE), supernatant (S), and pellet (P) fractions. Presence of Prp43-3HA, Pgk1, and Histone H3 was assayed in each fraction. **B.** Whole cell extracts were prepared by glass bead disruption. Bulk chromatin was immunoprecipitated with a histone H3-specific antibody. Prp43-HA was subsequently detected by SDS-PAGE and western blot analysis. Lane 1 is 1% input. Samples were incubated with RNase (20 U) where indicated.

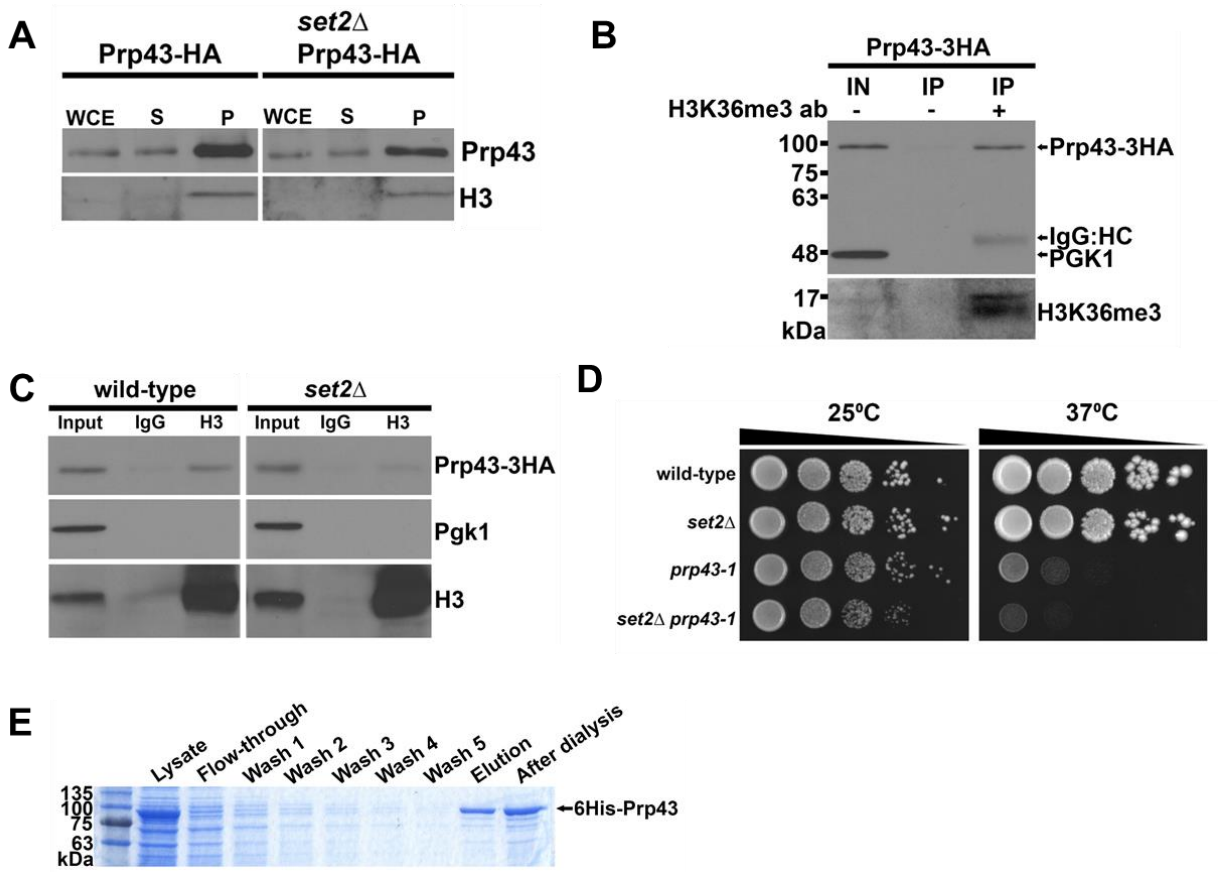

Figure 4.3. Set2-mediated H3K36 methylation is required for Prp43 binding to chromatin. **A.** Whole cell extracts from wild-type and *set2*Δ cells were subjected to a high-speed spin to separate soluble and insoluble fractions. Prp43, Pgk1, and Histone H3 levels were detected by Western blot analysis in the whole cell extract (WCE), supernatant (S), and insoluble chromatin-enriched pellet (P). **B.** Whole cell extracts were prepared from a Prp43-HA strain. H3K36me3 was immunoprecipitated using a polyclonal antibody against H3K36me3. Prp43 was then detected by SDS-PAGE and western blot analysis. Lane 1 is 1% input. **C.** Whole cell extracts were prepared by glass bead disruption. Bulk chromatin was immunoprecipitated with a histone H3-specific antibody. Prp43, Pgk1, and Histone H3 were subsequently detected by SDS-PAGE and western blot analysis. Lane 1 is 1% input. **D.** Growth analysis of wild-type, *set2*Δ, *prp43-1*, and *set2*Δ *prp43-1* cells on YPD plates at 25C and 37C. Each spot is a 10-fold dilution. Plates were incubated for 2–3 days prior to imaging. **E.** SDS-PAGE analysis of purified recombinant 6His-Prp43.

Samples were run on a 10% SDS-PAGE gel and was subsequently stained with SimplyBlue SafeStain.

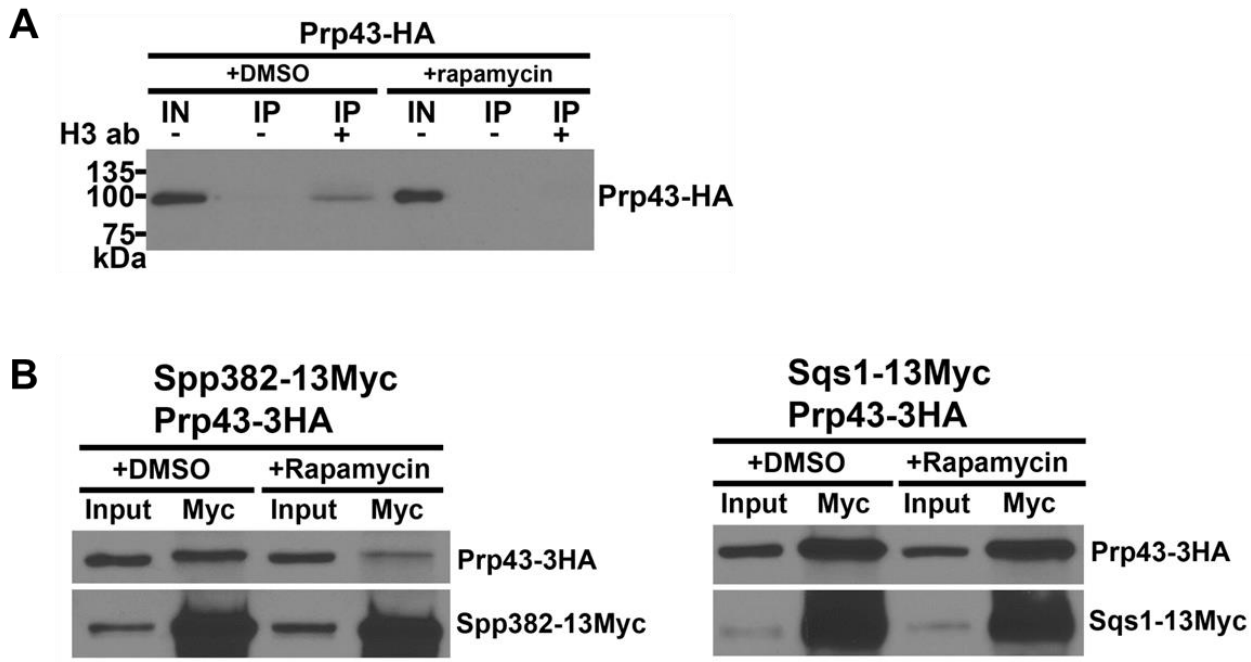

Figure 4.4. Prp43's interaction with chromatin depends on transcription of ICGs. A. Co-IP analysis between Prp43-3HA and Histone H3. Cells were incubated with DMSO or rapamycin where indicated. Samples were run on a 15% SDS-PAGE gel and western blot analysis was performed. Input is 1% of total lysate. **B.** Co-IP analysis between Spp382-13Myc and Prp43-3HA (left) and Sqs1-13Myc and Prp43-3HA (right). Cells were incubated with rapamycin where incubated with DMSO or rapamycin where indicated. Samples were run on a 10% SDS-PAGE gel and western blot analysis was performed. Input is 1% of total lysate.

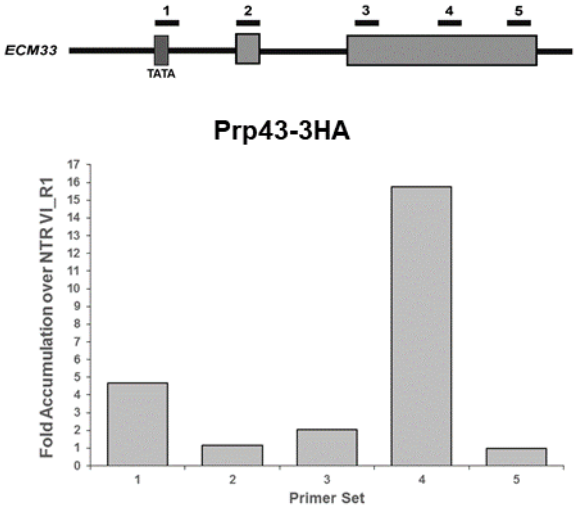

Figure 4.5. Prp43 is co-transcriptionally recruited to ICG *ECM33*. Occupancy of Prp43-3HA on *ECM33* relative to a non-transcribed region (NTR) on Chr. V.

Table 4.1. Yeast strains used in this study		
Name	**Genotype**	**Reference**
BY4741	MATa his3Δ1 leu2Δ0 met15Δ0 ura3Δ0	Open Biosystems
TJY7170	MATa set2Δ::KANMX4 his3Δ1 leu2Δ0 met15Δ0 ura3Δ0	GE Dharmacon
TJY7287	MATa PRP43-HA::KANMX4 his3Δ1 leu2Δ0 met15Δ0 ura3Δ0	This study
TJY7288	MATa set2Δ::KANMX4 PRP43-HA:HIS3MX6 his3Δ1 leu2Δ0 met15Δ0 ura3Δ0	This study
TJY7289	MATa PRP43-HA::HIS3MX6 SPP382-Myc::KANMX4 his3Δ1 leu2Δ0 met15Δ0 ura3Δ0	This study
TJY7290	MATa PRP43-HA::HIS3MX6 SQS1-Myc::KANMX4 his3Δ1 leu2Δ0 met15Δ0 ura3Δ0	This study

REFERENCES

Alpert, T., Herzel, L., and Neugebauer, K.M. (2017). Perfect timing: splicing and transcription rates in living cells. Wiley Interdiscip Rev RNA *8*.

Andersson, R., Enroth, S., Rada-Iglesias, A., Wadelius, C., and Komorowski, J. (2009). Nucleosomes are well positioned in exons and carry characteristic histone modifications. Genome Res *19*, 1732-1741.

Arenas, J.E., and Abelson, J.N. (1997). Prp43: An RNA helicase-like factor involved in spliceosome disassembly. Proc Natl Acad Sci U S A *94*, 11798-11802.

Ares, M., Jr., Grate, L., and Pauling, M.H. (1999). A handful of intron-containing genes produces the lion's share of yeast mRNA. RNA *5*, 1138-1139.

Bhatt, D.M., Pandya-Jones, A., Tong, A.J., Barozzi, I., Lissner, M.M., Natoli, G., Black, D.L., and Smale, S.T. (2012). Transcript dynamics of proinflammatory genes revealed by sequence analysis of subcellular RNA fractions. Cell *150*, 279-290.

Cardenas, M.E., Cutler, N.S., Lorenz, M.C., Di Como, C.J., and Heitman, J. (1999). The TOR signaling cascade regulates gene expression in response to nutrients. Genes Dev *13*, 3271-3279.

Chen, Y.L., Capeyrou, R., Humbert, O., Mouffok, S., Kadri, Y.A., Lebaron, S., Henras, A.K., and Henry, Y. (2014). The telomerase inhibitor Gno1p/PINX1 activates the helicase Prp43p during ribosome biogenesis. Nucleic Acids Res *42*, 7330-7345.

de la Mata, M., Alonso, C.R., Kadener, S., Fededa, J.P., Blaustein, M., Pelisch, F., Cramer, P., Bentley, D., and Kornblihtt, A.R. (2003). A slow RNA polymerase II affects alternative splicing in vivo. Mol Cell *12*, 525-532.

Fong, N., Kim, H., Zhou, Y., Ji, X., Qiu, J., Saldi, T., Diener, K., Jones, K., Fu, X.D., and Bentley, D.L. (2014). Pre-mRNA splicing is facilitated by an optimal RNA polymerase II elongation rate. Genes Dev *28*, 2663-2676.

Guo, R., Zheng, L., Park, J.W., Lv, R., Chen, H., Jiao, F., Xu, W., Mu, S., Wen, H., Qiu, J.*, et al.* (2014). BS69/ZMYND11 reads and connects histone H3.3 lysine 36 trimethylation-decorated chromatin to regulated pre-mRNA processing. Mol Cell *56*, 298-310.

Heininger, A.U., Hackert, P., Andreou, A.Z., Boon, K.L., Memet, I., Prior, M., Clancy, A., Schmidt, B., Urlaub, H., Schleiff, E.*, et al.* (2016). Protein cofactor competition regulates the action of a multifunctional RNA helicase in different pathways. RNA Biol *13*, 320-330.

Hnilicová, J., and Staněk, D. (2011). Where splicing joins chromatin. Nucleus *2*, 182-188.

Hoskins, A.A., and Moore, M.J. (2012). The spliceosome: a flexible, reversible macromolecular machine. Trends Biochem Sci *37*, 179-188.

Howe, K.J., Kane, C.M., and Ares, M., Jr. (2003). Perturbation of transcription elongation influences the fidelity of internal exon inclusion in Saccharomyces cerevisiae. RNA *9*, 993-1006.

Kai, M., Tanaka, H., and Wang, T.S. (2001). Fission yeast Rad17 associates with chromatin in response to aberrant genomic structures. Mol Cell Biol *21*, 3289-3301.

Kim, S., Kim, H., Fong, N., Erickson, B., and Bentley, D.L. (2011). Pre-mRNA splicing is a determinant of histone H3K36 methylation. Proc Natl Acad Sci U S A *108*, 13564-13569.

Kolasinska-Zwierz, P., Down, T., Latorre, I., Liu, T., Liu, X.S., and Ahringer, J. (2009). Differential chromatin marking of introns and expressed exons by H3K36me3. Nat Genet *41*, 376-381.

Koodathingal, P., Novak, T., Piccirilli, J.A., and Staley, J.P. (2010). The DEAH box ATPases Prp16 and Prp43 cooperate to proofread 5' splice site cleavage during pre-mRNA splicing. Mol Cell *39*, 385-395.

Kouzarides, T. (2007). Chromatin modifications and their function. Cell *128*, 693-705.

Lacadie, S.A., Tardiff, D.F., Kadener, S., and Rosbash, M. (2006). In vivo commitment to yeast cotranscriptional splicing is sensitive to transcription elongation mutants. Genes Dev *20*, 2055-2066.

Lebaron, S., Froment, C., Fromont-Racine, M., Rain, J.C., Monsarrat, B., Caizergues-Ferrer, M., and Henry, Y. (2005). The splicing ATPase prp43p is a component of multiple preribosomal particles. Mol Cell Biol *25*, 9269-9282.

Leung, C.S., Douglass, S.M., Morselli, M., Obusan, M.B., Pavlyukov, M.S., Pellegrini, M., and Johnson, T.L. (2019). H3K36 Methylation and the Chromodomain Protein Eaf3 Are Required for Proper Cotranscriptional Spliceosome Assembly. Cell Rep *27*, 3760-3769 e3764.

Li, J., and Stern, D.F. (2005). DNA damage regulates Chk2 association with chromatin. J Biol Chem *280*, 37948-37956.

Longtine, M.S., McKenzie, A., 3rd, Demarini, D.J., Shah, N.G., Wach, A., Brachat, A., Philippsen, P., and Pringle, J.R. (1998). Additional modules for versatile and economical PCR-based gene deletion and modification in Saccharomyces cerevisiae. Yeast *14*, 953-961.

Luco, R.F., Pan, Q., Tominaga, K., Blencowe, B.J., Pereira-Smith, O.M., and Misteli, T. (2010). Regulation of alternative splicing by histone modifications. Science *327*, 996-1000.

Mayas, R.M., Maita, H., Semlow, D.R., and Staley, J.P. (2010). Spliceosome discards intermediates via the DEAH box ATPase Prp43p. Proc Natl Acad Sci U S A *107*, 10020-10025.

Merkhofer, E.C., Hu, P., and Johnson, T.L. (2014). Introduction to cotranscriptional RNA splicing. Methods Mol Biol *1126*, 83-96.

Misteli, T., and Spector, D.L. (1999). RNA polymerase II targets pre-mRNA splicing factors to transcription sites in vivo. Mol Cell *3*, 697-705.

Neves, L.T., Douglass, S., Spreafico, R., Venkataramanan, S., Kress, T.L., and Johnson, T.L. (2017). The histone variant H2A.Z promotes efficient cotranscriptional splicing in S. cerevisiae. Genes Dev *31*, 702-717.

Nojima, T., Rebelo, K., Gomes, T., Grosso, A.R., Proudfoot, N.J., and Carmo-Fonseca, M. (2018). RNA Polymerase II Phosphorylated on CTD Serine 5 Interacts with the Spliceosome during Co-transcriptional Splicing. Mol Cell *72*, 369-379 e364.

Oesterreich, F.C., Herzel, L., Straube, K., Hujer, K., Howard, J., and Neugebauer, K.M. (2016). Splicing of Nascent RNA Coincides with Intron Exit from RNA Polymerase II. Cell *165*, 372-381.

Pertschy, B., Schneider, C., Gnadig, M., Schafer, T., Tollervey, D., and Hurt, E. (2009). RNA helicase Prp43 and its co-factor Pfa1 promote 20 to 18 S rRNA processing catalyzed by the endonuclease Nob1. J Biol Chem *284*, 35079-35091.

Robert-Paganin, J., Rety, S., and Leulliot, N. (2015). Regulation of DEAH/RHA helicases by G-patch proteins. Biomed Res Int *2015*, 931857.

Simon, J.M., Hacker, K.E., Singh, D., Brannon, A.R., Parker, J.S., Weiser, M., Ho, T.H., Kuan, P.F., Jonasch, E., Furey, T.S.*, et al.* (2014). Variation in chromatin accessibility in human kidney cancer links H3K36 methyltransferase loss with widespread RNA processing defects. Genome Res *24*, 241-250.

Sims, R.J., 3rd, Millhouse, S., Chen, C.F., Lewis, B.A., Erdjument-Bromage, H., Tempst, P., Manley, J.L., and Reinberg, D. (2007). Recognition of trimethylated histone H3 lysine 4 facilitates the recruitment of transcription postinitiation factors and pre-mRNA splicing. Mol Cell *28*, 665-676.

Sorenson, M.R., Jha, D.K., Ucles, S.A., Flood, D.M., Strahl, B.D., Stevens, S.W., and Kress, T.L. (2016). Histone H3K36 methylation regulates pre-mRNA splicing in Saccharomyces cerevisiae. RNA Biol *13*, 412-426.

Thomas, G., and Hall, M.N. (1997). TOR signalling and control of cell growth. Curr Opin Cell Biol *9*, 782-787.

Tsai, R.T., Tseng, C.K., Lee, P.J., Chen, H.C., Fu, R.H., Chang, K.J., Yeh, F.L., and Cheng, S.C. (2007). Dynamic interactions of Ntr1-Ntr2 with Prp43 and with U5 govern the recruitment of Prp43 to mediate spliceosome disassembly. Mol Cell Biol *27*, 8027-8037.

Venkataramanan, S., Douglass, S., Galivanche, A.R., and Johnson, T.L. (2017). The chromatin remodeling complex Swi/Snf regulates splicing of meiotic transcripts in Saccharomyces cerevisiae. Nucleic Acids Res *45*, 7708-7721.

Wilkinson, A.W., and Gozani, O. (2014). Histone-binding domains: strategies for discovery and characterization. Biochim Biophys Acta *1839*, 669-675.

CHAPTER 5:

Concluding remarks and perspectives

Since it was discovered that splicing is cotranscriptional, studies in yeast to higher eukaryotes have implicated the transcriptional machinery and chromatin in regulating splicing. An optimal rate of transcription elongation by RNAPII is necessary for proper constitutive and alternative splicing (Fong et al., 2014). Furthermore, the phosphorylation state of the CTD tail of RNAPII has been proposed affect splicing, possibly by recruiting splicing factors to sites of transcription (Das et al., 2007; Hirose et al., 1999; Komarnitsky et al., 2000). Chromatin has also been implicated in affecting splicing outcomes (Hnilicová and Staněk, 2011). In this dissertation, we demonstrate how chromatin, specifically chromatin modification, regulates cotranscriptional splicing and vice versa.

We show that the histone methyltransferase Set2 and its associated histone mark H3K36 methylation are important for constitutive splicing in *S. cerevisiae* (Leung et al., 2019). We demonstrate that Set2 is required for Eaf3 recruitment to ICGs and that Eaf3 interacts with all five spliceosomal snRNAs. Furthermore, we show that Eaf3 physically interacts with the splicing factor Prp45, the human ortholog of SKIP. Loss of Eaf3 results in inefficient cotranscriptional recruitment of Prp45 to nascent transcripts. This study reveals a novel mechanism by which a histone modification recruits the splicing machinery to chromatin for cotranscriptional splicing in yeast.

Although we have shown a role for Eaf3 to stabilize Prp45 for proper cotranscriptional spliceosome assembly, it does not rule out that transcription changes in the absence of Eaf3 or H3K36me may affect splicing outcomes. We plan on performing native elongating transcript sequencing (NET-seq) to quantitatively measure how RNAPII elongation changes in the mutants and relate them to the splicing changes we previously observed. It is important to note the experiments performed to determine Set2's role in regulating cotranscriptional splicing has been performed at steady state conditions. For future studies, we plan to perform metabolic labeling of newly synthesized RNAs with 4-thiouridine (4sU) to further dissect how transcription and splicing changes in the absence of H3K36me. By performing 4sU-sequencing at different time points, we

may see an even greater splicing defect in the H3K36me and *eaf3*Δ mutants since we will be able to capture these unspliced RNAs before they are degraded. Furthermore, we will be able to determine whether transcription changes have a role in affecting splicing outcomes in the mutants.

In addition to recruiting Prp45 to chromatin, we also demonstrate a role for H3K36me in recruitment of the spliceosome disassembly factor Prp43. Although it is understood that splicing occurs cotranscriptionally, it is not well understood how spliceosomes are disassembled and discarded cotranscriptionally. A study from the Smale group suggested that transcripts are retained on chromatin until fully spliced in mammals (Bhatt et al., 2012). We hypothesize that Prp43 is recruited to chromatin to release pre-mRNAs and disassemble spliceosomes. We show that Prp43 physically interacts with chromatin and that this interaction is not dependent on RNA, but dependent on presence of H3K36me. We also show that Prp43's interaction with chromatin is due to its splicing function and not due to its other functions in the cell. Lastly, we show that we can capture Prp43 on nascent transcripts via ChIP-qPCR which will allow further studies on how Prp43 is recruited to chromatin to perform its disassembly function cotranscriptionally.

Although there have been many studies on how chromatin affects splicing, there has been increasing interest in how splicing may affect the state of the chromatin. The Bentley and Carmo-Fonseca groups have shown that inhibition of splicing results in changes in normal H3K36me3 patterns in mammals (de Almeida et al., 2011; Kim et al., 2011). We hypothesized that splicing may have a role in establishing proper levels on H3K36me3 on ICGs to maintain a splicing/H3K36me feedback regulatory loop. By ChIP-seq, we show that ICGs are enriched for H3K36me3 throughout the gene body compared to non-ICGs. Furthermore, we show that a similar shift in H3K36me3 from the 5′ to 3′ end of genes occurs in yeast when splicing is inhibited with the *prp45*(1-169) temperature-sensitive mutant. We propose that this shift in H3K36me3 is a

signal for the spliceosome disassembly factor Prp43 to discard stalled spliceosomes on chromatin and to release the tethered pre-mRNA.

The studies presented here demonstrate a clear role for chromatin in directly regulating cotranscriptional splicing. H3K36 methylation has been shown to be critical for not only proper spliceosome assembly, but also possibly for spliceosome disassembly and discard. Future studies are needed to dissect the molecular mechanisms of the crosstalk between splicing and chromatin modifications, particularly how splicing affects normal patterns of histone modifications.

REFERENCES

Bhatt, D.M., Pandya-Jones, A., Tong, A.J., Barozzi, I., Lissner, M.M., Natoli, G., Black, D.L., and Smale, S.T. (2012). Transcript dynamics of proinflammatory genes revealed by sequence analysis of subcellular RNA fractions. Cell *150*, 279-290.

Das, R., Yu, J., Zhang, Z., Gygi, M.P., Krainer, A.R., Gygi, S.P., and Reed, R. (2007). SR proteins function in coupling RNAP II transcription to pre-mRNA splicing. Mol Cell *26*, 867-881.

de Almeida, S.F., Grosso, A.R., Koch, F., Fenouil, R., Carvalho, S., Andrade, J., Levezinho, H., Gut, M., Eick, D., Gut, I.*, et al.* (2011). Splicing enhances recruitment of methyltransferase HYPB/Setd2 and methylation of histone H3 Lys36. Nat Struct Mol Biol *18*, 977-983.

Fong, N., Kim, H., Zhou, Y., Ji, X., Qiu, J., Saldi, T., Diener, K., Jones, K., Fu, X.D., and Bentley, D.L. (2014). Pre-mRNA splicing is facilitated by an optimal RNA polymerase II elongation rate. Genes Dev *28*, 2663-2676.

Hirose, Y., Tacke, R., and Manley, J.L. (1999). Phosphorylated RNA polymerase II stimulates pre-mRNA splicing. Genes Dev *13*, 1234-1239.

Hnilicová, J., and Staněk, D. (2011). Where splicing joins chromatin. Nucleus *2*, 182-188.

Kim, S., Kim, H., Fong, N., Erickson, B., and Bentley, D.L. (2011). Pre-mRNA splicing is a determinant of histone H3K36 methylation. Proc Natl Acad Sci U S A *108*, 13564-13569.

Komarnitsky, P., Cho, E.J., and Buratowski, S. (2000). Different phosphorylated forms of RNA polymerase II and associated mRNA processing factors during transcription. Genes Dev *14*, 2452-2460.

Leung, C.S., Douglass, S.M., Morselli, M., Obusan, M.B., Pavlyukov, M.S., Pellegrini, M., and Johnson, T.L. (2019). H3K36 Methylation and the Chromodomain Protein Eaf3 Are Required for Proper Cotranscriptional Spliceosome Assembly. Cell Rep *27*, 3760-3769 e3764.

APPENDIX

Antisense splicing in *set2*Δ cells.

Deletion of the *SET2* gene leads to increased cryptic and antisense transcription in *S. cerevisiae* due to loss of binding of Rpd3S histone deacetyltransferase complex to transcribed regions (Carrozza et al., 2005; Joshi and Struhl, 2005; Keogh et al., 2005; Venkatesh et al., 2016). Although the implications of cryptic and antisense transcripts in yeast are still largely unknown, recent studies have begun to elucidate their functions. Set2 and H3K36me has been implicated in nutrient stress response in yeast (McDaniel et al., 2017). Upon nutrient stress, antisense transcripts interfere with transcription of sense transcripts, implying that Set2 is required for transcriptional fidelity (McDaniel et al., 2017). A subsequent study revealed that loss of Set2 lead to increased antisense transcription of cell cycle regulated genes and thus misregulating transcription of the sense transcript (Dronamraju et al., 2018). Through stranded RNA-seq of wild-type and *set2*Δ cells, we confirm that loss of *SET2* leads to an accumulation of antisense transcription genome-wide (Figure A.1). Furthermore, lowly expressed genes are more susceptible to having increased antisense transcription (Figure A.1).

Interestingly, some of these antisense transcripts have novel splicing events. *LEU4*, a gene encoding a protein involved in the leucine biosynthesis pathway, was determined to show a strong and significant increase in antisense splicing events. We performed antisense-specific PCR and confirmed the presence of a spliced RNA that arises from the *LEU4* gene in *set2*Δ cells (Figure A.2). Under wild-type conditions, these splicing events are not observed because antisense *LEU4* transcripts are low. However, when *SET2* is deleted, antisense transcription of *LEU4* increases, and therefore makes it possible to observe spliced antisense transcripts. Future studies will focus on determining the conditions under which this antisense transcript is abundant and whether this transcript is involved in regulating the leucine biosynthesis pathway.

FIGURES

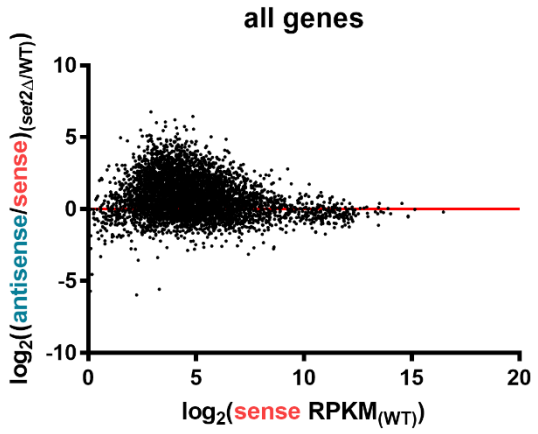

Figure A.1. Lowly abundant genes have more antisense transcription. XY-scatter plot of wild-type sense RPKM levels compared to antisense/sense ratio in *set2*Δ cells.

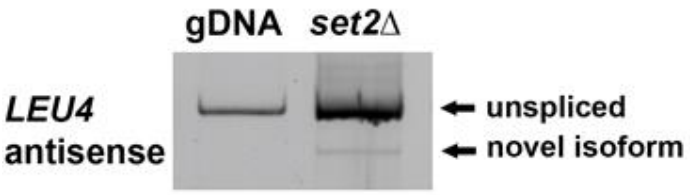

Figure A.2. *LEU4* undergoes antisense splicing. *LEU4* antisense-specific RT-PCR. Samples were run on an 8% PAGE gel.

REFERENCES

Carrozza, M.J., Li, B., Florens, L., Suganuma, T., Swanson, S.K., Lee, K.K., Shia, W.J., Anderson, S., Yates, J., Washburn, M.P.*, et al.* (2005). Histone H3 methylation by Set2 directs deacetylation of coding regions by Rpd3S to suppress spurious intragenic transcription. Cell *123*, 581-592.

Dronamraju, R., Jha, D.K., Eser, U., Adams, A.T., Dominguez, D., Choudhury, R., Chiang, Y.C., Rathmell, W.K., Emanuele, M.J., Churchman, L.S.*, et al.* (2018). Set2 methyltransferase facilitates cell cycle progression by maintaining transcriptional fidelity. Nucleic Acids Res *46*, 1331-1344.

Joshi, A.A., and Struhl, K. (2005). Eaf3 chromodomain interaction with methylated H3-K36 links histone deacetylation to Pol II elongation. Mol Cell *20*, 971-978.

Keogh, M.C., Kurdistani, S.K., Morris, S.A., Ahn, S.H., Podolny, V., Collins, S.R., Schuldiner, M., Chin, K., Punna, T., Thompson, N.J.*, et al.* (2005). Cotranscriptional set2 methylation of histone H3 lysine 36 recruits a repressive Rpd3 complex. Cell *123*, 593-605.

McDaniel, S.L., Hepperla, A.J., Huang, J., Dronamraju, R., Adams, A.T., Kulkarni, V.G., Davis, I.J., and Strahl, B.D. (2017). H3K36 Methylation Regulates Nutrient Stress Response in Saccharomyces cerevisiae by Enforcing Transcriptional Fidelity. Cell Rep *19*, 2371-2382.

Venkatesh, S., Li, H., Gogol, M.M., and Workman, J.L. (2016). Selective suppression of antisense transcription by Set2-mediated H3K36 methylation. Nat Commun *7*, 13610.